NUCLEAR PHYSICS LABORATORY

UNIVERSITY OF
WASHINGTON

ANNUAL REPORT

JUNE 1967

U.S. ATOMIC ENERGY COMMISSION
CONTRACT A.T. (45-1)-1388

ANNUAL REPORT

Nuclear Physics Laboratory
University of Washington
June, 1967

Program "A" --
Experimental Nuclear Physics
Program (Cyclotron)
under
U. S. Atomic Energy Commission
Contract A. T. (45-1) - 1388

PREFACE

This report reviews the research and technical development conducted at the Nuclear Physics Laboratory at the University of Washington during the year ending June 15, 1967. Two accelerators are presently in use, a 60-inch cyclotron and a two-stage FN tandem Van de Graaff. The installation of a second, injector stage, FN tandem is nearly complete; it is expected to be available for research very shortly.

Research at this Laboratory is performed by the faculty and graduate students of the Departments of Physics and Chemistry of the University of Washington. Support for these projects is provided by the State of Washington, the U.S. Atomic Energy Commission, and the National Science Foundation.*

The arrangement of this report follows the pattern of previous years in that it is broken into subsections. Some of the project reports could have been included in more than one subsection; for these the decision as to the most appropriate section was somewhat arbitrary. The project reports are numbered consecutively. As has been our practice in the past, the names of the investigators participating in each project are listed at the end of each project report in alphabetical order.

The investigations described in the report for the most part continue and extend experimental work described in earlier reports, to which reference is generally made. Continued emphasis is placed on elastic and inelastic scattering, pickup and stripping reactions, reactions involving spin flip, photons emitted in nuclear reactions, compound nuclear reactions, and nuclear fission. This year's report also includes two project reports of research which originated within the University but outside the Nuclear Physics Laboratory. While these projects make use of the cyclotron, their financial support comes from sources other than those which support the Nuclear Physics Laboratory.

This report concludes with sections describing new instruments for research, accelerator research and development, a list of laboratory personnel, a list of advanced degrees granted during the past year, and a list of laboratory publications since last year's report.

---

* The National Science Foundation provided the funds to purchase the three-stage tandem Van de Graaff accelerator and some of its associated equipment, and a portion of the funds to construct the laboratory building to house them.

TABLE OF CONTENTS

I. ELASTIC AND INELASTIC SCATTERING

1. A Search for Excited States in He^3

Kim *et al.*[1] recently reported He^3 excited states of excitation energy 8.2, 10.2 and 12.6 MeV, seen in the inelastic scattering of protons by He^3. The experiment here described is a search for effects of these states in the elastic scattering of protons by deuterons. Excitation functions near energies where the excited states are expected were obtained. It should be noted that anomalies in these excitation functions would most likely correspond to He^3 states with isotopic spin T=1/2 but not states with T=3/2.

The target consisted of a 1 in. diameter cylindrical gas cell with 0.1 mil Havar[2] windows, filled with deuterium to about one half atmospheric pressure. Two detectors were used simultaneously; by detecting both scattered protons and recoil deuterons in each detector, we could measure differential cross sections at as many as four c.m. angles in one run. Protons of about 4, 7, and 10.6 MeV were used. Excitation functions were measured with energy steps of less than 60 keV.

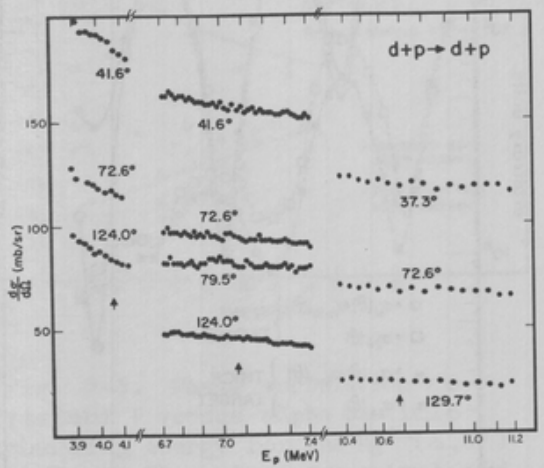

Fig. 1-1. Excitation function of the differential cross section for elastic scattering of protons by deuterons. The proton energy E_p is in the lab system; angles are in the c.m. system. Arrows indicate energies at which resonances are expected.

Figure 1-1 shows the excitation functions which were obtained. Angles are in the c.m. system; incident proton energy is in the lab system. Points are normalized by interpolating between absolute differential cross section measurements available in the literature.[3] The arrows indicate where resonances corresponding to the He^3 excited states are expected. No anomaly is observed at these energies or elsewhere on the curves. This finding has been amply supported by recently reported evidence.[4] (C. C. Ling, D. W. Storm and W. G. Weitkamp)

---

1. C. C. Kim, S. M. Bunch, D. W. Devins, and H. H. Forster, Phys. Letters *22*, 314 (1966).
2. Supplied by the Hamilton Watch Company.
3. W. T. H. Van Oers and K. W. Brockman, Jr., Nucl. Phys. *21*, 189 (1960).
4. J. C. Legg, A. S. Wilson, M. A. Crosby, and G. C. Phillips, Bull. Am. Phys. Soc. *11*, 895 (1966).

2. Phase Correlations in $Mg^{24}(\alpha,\alpha')$

An approach to the study of nuclear reaction mechanisms using the Blair Phase Rule in the case of $Mg^{24}(\alpha,\alpha')$ scattering was reported last year.[1] In this work the phase relationship between two angular distributions was put on a quantitative basis by constructing a function P which described the correlation in phase of the maxima and minima of two distributions, in this case the elastic angular distribution and inelastic first-excited-state (2^+, 1.368 MeV) angular distribution of the $Mg^{24}(\alpha,\alpha')$ reaction. This work has been expanded and refined to include: 1) a fine grain quantitative picture of the energy dependence of the phase rule in the region 15 MeV to 22 MeV; 2) an investigation of the validity of this analysis; and 3) a comparison of the experimental values of P with those predicted by DWBA analysis.

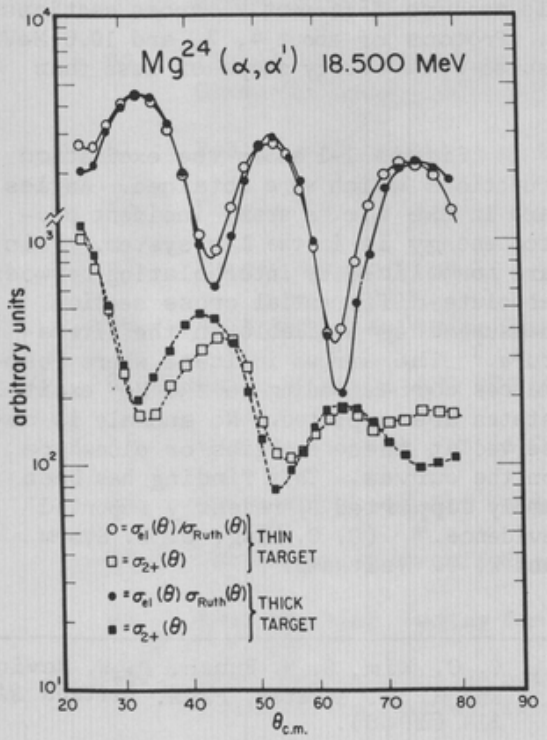

Fig. 2-1. Angular distributions of elastic and 2^+ first excited state for thin and thick targets for $Mg^{24}(\alpha,\alpha')$ at 18.5 MeV.

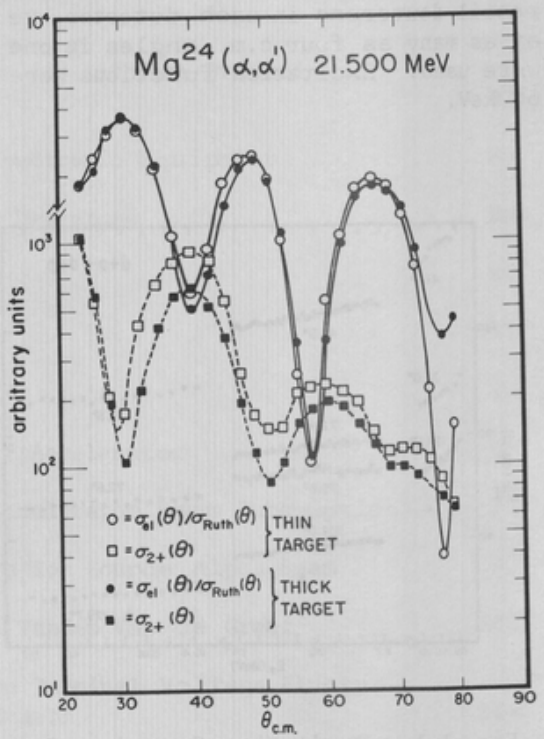

Fig. 2-2. Angular distributions of elastic and 2^+ first excited state for thin and thick targets for $Mg^{24}(\alpha,\alpha')$ at 21.5 MeV.

For these more recent investigations of phase correlation, a thinner Mg^{24} target (0.13 mg/cm^2) was used, in contrast to the earlier work with a thick (1.8 mg/cm^2) target. The thick target would average out compound nuclear Ericson-type energy variations that a thinner target would show. Figures 2-1 and 2-2 show

two sets of distributions (thin and thick targets) for 18.5 and 21.5 MeV. For 18.5 MeV one can see the differences in the inelastic angular distribution between the two targets. These differences are reduced at 21.5 MeV.

The phase correlation coefficient was calculated for the elastic and inelastic 2^+ pair of distributions at each energy for the thin and thick targets. Figure 2-3 shows the value of P as a function of α particle bombarding energy. Its large fluctuations, especially for the thin target at lower energies, is of interest. For comparison with experiment, distorted wave calculations (based upon optical model fits to the thick target data) were made at several energies to provide an estimate of the expected phase correlation coefficient predicted by a direct reaction model. Statistical compound-nucleus predictions were similarly obtained from a Hauser-Feshbach calculation, which gives a prediction of inelastic angular distributions averaged over a large energy interval. P corresponding to the predictions of these models are shown in Fig. 2-4, along with additional data of Eidson,[2] McDaniels,[3] and Hendrie,[4] which were used to provide indications of the phase relation at lower and higher energies.

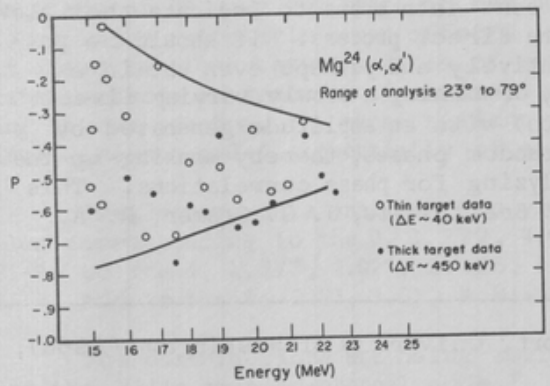

Fig. 2-3. Phase correlation coefficient P versus alpha particle bombarding energy for the $Mg^{24}(\alpha,\alpha')$ reaction. The values are calculated for the thin target (0.13 mg/cm^2) and thick target (1.8 mg/cm^2) data.

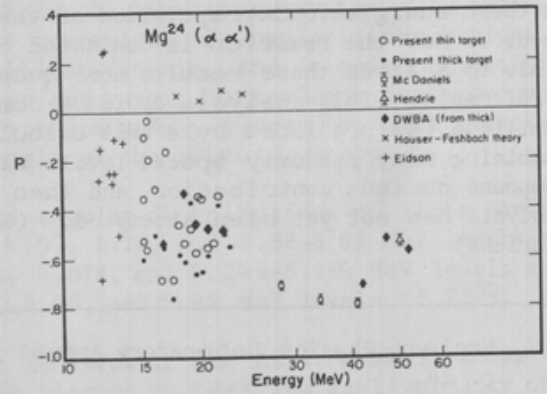

Fig. 2-4. Phase correlation coefficient P versus alpha particle bombarding energy for the $Mg^{24}(\alpha,\alpha')$ reaction. The data of Fig. 2-3 are shown along with other data at higher and lower bombarding energies.

Besides choosing a suitable index for the phase relationship, there are several problems that arise in its use. One of these is the selection of the angular range over which to calculate P; another is the dependence of P upon the step size $\Delta\theta$ taken. We used an angular range between 20° and 75°. It was found that the phase rule holds fairly consistently in this region, and that small changes in the end points of this range were followed by only small changes in the values of P. The step size used was that of the experiment, $\Delta\theta=2°$. By using Lagrange interpolation, we could vary the size of $\Delta\theta$ used, but found no change in the form of P as a function of energy.

Figures 2-3 and 2-4 show the energy dependence of the phase correlation coefficient P. The points are seen to be widely distributed and show rapid energy variations. The important features of this behavior are the dispersion of the points and the average value of the points. Inspection of the curve shows that the dispersion is progressively reduced as the bombarding energy is increased, while the average value of the data remains fairly constant and is fairly consistent with the theoretical distorted wave predictions. These results we can interpret as follows: in this region of excitation in the $Mg^{24}+\alpha$ system, there is strong competition in the inelastic 2^+ channel between direct inelastic scattering and the alpha decay of the Si^{28} compound nucleus, the latter producing Ericson-type fluctuations with a coherence width which is estimated to be about 100 keV. While the phase relation of the direct component of the cross section is fairly strong, the fluctuating compound-nucleus contribution has no consistent phase relation, and drives the value of P to more positive or more negative values at random. One would thus expect the average value to be zero, which is seen in the Hauser-Feshbach calculations shown in Fig. 2-4. Thus the average value of P will reflect the contribution of the direct reaction component, while the dispersion of the data points about this central value will reflect the contribution of the fluctuating compound nucleus component. The reduced dispersion of P at higher energies is thus taken as an indication that the direct component is "winning" at these energies. Extrapolation of the present data seems to indicate that above about 25 MeV the reaction is dominated by the direct process. It should be possible to analyze these results more quantitatively and perhaps even obtain a CN/DI ratio. This analysis could be done by combining a slowly varying direct amplitude (as predicted by a DWBA calculation) with an amplitude generated by combining many randomly spaced levels with random phases, thereby mocking-up the compound nucleus contribution, and then analyzing for phase correlations. This analysis has not yet been attempted. (W. J. Braithwaite, J. G. Cramer, R. A. Hinrichs)

---

1. Nuclear Physics Laboratory Annual Report, University of Washington (1966), p. 14.
2. W. W. Eidson, Indiana University, private communication.
3. D. McDaniels, Ph.D. Thesis, University of Washington (1960).
4. D. Hendrie, University of California, Berkeley, private communication.

---

3. Inelastic Alpha Scattering on Silicon Isotopes

A study of elastic and inelastic scattering of 42 MeV alpha particles from the three naturally occurring isotopes of silicon has been initiated for two reasons: to investigate the nature of the inelastic process itself with regard to recent theoretical descriptions of this process,[1,2] and to obtain nuclear structure information about the character of the energy levels excited by the scattering. A similar measurement[3] carried out on the Al^{27} and Si^{28} nuclear systems has shown, for example, that the inelastic scattering cross sections of Al^{27} may be interpreted within the framework of an excited core-hole model. Further interest is attached to the silicon nuclei because of the suggestion by Bromley *et al.*[4] that the collective deformations of sd-shell nuclei are changing

sign (from prolate to oblate) in this immediate mass region.

Because of the substantial isotopic contamination encountered in a preliminary experiment[5] on Si^{28} where a natural silicon target was used, an effort was made to obtain for the present measurement nearly pure mono-isotopic targets. The isotopic purities were 99.8% for Si^{28}, 95.3% for Si^{29}, and 95.6% for Si^{30}. Each target was evaporated on a 50 $\mu g/cm^2$ carbon backing with overall target thicknesses corresponding to between 60 and 100 keV energy loss for the incident alpha beam. The energy resolution (FWHM) of the alpha peaks of interest was typically 130 keV. Four lithium-drifted silicon detectors, fabricated in this laboratory, were spaced at 2° separations and employed simultaneously in detecting the scattered particles. The linear signals from each counter were fed through four separate preamplifier-amplifier systems; the signals in the energy regions of interest were then selected with four biased amplifiers and presented to the SDS-930 computer for pulse-height analysis and storage into a separate 512-channel data array for each detector. Dead time corrections were made for each ADC individually by recording both the number of pulses presented to, and the number of pulses analyzed by, each ADC. These corrections were typically less than 2% except at the forward-most angles where the largest correction was 12%. Measurements were taken in steps of 1° over the angular range of 10° to 62° and in steps of 2° over the range of 62° to 85° in the laboratory system. In order to minimize systematic error effects in the comparison of angular distributions of cross sections between states of each silicon isotope, and in order to facilitate accurate subtraction of unwanted oxygen and carbon contaminant peaks appearing in the spectra, the three silicon targets and a MoO_3 target (on carbon backing) were bombarded sequentially at each angle of the detector array.

Preliminary data analysis has yielded angular distributions of alpha particles corresponding to the 0, 1.772, 4.61, 4.97, 6.27, and 6.88-6.89 MeV levels of Si^{28}; to the 0, 1.277, 2.027, 2.425, 3.621, 4.078, and 5.249-5.279 MeV levels of Si^{29}; and to the 0, 2.23, 3.51, 4.81-4.83, 5.48, and 5.95 MeV levels of Si^{30}.

The distributions are being analyzed in terms of the Austern-Blair model[1] and the Wills coupled-channel code.[6] It is planned to test the applicability of both the strong-coupling and the weak-coupling approximations of the collective model in predicting the relative cross sections of excitation. It is hoped that this will provide some insight as to the possible collective character of the individual nuclear states involved. (J. Allen, W. Braithwaite, J. G. Cramer, and E. Preikschat)

---

1. N. Austern and J. S. Blair, Ann. Phys. *33*, 15 (1965).
2. T. Tamura, Rev. of Mod. Phys. *37*, 679 (1965).
3. J. Kokame, K. Fukanaga, H. Nakamura, Phys. Letters *14*, 234 (1965).
4. D. A. Bromley, H. E. Gove, and A. E. Litherland, Can. J. Phys. *35*, 1057 (1957).
5. Nuclear Physics Laboratory Annual Report, University of Washington (1965), p. 7.
6. J. G. Wills, Ph.D. Thesis, University of Washington, 1965.

---

4. Elastic Scattering of Alpha Particles from Calcium Isotopes and the Isotopic Dependence of Nuclear Radii

A brief account was given in the 1966 Annual Report[1] of an analysis of the cross sections as measured for the elastic scattering of 42 MeV alpha particles by nuclei ranging from K^{39} to Fe^{54}. This analysis had been motivated in part by careful measurements of electron scattering[2] and mu-mesic x-ray spectra[3] which revealed some surprising differences in the electric charge distributions of the Ca isotopes. It is well known that angular distributions for elastic scattering of alpha particles show a sharp diffraction structure and that the locations of the minima in the cross sections are particularly sensitive to the value for the strong absorption radius characterizing the scattering amplitudes. Unfortunately the experiments analyzed last year[4] had not been explicitly designed to point up the anticipated small differences between neighboring isotopes; the available data points in regions of sharp minima were neither plentiful enough nor of high enough accuracy to determine the locations of minima to better than ±0.5°. Consequently, although the analysis suggested that the strong absorption radii of the Ca isotopes were not increasing as rapidly with A as one might expect, not a great deal of confidence could be attached to that conclusion.

Accordingly, a new series of measurements of the cross sections for elastic scattering from Ca isotopes have been carried out in which special attention has been given to the accuracy of the angular distributions and to the locations of the minima which occur in the neighborhood of 35° (c.m.) and 24° (c.m.). To minimize the angular spread and the variation of the mean scattering angle with time, the beam was defined by two 1/32 in. collimators, separated by 20 in.; the target was located 8 in. from the second collimator, and the detector was set 20 in. from the target, with a 1/32 in. aperture in front of it. With this geometry the over-all angular spread was of the order of 0.2 deg.

Elastic angular distributions have been measured for the four isotopes $Ca^{40,42,44,48}$, in steps of 1° or 2° from 15° to 45° (lab); in the minima near 24° and 35° (c.m.), the angular distributions have been measured in steps of 0.2°. The observed cross sections near 35° are shown in Fig. 4-1. We here determined that the minima for $Ca^{40,42,44,48}$ occur at 35.05°, 34.63°, 34.19°, and 33.81°, respectively. It is estimated that there is a possible error of ±0.05° for the differences in minimum angles and a further over-all error of ±0.05° in the absolute values of the minimum angles.

The cross sections have been analyzed in terms of three models: (i) The Fraunhofer model, (ii) a parameterized phase shift model where we have used the parameterization of Springer and Harvey,[5] (iii) a four-parameter optical model.

(i) Of these, the Fraunhofer model[6] contains the least ambiguity since the minima in the angular distributions may be directly related to the strong absorption radius. The accurately measured minima near 35° have been used to determine values for the Coulomb corrected Fraunhofer radii, R_{FC}, and these are plotted versus $A^{1/3}$ in Fig. 4-2.

(ii) The five parameters of the parameterized phase shift model have been determined by searching for the best least squares fit of the measured angular

distributions over the angular range 15° to 45°. Rather than relating the cutoff angular momentum parameter, L, directly to a radius, we have defined two strong absorption radii, $R_{pl/2}$ and $\mathcal{R}_{pl/2}$, which correspond to the angular momenta, $\ell_{pl/2}$, at which $Re(\eta_{\ell pl/2}) \equiv 1/2$, and $\mathcal{L}_{pl/2}$, at which $T_{\mathcal{L}pl/2} \equiv 1-|\eta_{\mathcal{L}pl/2}|^2 \equiv 1/2$, respectively. Here η_ℓ is the outgoing amplitude of the ℓ^{th} partial wave. Again these radii are shown in Fig. 4-2.

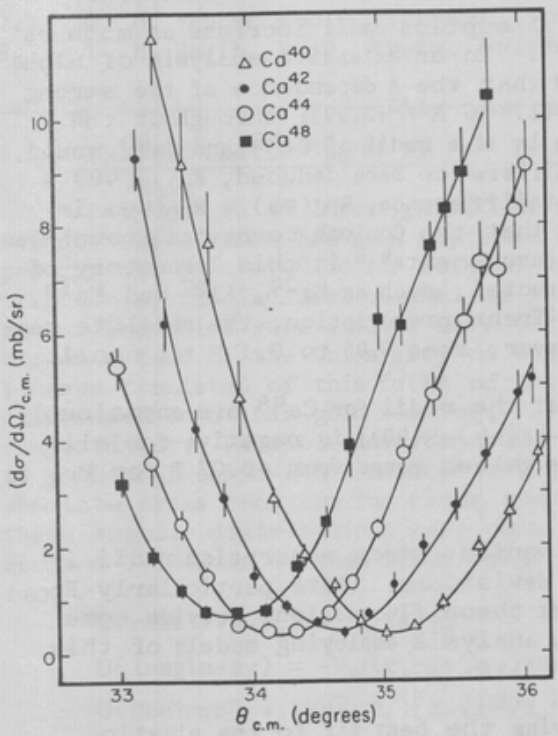

Fig. 4-1. Cross sections in the vicinity of 35° for the elastic scattering of 42 MeV α particles from the calcium isotopes.

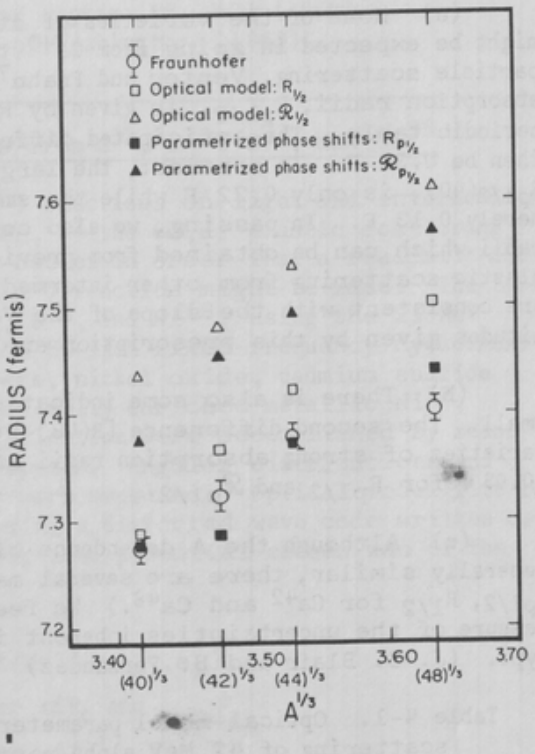

Fig. 4-2. Radii derived for the calcium isotopes.

(iii) An optical model potential has been assumed which has the same Woods-Saxon form factor for both the real and imaginary parts. The four parameters of the model are thus the depths of the real and imaginary potential, V and W, the radius, R_{opt}, and the diffuseness, a. "Best fit" parameters were determined by a least squares search, in which all four parameters were allowed to vary. In this search, the initial value of real depth, V, was chosen to be 200 MeV. The "best fit" parameters are listed in Table 4-1. We note that only the imaginary depth, W, and the radius, R_{opt}, vary appreciably from one isotope to another.

Because of the well known ambiguities in the optical model parameters in situations of strong absorption, we have not attached too much importance to the deduced values of R_{opt}. Rather, we feel that it is more significant to examine the partial wave amplitudes which emerge from this analysis and to define in terms of these amplitudes strong absorption radii which are completely analogous to those of the paramterized phase shift model. The resulting radii, $R_{1/2}$ and $\mathcal{R}_{1/2}$, are also displayed in Fig. 4-2. It is worth noting that the differences in R_{opt} are only slightly less than those in $\mathcal{R}_{1/2}$.

Inspection of Fig. 4-2 leads to the following conclusions:

(a) None of the varieties of strong absorption radii increase as much as might be expected in going from Ca^{40} to Ca^{48}. In an extensive analysis of alpha particle scattering, Venter and Frahn[7] find that the A dependence of the strong absorption radii, $R_{pl/2}$, is given by $R_{pl/2}=(1.446\ A^{1/3}+2.29)F$ throughout the periodic table. The anticipated difference in the radii of Ca^{48} and Ca^{40} would then be 0.31 F. In contrast, the largest difference here deduced, $R_{pl/2}(48) - R_{pl/2}(40)$, is only 0.22 F while the smallest difference, $R_{FC}(48) - R_{FC}(40)$ is merely 0.13 F. In passing, we also comment that the Coulomb corrected Fraunhofer radii which can be obtained from previous measurements[4,8] in this laboratory of elastic scattering from other intermediate nuclei, such as Mg^{24}, Al^{27} and Fe^{54}, are consistent with the slope of the Vanter-Frahn prescription; the absolute magnitudes given by this prescription are, however, some 0.05 to 0.1 F too small.

(b) There is also some indication that the radii for Ca^{48} are anomalously small. The second difference [R(48)-R(44)]-[R(44)-R(40)] is negative for all varieties of strong absorption radii and the values range from -0.07 F for R_{FC} to -0.03 F for $R_{pl/2}$ and $\mathcal{R}_{pl/2}$.

(c) Although the A dependence of the various strong absorption radii is generally similar, there are several marked deviations. (Note particularly R_{FC}, $R_{pl/2}$, $R_{1/2}$ for Ca^{42} and Ca^{48}.) We feel that these fluctuations provide some measure of the uncertainties inherent in any analysis employing models of this type. (J. S. Blair and B. Fernandez)

Table 4-1. Optical model parameters giving the best fit to the elastic scattering of 42 MeV alpha particles from the calcium isotopes.

A =	40	42	44	48
V	200.525	204.460	199.175	200.489
W	20.657	27.007	25.808	28.177
r_0	1.425	1.413	1.4045	1.3805
R_{opt}	4.872	4.910	4.957	5.015
a	.562	.559	.564	.562

1. Nuclear Physics Laboratory Annual Report, University of Washington (1966), p. 10.
2. Hofstadter, Nödelke, Van Oostrom, Suelze, Yearian, Clark, Herman, and Ravenhall, Phys. Rev. Letters *15*, 758 (1965).
3. Bjorkland, Raboy, Trail, Ehrlich, and Powers, Phys. Rev. *136*, B341 (1964).
4. R. J. Peterson, Ph.D. Thesis, University of Washington (1966).
5. A. Springer and B. G. Harvey, Phys. Letters *14*, (1965) 116.
6. See for example, J. S. Blair, Lectures in Theoretical Physics, Vol. VIII-C, University of Colorado Press (1966), p. 343.
7. R. H. Venter and W. E. Frahn, Annals of Physics *27*, 401 (1964).
8. I. M. Naqib, Ph.D. Thesis, University of Washington (1962).

5. Elastic Scattering of 21 MeV Deuterons from C^{12}, O^{16}, S^{32}, and Ni^{58}

Persuant to an investigation of (d,Li^6) reactions on light and intermediate weight nuclei which has been reported earlier,[1,2] the (d,d) elastic scattering process has been studied for several target nuclei in order that a realistic description of the incident channel of the (d,Li^6) reaction might be made. The target nuclei which were studied were C^{12}, O^{16}, S^{32}, and Ni^{58}, using the 21 MeV deuteron beam of the University of Washington 60-inch fixed-frequency cyclotron. Targets consisted of thin foils of polystyrene, nickel oxide, cadmium sulfide evaporated on a thin gold backing, and isotopically enriched metallic Ni^{58}, respectively. Particle detection and identification were accomplished by means of a dE/dx-E solid-state counter telescope system. Angular distributions and absolute cross sections for these reactions were measured. Optical model fits to these angular distributions were obtained using a distorted wave code written by Bernard Fernandez of this laboratory. The optical potential chosen was of the form

$$U(\text{real}) = -V_s f(r,r_{os},a_s),$$

$$U(\text{imaginary}) = -W_s f(r,r_{oI},a_I)+4a_I W_D(d/dr)f(r,r_{oI},a_I),$$

$$U(\text{Coulomb}) = (Ze^2/2R_c)[3-(r^2/R_c^2)] \text{ for } r \leq R_c \text{ and}$$

$$= Ze^2/r \text{ for } r > R_c, \text{ where } R_c = r_{oS}A^{1/3},$$

and $f(r,r_o,a)=\{1+\exp[(r-r_oA^{1/3})/a]\}^{-1}$.

The well parameters obtained in fitting the (d,d) elastic scattering angular distribution from the Ni^{58} target are in excellent agreement with those reported by Perey and Perey[3] for this deuteron energy, and serve as a significant check on the validity of the remainder of the present scattering data. In lieu of presenting these angular distributions here, the results of the optical model search for each of these reactions are summarized in Table 5-1. (J. B. Gerhart, P. F. Mizera, and F. W. Slee)

Table 5-1. Well Parameters for 21 MeV Elastically Scattered Deuterons

Target	V_s (MeV)	W_s (MeV)	W_D (MeV)	R_{os} (F)	a_s (F)	r_{oI} (F)	a_I (F)
C^{12}	59.1239	0.0	10.7548	1.4286	0.6461	1.0671	0.8263
O^{16}	59.0374	0.0	6.6706	1.5230	0.6737	1.4973	0.6114
S^{32}	60.3882	0.0	9.0541	1.1196	0.5894	1.1092	0.8459
Ni^{58}	56.3001	0.0	14.3702	1.0996	0.9223	1.3835	0.6816

1. Nuclear Physics Laboratory Annual Report, University of Washington (1965), p. 28.
2. *ibid.* (1966), p. 36.
3. C. M. Perey and F. G. Perey, Phys. Rev. *132*, 755 (1963).

6. Elastic and Inelastic Scattering of Alpha Particles from Rb^{87}

A study of the elastic and inelastic scattering of 42 MeV alpha particles from Rb^{87} has been started. The prime motivation for this experiment is the lack of information about the states of Rb^{87}. Excited states have been reported at 0.403, 0.843, and 2.97 MeV,[1] and of these only the 0.403 MeV state has a spin and parity assignment $(5/2^-)$.[1,2] The ground state has a spin and parity of $3/2^-$. The goal of the present experiment was to look for additional low-lying states and to measure the corresponding angular distributions of the scattered α particles. These angular distributions could then be used to establish parities, angular momentum transfers, and transition rates for these states.[3] It was also hoped that a comparison of the angular distributions for the excitation of these states with those for the excitation of the states of Sr^{88} would be useful.

Preliminary data were taken using a 200 μg/cm^2 Rb_2SO_4 target, isotopically enriched to 99% Rb^{87}, evaporated on a 50 μg/cm^2 carbon backing. This target proved to be somewhat less than ideal because of the many contaminants present. The data taken with this target seem to indicate that states, other than those listed above, are located at approximately 1.35, 1.70, 1.95, 2.28, 2.42, and 2.70 MeV. The uncertainty in energy for each of these states is estimated to be approximately ±50 keV. Partial angular distributions were obtained for the excitation of the states listed above and are shown in Figs. 6-1 and 6-2. The dashed curves are the results of an Austern-Blair[4] adiabatic approximation for 42 MeV alpha particles scattered from Sr^{88}.[5] The angular distributions for the 0.403, 1.35, 1.70, 1.95, and 2.28 MeV states (Fig. 6-1) seem to be out of phase with the elastic angular distribution which, according to the Blair phase rule,[3] would indicate that the parities of all these states are negative (i.e., the same as the ground state). The angular distributions for the excitation of the 2.42, 2.70, and 2.97 MeV states seem to be in phase with the elastic angular

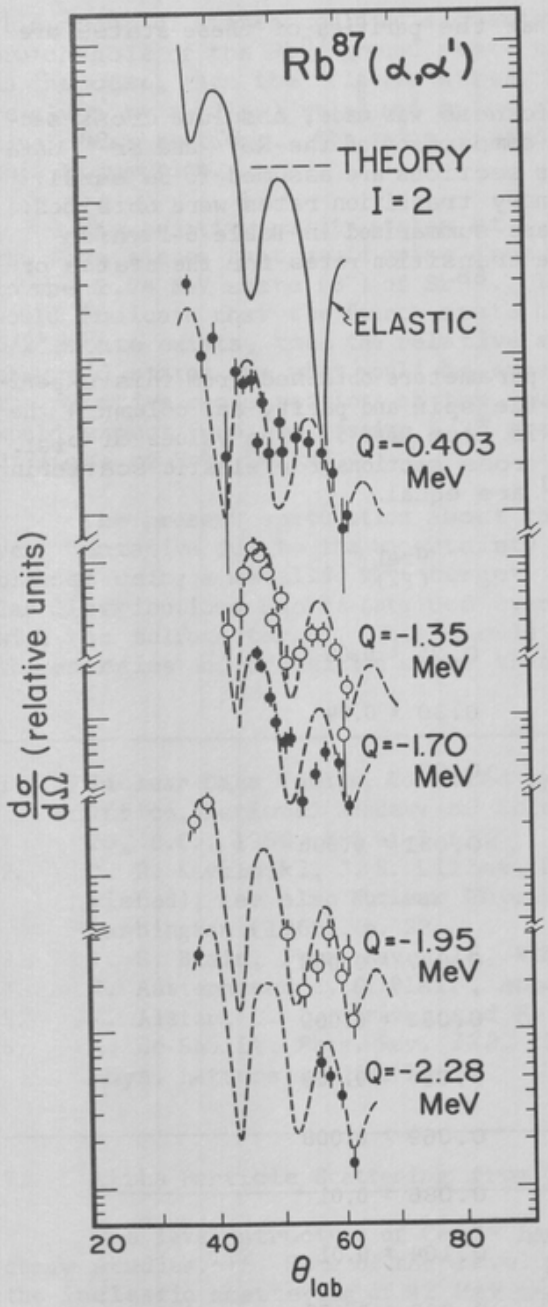

Fig. 6-1. Angular distributions for 42 MeV alpha particles exciting the 0.403, 1.35, 1.70, 1.95, and 2.28 MeV states of Rb^{87}. The curves are Austern-Blair model adiabatic approximations for an I=2 transition calculated for 42 MeV alpha particles incident on Sr^{88} (see ref. 5). The elastic cross section is shown for comparison.

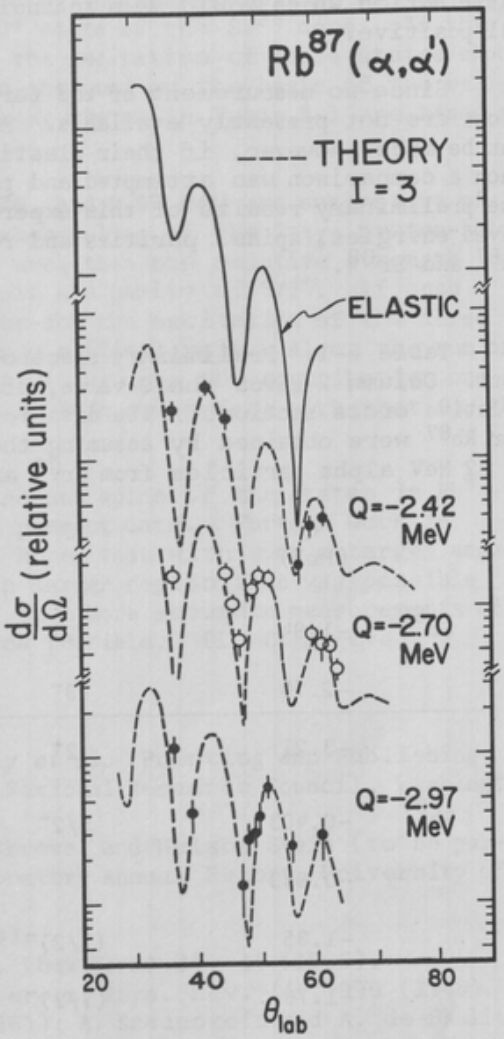

Fig. 6-2. Angular distributions for 42 MeV alpha particles exciting the 2.42, 2.70 and 2.97 MeV states of Rb^{87}. The curves are Austern-Blair adiabatic approximations for an I=3 transition calculated for 42 MeV alpha particles incident on Sr^{88} (see ref. 5). The elastic cross section is shown for comparison.

distribution which would seem to indicate that the parities of these states are all positive.

Since no measurement of the target thickness was made, absolute cross sections are not presently available. A rough comparison of the Rb^{87} and Sr^{88} data can be made, however, if their elastic cross sections are assumed to be equal. Such a comparison was attempted and preliminary transition rates were obtained. The preliminary results of this experiment are summarized in Table 6-1 which gives energies, spins, parities and relative transition rates for the states of Rb^{87} and Sr^{88}.

Table 6-1. Preliminary spectroscopic parameters obtained from this experiment. Column 2 gives the Q-value, column 3 the spin and parity and column 4 the relative cross sections. The data for Sr^{88} is from Ref. 5. The values of $\sigma_{rel.}$ for Rb^{87} were obtained by assuming that the cross sections for elastic scattering of 42 MeV alpha particles from Sr^{88} and Rb^{87} are equal.

	Q (MeV)	J^π	σ_{rel} (F^2)
Sr^{88}	-1.84	2^+	0.25 ± 0.03
	-2.74	3^-	0.30 ± 0.04
	-3.21	2^+	∿0.02
Rb^{87}	-0.403	$5/2^-$	0.031 ± 0.006
	-0.843		
	-1.35	$(1/2)^-$	0.047 ± 0.008
	-1.70	$(7/2)^-$	0.083 ± 0.009
	-1.95	$(3/2)^-$	0.055 ± 0.009
	-2.25	$(5/2)^-$	0.069 ± 0.008
	-2.42	$(7/2)^+$	0.086 ± 0.01
	-2.70	$(9/2)^+$	0.104 ± 0.01
	-2.97	$(3/2)^+$	0.036 ± 0.008

These preliminary results suggest several things. First, they suggest that the experiment should be redone with a different Rb^{87} target. Second, the summed strengths for the negative parity 1.35, 1.70, 1.95, and 2.28 MeV states of Rb^{87} are very nearly equal to that for the 1.84 MeV (2^+) state of Sr^{88}.[5] Also, the average energy of this group of states is 1.82 MeV. These results suggest that

this group of states could be a quartet formed by the weak-coupling[6] of the $2p_{3/2}$ proton-hole of the Rb^{87} ground state to the 2^+ state of the Sr^{88} core. If this is the case, then the relative strengths for the excitation of these states should be given by a (2j+1) rule[5] and spins might be assigned on the basis of the relative cross sections. The spins listed for these states in Table 6-1 are based on this assumption.

The positive parity states at 2.42, 2.70, and 2.97 MeV are suggestive of the four states that could arise from the weak-coupling of the $2p_{3/2}$ proton-hole to the 2.74 MeV state (3^-) of Sr^{88}. If they are, then the relative strength would indicate that the fourth state has a spin and parity of $5/2^+$. If such a $5/2^+$ state exists, then the relative strengths for the excitation of the three observed states are what would be expected from a (2j+1) rule. Also, the sum of the relative cross sections of the four states (including the contribution one would expect from the missing $5/2^+$ state) is 0.28 in comparison with that for the 3^- state of Sr^{88} (0.30).

The present speculation about the nature and spins of the states in Rb^{87} is very tentative due to the uncertainty in the present data. Further work is planned using a metallic Rb^{87} target. It is hoped that with such a target angular distributions can be obtained over a much larger region than was possible with the sulfate target. This should permit much more accurate measurements of the energies and transition rates than are now possible. (D. C. Shreve)

---

1. Nuclear Data Tables, Compiled by K. Way *et al.* (Printing and Publishing Office, National Academy of Sciences, National Research Council, Washington 25, D.C., 1960) NRC 61-3-51.
2. C. D. Kavaloski, J. S. Lilley, D. C. Shreve, and Nelson Stein (to be published); see also Nuclear Physics Laboratory Annual Report, University of Washington (1966), p. 22.
3. J. S. Blair, Phys. Rev. *115*, 928 (1959).
4. N. Austern and J. S. Blair, Ann. Phys. (New York) *33*, 15 (1965).
5. J. Alster, D. C. Shreve, and R. J. Peterson, Phys. Rev. *144*, 999 (1966).
6. A. de-Shalit, Phys. Rev. *122*, 1530 (1961); A. Braunstein and A. de-Shalit, Phys. Letters 1, 264 (1962).

---

7. Alpha Particle Scattering from Ce^{140}

The level structure of Ce^{140} has been known so far only from β and γ decay studies.[1,2] Some of the level properties have been investigated through the inelastic scattering of 42 MeV α-particles from a target of natural Ce (88.48% Ce^{140}). This nucleus is of special interest since it has a closed neutron shell and a large gap in energy between the ground and first excited states.

Angular distributions have been obtained for the elastic scattering (Fig. 7-1) and for some inelastic peaks (Fig. 7-2), using solid state detectors, with an overall resolution of about 110 keV. The elastic angular distribution has been analyzed in terms of a four-parameter optical model. It is assumed that

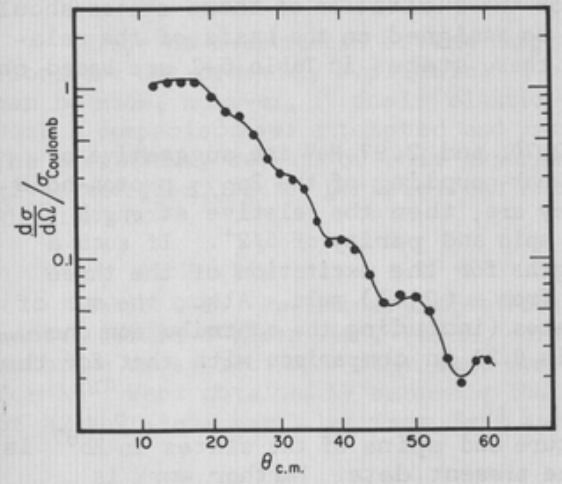

Fig. 7-1. Angular distribution of 42 MeV α particles elastically scattered from Ce^{140}.

the same Woods-Saxon form factor applies to both the real and imaginary parts. The four parameters are then the depths of the real and imaginary potential, V and W, the radius, R_{opt}, and the diffuseness, a. Four sets of parameters have been found which give equally good fits to the data; these are listed in Table 7-1.

The inelastic angular distributions have been analyzed by means of the Austern-Blair model,[3] where in addition to the adiabatic approximation, the radial integral

$$\int \chi_{\ell'} \frac{\partial V}{\partial R}_{opt} \chi_{\ell} \, dr$$

is approximated by

$$\frac{iE}{2k} \cdot \frac{\partial \eta_{\bar{\ell}}}{\partial R}_{opt}$$

where

$$\bar{\ell} = \frac{\ell+\ell'}{2} \quad .$$

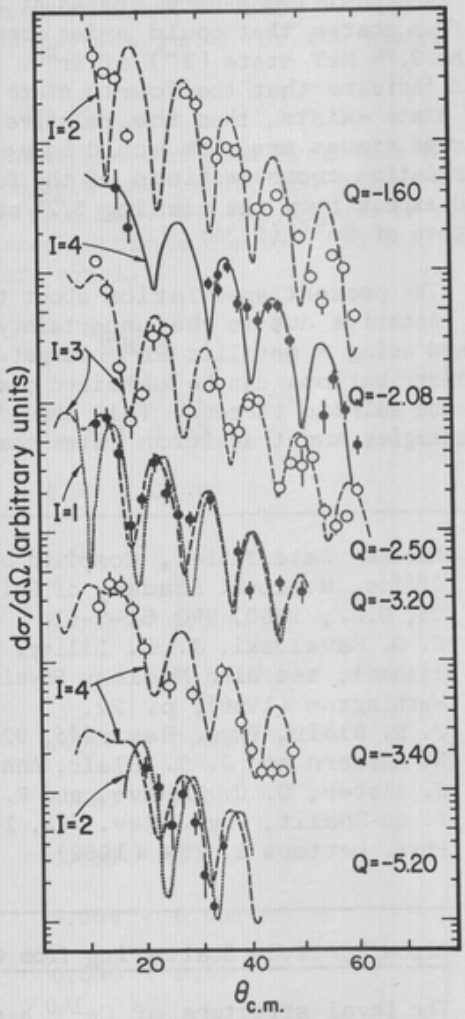

Fig. 7-2. Angular distributions of 42 MeV α particles inelastically scattered from Ce^{140}. The curves are Austern-Blair calculations.

The derivatives

$$\frac{\partial \eta_\ell}{\partial R_\ell}$$

have been obtained from the optical model (Table 7-2). This is the first time that this variation of the Austern-Blair model has been used to analyze experimental data; hitherto, the partial wave amplitudes and their derivatives have been obtained from a parameterized phase shift model.

Table 7-1. Optical model parameters for $Ce^{140}(\alpha,\alpha)$ giving nearly nearly equivalent fits to the observed cross sections

V(MeV)	W(MeV	r_o(F)	R_{opt}(F)	a(F)
- 60.634	-18.024	1.483	7.701	.582
- 70.018	-15.664	1.479	7.680	.571
-151.019	-19.155	1.404	7.291	.555
-253.144	-32.596	1.350	7.01	.555

Table 7-2. Observed excited levels of Ce^{140} in α particle inelastic scattering and corresponding spin-parity assignments and values for deformation distance, δ_I.

Q(MeV)	I^π	$\delta_I(=\beta_I R)$(F)
-1.60[a]	2^+	.66
-2.08[a]	4^+	.29
-2.50[a]	3^-	.67
-3.20	$(1^-,3^-)$	.29
-3.40	(4^+)	.31
-5.20	$(2^+,4^+)$	.23

[a] Spin-parity assignments are known from previous work. See ref. 7-1.

The spin-parity assignments for the first three levels are already known.[1,2] In Fig. 7-2, the angular distributions to these three levels are compared to the predictions of the Austern-Blair model for single excitation. Although the observed angular distribution to the lowest 2^+ level conforms to the predicted

phase relations beyond 30°, there appear to be some significant differences between theory and experiment at small angles; it is quite likely that these can be attributed to the neglect of Coulomb excitation in our calculations. Unfortunately, the spectra for angles between 18° and 28° are obscured by contaminant peaks.

Much of the weak cross section for excitation of the first 4^+ level is similarly obscured between 18° and 32°. It is significant that the pattern beyond 30° is consistent with that predicted for single excitation, rather than double excitation, of the 4^+ state. This suggests that the Q = -2.08 MeV level is more appropriately described as a 2-quasi-particle state than as a 2-quadrupole-phonon or rotational excitation, a conclusion which is not surprising in view of the fact that the 82 neutrons in Ce^{140} form a closed shell. The angular distribution for excitation of the group with Q = -2.50 MeV displays a good octupole pattern out to an angle of 55°.

Concerning the three angular distributons to levels at higher excitation, a strong statement can be made only for that corresponding to Q = -3.20 MeV. Here the angular distribution at angles less than 35° definitely favors a 3^- assignment but a 1^- assignment cannot be excluded. Parts of the Q = -3.40 MeV angular distribution suggest a 4^+ assignment but there are some clear points of discrepancy. The sparse angular distribution for the group at Q = -5.20 MeV suggests either a 2^+ or 4^+ assignment; the data clearly contradict a 1^- or 3^- assignment. None of these three angular distributions gives any hint of a possible double excitation contribution.

Preliminary values of the deformation distances[3] corresponding to these transitions are given in Table 7-2. (B. Fernandez)

---

1. H. W. Baer, J. J. Reidy, and M. L. Wiedenbeck, Nucl. Phys. *86*,332 (1966). This article contains references to earlier studies of Ce^{140}.
2. The 2^+ state at 1.596 MeV excitation and the 3^- state at 2.47 MeV excitation have been observed in Coulomb excitation: O. Nathan and V. I. Popov, Nucl. Phys. *2*, 631 (1960); O. Hansen and O. Nathan, Nucl. Phys. *42*, 197 (1963).
3. N. Austern and J. S. Blair, Annals of Physics *33*, 15 (1965).

---

8. Inelastic Alpha Particle Scattering to Highly Excited States in Heavy Nuclei

In earlier progress reports[1,2] we have reported measurements of α-particle spectra observed from Sn and heavier elements bombarded with 42 MeV α particles. From the shapes of these spectra and their strong forwardness, it is clear that the observed α particles come from a direct interaction. To help determine the nature of the interaction responsible for the inelastic scattering it was decided to make some measurements at smaller angles to the beam than the most forward angle (40°) that had been studied so far. The reasons for going forward stem from the observation that at 40°, $d\sigma/d\Omega$ is still increasing rapidly as θ decreases. It is of interest to know if $d\sigma/d\Omega$ folds over at forward angles, and it is also

of interest to obtain enough values of $d\sigma/d\Omega$ where it is large to permit an integration over angle to obtain a total cross-section.

The reasons that forward angle measurements had not been carried out earlier were largely technical.[1] The background due to target impurities (carbon, oxygen) increase more rapidly than the signal does as one goes forward.[2] The elastic cross-section increases faster than the inelastic cross-section as one goes forward and there may be a significant contribution of apparent inelastic α particles from the low energy tail on the elastic line produced in the counter system. The lowest energy α particles seen have an energy in the neighborhood of the Coulomb barrier. Their cross-section is found to increase rather slowly with decreasing angle. Consequently any particles of this energy which may be present in the incident beam would become increasingly troublesome at forward angles because they would be scattered into the detector elastically, i.e., with Rutherford cross-sections. In short, a relatively small amount of degraded beam accompanying the main beam could give spurious contributions to the spectrum at forward angles.

To minimize the role of target impurities, presumably mainly surface impurities, the thickness of typical targets was increased to 1 to 2 mg/cm^2. In addition, a special effort was made to prepare particularly clean targets. To reduce the possible effects of a tail on the elastic line in the detector system, a small magnet[3] was used to disperse the scattered beam and separate away the elastic line. The properties of the magnet were studied at backward angles by comparing "magnet-on" and "magnet-off" observations taken with a broad α particle spectrum. To reduce the amount of degraded beam present in the incident beam the beam spot on the target was defined by the duct slits before the analyzing magnet. Between these slits and the target there was only a very large diameter clean-up aperture.

Preliminary results indicate that (1) the inelastic cross-section from heavy elements is continuing to increase as one goes from 40° to 25° and that (2) it will not be possible to make measurements at angles less than 25° unless the amounts of oxygen and carbon in the targets can be even further reduced.

In addition to the work done at 42 MeV at our cyclotron, one run was performed at the Berkeley 88" cyclotron in collaboration with Drs. B. G. Harvey, D. Hendrie and N. Mangelson. The main object of this run was to see whether the probability for very high excitations in (α,α') reactions persist at higher bombarding energies. For example, does one still see scattered α particles with Coulomb Barrier energies ($\sim$20 MeV) when the incident α particle energy is raised above 42 MeV? The energies of the Berkeley bombardments were 42, 50, 65 and 90 MeV. Broad spectra of inelastic α particles were observed at all energies. They are in the process of being analyzed. (G. Chenevert and I. Halpern)

---

1. Cyclotron Research, University of Washington (1964), p. 13.
2. Nuclear Physics Laboratory Annual Report, University of Washington (1966), p. 6.
3. Cyclotron Research, University of Washington (1964), p. 51.

9. Proton Scattering from Isobaric Analog States in the Lead Region

The study[1] of isobaric analogs of the low-lying states of Pb^{207} by proton elastic and inelastic scattering on Pb^{206} has been extended, and new results have been obtained. The improvements in the previous data consist of obtaining purer targets of Pb and obtaining better resolution in the particle spectrum. As a result we were able to resolve some of the weaker inelastic proton groups which were not previously observed. In addition, angular distributions were taken on the previously reported resonances as well as those more recently observed.

Excitation functions in the region of the first three analog states (E_p=11.5-14.5 MeV) were measured at 105°, 125°, 145° and 165°. In addition to the previously reported resonances at the ground state analog (E_p=12.23 MeV) for the g.s. (0^+), 0.804 (2^+), 1.47 (2^+) and the 1.71 MeV (1^+) states of Pb^{206}, new resonances were observed there for the 1.15 (0^+) and the 1.34 MeV (3^+) states.

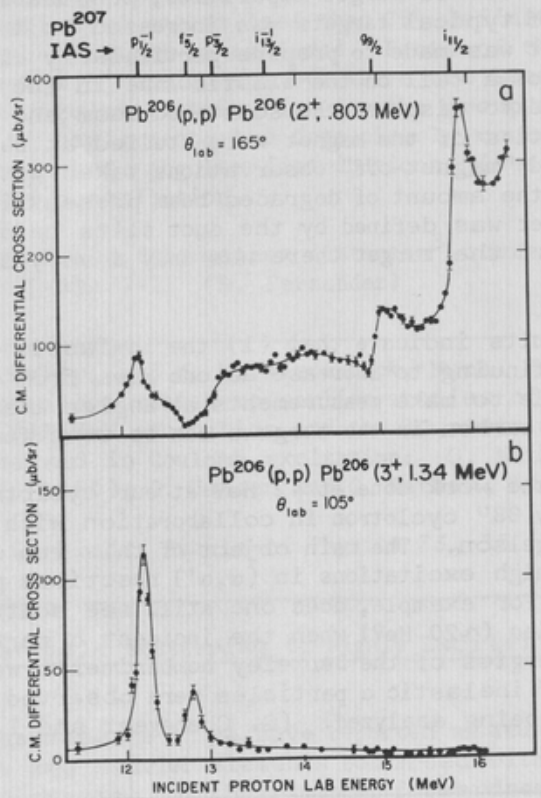

Fig. 9-1. Inelastic scattering excitation functions for the Pb^{206} (p,p') to the 2^+ (.803 MeV) (a) and 3^+ (1.34 MeV) (b) states of Pb^{206}.

Figure 9-1(b) contains the excitation function for the decay to the 3^+ (1.34 MeV) state of Pb^{206} at 105° in the laboratory frame. In the entire

energy range studied resonances are seen only at the g.s. ($1/2^-$) and first excited state ($5/2^-$) analogs of Pb^{207}. In addition, the on-resonance angular distributions as shown in Fig. 9-2 for both of these states are isotropic. Deviations from isotropy in the $f_{5/2}$ angular distribution would indicate contributions other than $p_{1/2}$ particle decay. This demonstrates that the 3^+ state has a dominant two neutron particle-hole configuration such that $\Psi(3^+)$ (1.34 MeV) $\approx 1.00(p_{1/2}\ f_{5/2}^{-1})$. This agrees with the shell model calculations of True and Ford[2] who obtain a $.999(p_{1/2}\ f_{5/2}^{-1})+.05(p_{3/2}^{-1}\ f_{5/2}^{-1})-.038(p_{1/2}^{-1}\ f_{7/2}^{-1})$. In order to appreciate the simplicity of this state, the excitation function for decay to the 2^+(.803 MeV) state of Pb^{206} is shown directly above in Fig. 9-1(a). The highly collective 2^+ state exhibits resonances or interference effects at the position of nearly every analog state in the energy region studied.

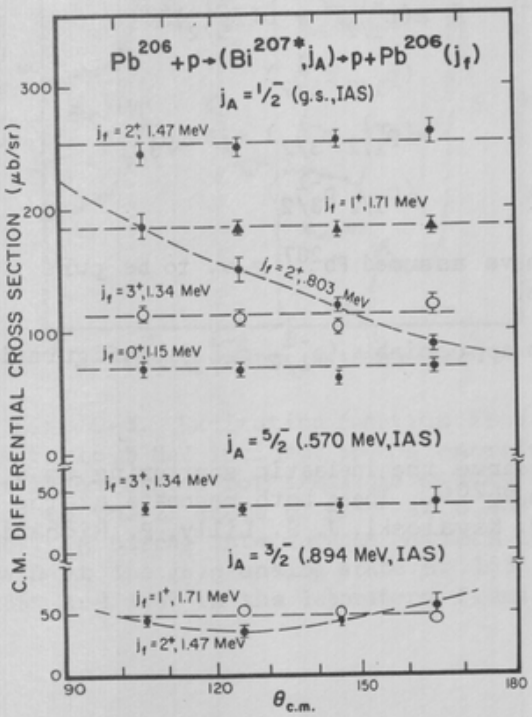

Fig. 9-2. Inelastic scattering angular distributions at the resonance energy of the three lowest energy analogs of Pb^{207}(*i.e.*, $1/2^-$, $5/2^-$ and $3/2^-$ states).

The inelastic scattering excitation function to the 1.15 MeV(0^+) state of Pb^{206} is not shown here. For this state a resonance is seen at the analog of the Pb^{207} ground state and a very small effect at the analog of the Pb^{207} $5/2^-$ state at .570 MeV excitation.

At the resonance energy for the $p_{1/2}$ g.s. IAS the angular distributions of the five inelastic groups were taken. The entrance channel ($p_{1/2}$ proton capture) requires all these angular distributions to be isotropic. Any deviations from isotropy in these cases implies that there is interference between the resonance and the background cross-section. From fig. 9-2 we see that the 2^+(.803 MeV) angular distribution is definitely not isotropic, even though the resonances at each angle appear to be Lorentzian in shape. The other four angular distributions are isotropic within the experimental errors. The total resonance width was obtained from the data and found to be 200 keV. Since this analog was observed in the elastic scattering a value of Γ_p could be extracted. In turn the inelastic widths could be calculated. Table 9-1 gives the results of this analysis.

At higher bombarding energies (14 to 16.5 MeV) we have taken excitation functions at eight different angles in order to study the interference pattern previously observed in the 2^+ state at the energy of the analog of the $g_{9/2}$ state of Pb^{207}. Figure 9-3 contains a plot of these data. For the $g_{9/2}$ resonance it is seen that the interference pattern goes through a zero at some

angle between 145° and 155°. A similar observation seems to be true for the $i_{11/2}$ analog resonance. These data have not been analyzed.

Table 9-1. Results of the analysis of proton elastic and inelastic scattering on Pb^{206} at the position of the resonance (E_p=12.23 MeV) for the $p_{1/2}$ g.s. analog of Pb^{207}. Included also is the dominant neutron configuration for the final state, which is based on the angular distributions at the position of the analogs of all the neutron hole state of Pb^{207}.

Final State	$\Sigma\Gamma_p$, (keV)	Dominant Configurations*
Pb^{206} 0^+(g.s.)	13	
2^+(.803)	--	many configurations
0^+(1.15)	11.9	$a(p_{1/2}^{-1})^2 + b(f_{5/2}^{-1})^2$
3^+(1.34)	19.9	$(p_{1/2}\ f_{5/2}^{-1})$
2^+(1.47)	44.8	$a(p_{1/2}^{-1}\ p_{3/2}^{-1}) + b\ (p_{3/2}^{-2})^{2\dagger}$
1^+(1.71)	32.8	$(p_{1/2}\ p_{3/2}^{-1})$

* Infered from this experiment. We have assumed Pb^{207} g.s. to be pure $p_{1/2}$ neutron hole in the Pb^{208} core.

† This state shows no evidence for an appreciable $(p_{1/2}^{-1}\ f_{5/2}^{-1})$ configuration as calculated in ref. 2.

In this higher energy range we also observe the inelastic scattering to a state at 3.76 MeV and a state at 2.38 MeV in Pb^{206}. These both resonate at the position of the $g_{9/2}$ analog of Pb^{207}. (C. D. Kavaloski, J. S. Lilly, P. Richard, and N. Stein)

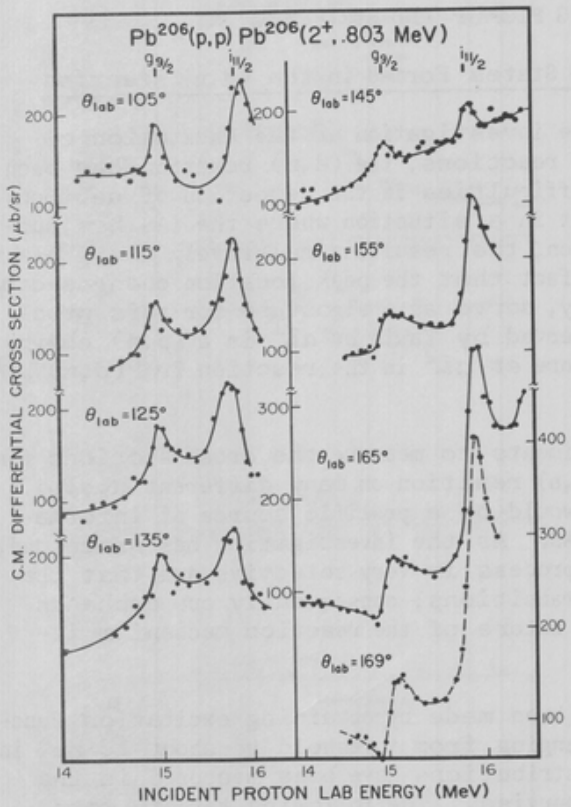

Fig. 9-3. Excitation function from 14 to 16.5 MeV incident proton energies at light angles for inelastic scattering to the 2^+ state of Pb^{206} at 0.803 MeV. A strong interference pattern is seen at the $g_{9/2}$ analog state at 155°, 165° and 169° in the laboratory frame.

1. C. D. Kavaloski, J. S. Lilly, P. Richard and N. Stein, Phys. Rev. Letters *16*, 807 (1966).
2. W. W. True and K. W. Ford, Phys. Rev. *109*, 1675 (1958).

II. REACTIONS INVOLVING PICKUP AND STRIPPING

10. Proton Decay from Isobaric Analogue States Formed in the (d,n) Reaction

Although there has been considerable investigation of the excitation of isobaric analogue states (IAS) with other reactions, the (d,n) reaction has been little used for this purpose. Obvious difficulties in the detection of neutrons help explain this lack of popularity. But in a situation where the IAS has sufficient energy for decay by proton emission, the resulting relatively sharp peaks in the proton spectrum, coupled with the fact that the peak location changes only slightly with changes in bombarding energy, serve as a signature for this process. Proton decay from IAS was first observed by Yavin *et al.*[1] in a (p,n) charge exchange reaction and more recently by Moore *et al.*[2] in the reaction $Zr^{90}(d,n)Nb^{91*}$ (IAS) → p + Zr^{90}(g.s.).

We have initiated a series of experiments to measure the cross sections for proton decay of IAS formed through the (d,n) reaction on many different nuclei. It was our first hope that this reaction would be a prolific source of information concerning the decay properties of IAS. As the investigation has proceeded, however, we have learned that the (d,np) process is very selective and that the cross sections are large for only a few transitions; consequently our emphasis has been shifted to an elucidation of the nature of the reaction mechanism itself.

A survey of the (d,np) reaction has been made by obtaining excitation functions, at 170° in the laboratory frame, ranging from threshold to about 16 MeV in the incident energy. Further, angular distributions have been measured in the backward hemisphere at various incident energies. The following targets were studied: Al^{27}, Ni^{64}, Zn^{68}, Y^{89}, $Zr^{90,92,94}$, $Mo^{92,94,98}$, $Sn^{114,116,118,120}$, and Pb^{206}.

Since the narrow proton decay peaks ride on a substantial background, it is necessary that the detection system have good energy resolution as well as the ability to discriminate protons from other charged particles. A ΔE-E detector telescope having a combined energy resolution of about 32 keV(FWHM), which was developed for the study of spectral fluctuations in the Al^{27}(d,p) reaction,[3] was admirably suited for this purpose.

Some feeling for the characteristics of the reaction may be obtained from inspection of representative proton spectra. The proton spectra following the d + Zr^{90} reaction are shown in Fig. 10-1a at two incident energies. The $d_{5/2}$ (g.s.)-IAS → 0^+(g.s.) transition [P_0^0] can be seen unambiguously at both energies. In the higher energy spectrum there are indications of the following transitions: $s_{1/2}$(1.21 MeV)-IAS → 0^+(g.s.)[P_0^1]; $d_{3/2}$(2.06 MeV)-IAS to both 0^+(g.s.)[P_0^2] and 2^+(2.21 MeV)[P_2^2]; and $g_{7/2}$(2.19 MeV)-IAS → 0^+(g.s.)[P_0^3].

In Fig. 10-1b, the protons from the d + Mo^{92} reaction are shown. Again the $d_{5/2}$(g.s.)-IAS → 0^+(g.s.) transition [P_0^0] is readily seen. Indications of other transitions are less obvious, even though the general background structure is relatively smoother than for the case of d + Zr^{90}. It is worth noting that the $d_{5/2}$(g.s.)-IAS does not give a discernable resonance in the proton scattering

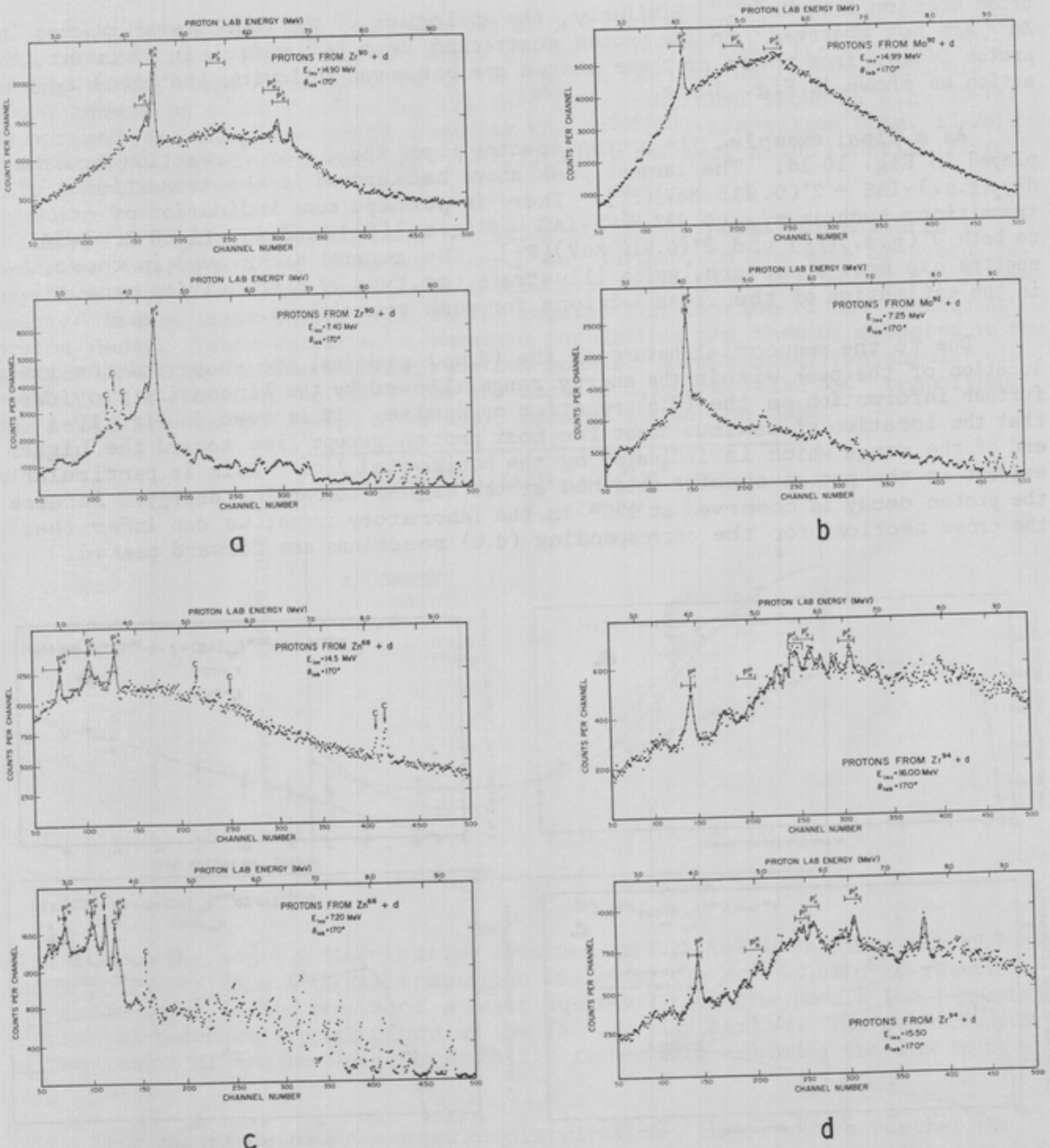

Fig. 10-1. Protons from deuterons bombardment of a variety of target nuclei: a - Zr^{90}, b - Mo^{92}, c - Zn^{68}, d - Zr^{94}; at incident energies near and far above the (d,n) threshold for the g.s. IAS. The horizontal lines indicate the energy range wherein the proton group corresponding to a particular decay of the IAS could lie. In the labeling of peaks superscripts refer to the IAS; the g.s. analogue is designated by the number 0, the analogue of the next excited state with reasonable spectroscopic factor is designated by the number 1, etc. Similarly, the subscripts refer to the final states.

cross section from Mo^{92}.[4] Similarly, the analogues of the four lowest states in Zn^{69} are not observed[5] in the proton scattering from Zn^{68} while, in contrast, the proton decays from three of these states are observed following the (d,n) reaction as shown in Fig. 10-1c.

As a final example, the proton spectra from the d + Zr^{94} reaction are displayed in Fig. 10-1d. The largest peak above background is the transition: $d_{5/2}$(g.s.)-IAS → 2^+(0.916 MeV)[P_1^0]. There is perhaps some indication of other transitions such as $s_{1/2}$(0.932 MeV)-IAS → 0^+(g.s.)[P_0^1], and $d_{3/2}$(1.68 MeV)-IAS to both 0^+(g.s.)[P_0^2] and 2^+(0.916 MeV)[P_1^2]. The general background in these spectra has more structure, which illustrate the type of difficulties encountered in the estimation of the cross sections for weak transitions.

Due to the sequential nature of the (d,np) process, the shape and the exact location of the peak within the energy range allowed by the kinematics provides further information on the (d,n) reaction mechanism. It is seen in Fig. 10-1 that the location of maximum count for most proton groups lies toward the higher end of the range which is indicated by the horizontal line. This is particularly evident in the proton spectra obtained at the higher bombarding energy. Because the proton decay is observed at 170° in the laboratory frame, we can infer that the cross sections for the corresponding (d,n) reactions are forward peaked.

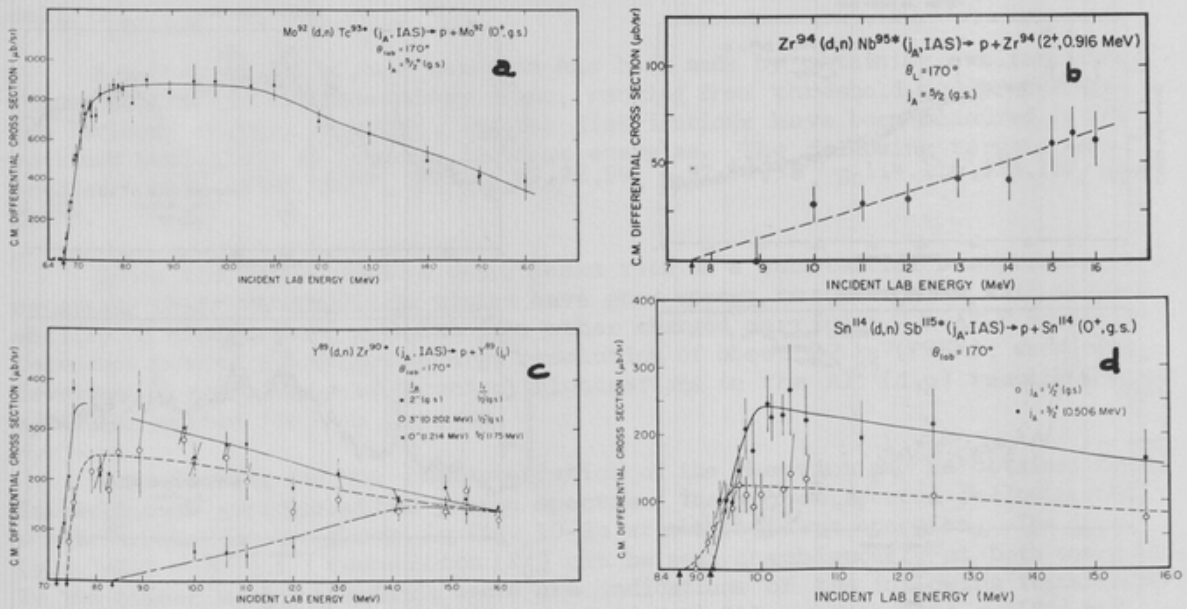

Fig. 10-2. The excitation functions obtained at 170° in the laboratory frame for the various transitions following the (d,n) reaction. Each (d,n) threshold for the IAS is indicated by an arrow on the energy axis. The errors shown include contributions from both the counting statistics and the uncertainties in background subtraction. Error of 10% in the absolute normalization has not been included. The smooth curve drawn through the data has no special significance.

The excitation functions measured at 170° are shown in Fig. 10-2 for several of the cases where cross sections can be extracted readily. The majority of the strong transitions exhibit an excitation function which rises sharply above threshold as is typified by the $Tc^{93*}[P_0^0]$-transition shown in Fig. 10-2a. Exceptions to this shape can be seen for the $Nb^{95*}[P_1^0]$-transition (Fig. 10-2b) and the $Zr^{90*}[P_3^2]$-transition (Fig. 10-2c), where the excitation function rises only slowly with energy.

A few angular distributions of the decay protons have been measured in order to determine total cross sections. But further, in the case of proton decay to a zero spin final state, the m-substate populations of the IAS can be extracted from a least squares fit to the angular distribution of the subsequent proton decay. These extracted m-substate populations can then be compared to the predictions from various nuclear reaction models. A representative angular distribution is shown in Fig. 10-3 for the case of $d_{5/2}$(g.s.)-IAS → 0^+ transition. The solid line is the result of a least squares fit to the data.

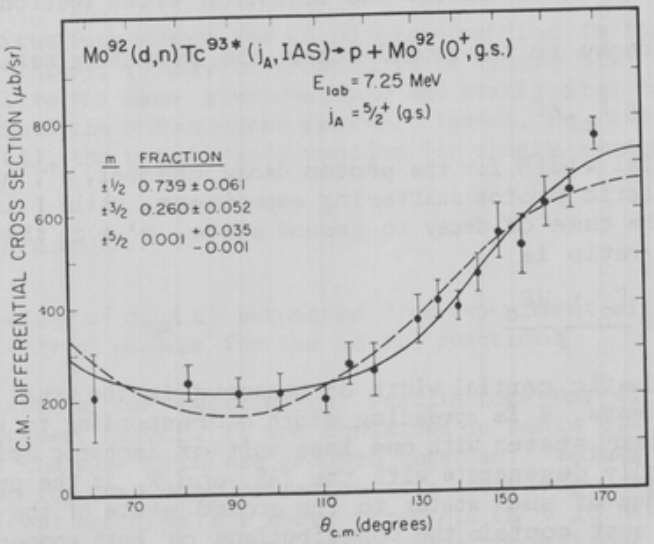

Fig. 10-3. The angular distribution obtained at 7.25 MeV bombarding energy for the $d_{5/2}$(g.s.)-IAS → 0^+(g.s.) transition following the $Mo^{92}(d,n)Tc^{93*}$ reaction. The solid curve is the result of a least squares fit to the data. The extracted fractional m-substate populations of the IAS are also listed. The dashed curve is the result of another least squares fit to the data assuming the IAS to be a $d_{5/2}$ state.

From the study of these angular distributions, there exists further the possibility of assigning definite spin value to the decaying state if the orbital angular momentum of the decay proton, ℓ, is known from other reactions. This is due mainly to the fact that the angular distributions from the lowest m-substates, $|\mathcal{Y}^{1/2}_{\ell 1/2 j}|^2$, are moderately different for the two values of j, $\ell + 1/2$ and $\ell - 1/2$; here $\mathcal{Y}^{m}_{\ell 1/2 j}$ is the angle-spin function corresponding to substate m. The dashed curve in Fig. 10-3 is the result of a least squares fit to the data assuming the

IAS to be a $d_{3/2}$ state. The calculated variance of the $d_{5/2}$ fit is a factor 2 smaller than the corresponding $d_{3/2}$ fit. Furthermore, the $d_{3/2}$ assignment requires a 99% m = ± 1/2 population in the IAS formed in the (d,n) reaction. This seems unwarranted since the emerging neutron has an energy of roughly 500 keV and thus can carry off a finite amount of angular momentum.

Our interpretation of the experimental results is based on the following theoretical considerations. With the assumption that the (d,np) process is sequential, the total cross section for proton decay to a given final state, $\sigma(d,np)$, may be written as the product

$$\sigma(d,np) = \sigma(d,n)G_{c'} \tag{1}$$

where $\sigma(d,n)$ is the total cross section for the formation of the IAS through the (d,n) reaction and $G_{c'}$ is the branching ratio for proton decay via channel c'. Knowledge of the branching ratio, $G_{c'}$, and the total cross section for proton decay, $\sigma(d,np)$ enables us to extract the formation cross section, $\sigma(d,n)$.

Except for decay to the ground state, the branching ratio is given by

$$G_{c'} = \Gamma_{c'}/\Gamma \tag{2}$$

where $\Gamma_{c'}$ is partial width for the proton decay channel, c', as measured, for example, in an inelastic proton scattering experiment, while Γ is the total width of the IAS. In the case of decay to ground state, c' = c, the correct expression for the branching ratio is

$$G_c = \frac{\Gamma_c + WP_c}{\Gamma} \tag{3}$$

where Γ_c is the elastic partial width as measured in the usual proton elastic scattering experiments, W is spreading width corresponding to decay of the IAS into compound nuclear states with one less unit of isobaric spin (normal states) which are essentially degenerate with the IAS, and P_c is the probability for subsequent proton decay of such states to the ground state of the target. Stated alternatively, G_c must contain the contributions of both compound and shape elastic widths. The reason Eq. (3) is not used for the other proton channels is that the $\Gamma_{c'}$ as deduced from inelastic scattering experiments includes implicitly the width for the roundabout decay through the normal states as well as the width for immediate decay of the IAS into exterior channel c'.

When there are many channels open for neutron decay, the probability for proton decay of the normal states is presumably small so that the product WP_c in Eq. (3) may be neglected. On the other hand when the neutron channels are closed, this second term in the numerator can become very important. It is often true that proton decay to the ground state is greatly favored over decay to excited states, because of the respective barrier penetrabilities. Thus, when the neutron channels are closed, the branching ratio for decay to the ground state, G_c, approaches unity. For a given Z, IAS which are closed for neutron decay will occur only (if at all) in the lighter isotopes; one therefore expects that the cross sections for corresponding (d,np) reactions in a given series of isotopes will decrease markedly with increasing A at that value for which many neutron

channels become open.

If it is assumed that an IAS is formed by the mechanism of direct (d,n) stripping, the formation cross section, $\sigma(d,n)$, can be estimated by means of the standard DWBA model.[6] The total cross section for the (d,np) reaction would then be given by the expression

$$\sigma(d,np) = \left[\frac{(2J_f + 1)}{(2J_i + 1)} \frac{S_{dp}}{2T_0 + 1} G_{c'}\right] \sigma_{DWB}(\ell) \qquad (4)$$

where J_f is the spin of the IAS, J_i and T_0 are respectively the spin and isotopic spin of the target nucleus, S_{dp} is the spectroscopic factor deduced from analysis of the (d,p) stripping reaction leading to the parent of the IAS, and $\sigma_{DWB}(\ell)$ is the total cross section for adding a proton of orbital angular momentum ℓ as computed by the DWBA model. In what follows the factor in brackets will be called the enhancement factor, F.

But even in situations where the (d,n) cross section is inadequately described by the DWBA theory, it may be reasonable to assume that the cross section will be proportional to the same spectroscopic and statistical factors which have been separated out into the enhancement factor. Indeed, Eq. (4) can be inverted so as to define $\sigma_{sp}(\ell)$, the total cross section for single proton transfer, through the relation

$$\sigma_{sp}(\ell) \equiv \sigma(d,np)/F. \qquad (5)$$

Comparison of the values of $\sigma_{sp}(\ell)$ extracted from experiment will then serve to measure the consistency of models for the (d,np) reaction.

A summary of some of our experimental results together with the calculated values of the enhancement factor, F, are contained in Table 10-1. Information concerning IAS with the same spin are grouped together. Values of the differential cross section for the (d,np) reaction at a laboratory angle of 170° are given both for incident energies far above threshold ($E \sim 16$ MeV) and at maxima near threshold for the IAS in question. (For those transitions where the corresponding groups are not discernable above background, we have assigned upper limits to the cross sections.) In calculating F we have used the values of S_{dp}, Γ, Γ_p and $\Gamma_{p'}$ which are available in the literature. The uncertainties in the enhancement factor can be as large or larger than 50% in many instances.

Also listed in Table 10-1 are preliminary values for $\sigma_{sp}(\ell)$ as defined by Eq. (5). In order to calculate this quantity it is necessary to know the total (angle integrated) (d,np) cross sections. For decay from a $s_{1/2}$ IAS, the total (d,np) cross section is simply 4π times the differential cross section at 170°. For decay from some of the $d_{5/2}$ IAS to the ground state of the target, the angular distributions have been measured at enough energies to allow us to extract a meaningful total cross section at all energies; for the weaker transitions from $d_{5/2}$ states, we have assumed that the angular distributions are the same as those measured for the stronger transitions at corresponding values of the outgoing neutron energy. Only one angular distribution has been measured for the decay of a $d_{3/2}$ IAS to a ground state; this, together with some information concerning

Table 10-1. Summary of results for the $2d_{5/2}$, $3s_{1/2}$, and $2d_{3/2}$ IAS as observed in the (d,np) reaction. The enhancement factor F as well as the differential cross section near and far ($E_d \sim 16$ MeV) from the threshold of the (d,n) reaction to IAS are given. The final two columns give the single particle cross sections for the (d,n) reaction. These values have been either calculated from measured angular distributions or estimated from related angular distributions (see discussion in text).

S.P. State	Parent	E_x	IAS(d,n) Threshold	Final State	F×10	$\sigma(170°)_{d,np}$ μb/sr Near	Far	Estimated $\sigma_{sp}(\ell)$ mb Near	Far
$2d_{5/2}$	Zr^{91}	g.s.	7.06	0^+(g.s.)	4.85	909±32	385±55	12.96±1.42†	8.49±1.22
	Zr^{93}	g.s.	7.38	0^+(g.s.)	0.482	76±23	32±11	9.75±2.91	7.12±2.45
	Zr^{95}	g.s.	7.57	0^+(g.s.)	0.134	---	16±10	---	12.76±7.46
				2^+(0.916)	0.264	24 UL	65±14		
	Mo^{93}	g.s.	6.69	0^+(g.s.)	5.80	875±53	350±75	10.01±0.61	8.32±0.89†
	Mo^{95}	g.s.	7.29	0^+(g.s.)	4.04	540±40	217±26	8.28±0.62	5.75±0.69
	Mo^{99}	0.18	8.66	0^+(g.s.)	0.127	3 UL	9 UL	1.50 UL	7.56 UL
$3s_{1/2}$	Zr^{91}	1.21	8.26	0^+(g.s.)	1.31	90±35	90±35	8.67±3.39	8.67±3.39
	Zr^{93}	0.96	8.40	0^+(g.s.)	0.616	---	---	---	---
	Zr^{95}	0.95	8.53	0^+(g.s.)	0.631	30±15	20 UL	5.91±3.02	4.02 UL
	Mo^{93}	0.93	7.64	0^+(g.s.)	1.56	80±45	75±25	6.41±3.64	6.03±2.01
	Mo^{95}	0.77	8.07	0^+(g.s.)	0.964				
	Mo^{99}	g.s.	8.48	0^+(g.s.)	0.364	14 UL	15 UL	4.90 UL	5.15 UL
	Sn^{115}	g.s.	8.73	0^+(g.s.)	1.28	120±25	75±40	11.81±2.51	7.41±3.90
	Sn^{117}	g.s.	9.25	0^+(g.s.)	0.300	11 UL	32±11	4.65 UL	13.45±4.65
	Sn^{119}	g.s.	9.64	0^+(g.s.)	0.211	13 UL	13 UL	7.41 UL	7.41 UL
	Sn^{121}	0.069	9.95	0^+(g.s.)	0.149	25 UL	---	21.1 UL	---
$2d_{3/2}$	Zr^{91}	2.06	9.23	0^+(g.s.) + 2^+(2.21)	1.64	58±20	100±30 + 150±30	2.59±0.88	15.61±3.77*
	Zr^{93}	1.45	8.93	0^+(g.s.)	0.377				
	Zr^{95}	1.64	9.26	0^+(g.s.)	0.369	8 UL	20±13	1.63 UL	5.51±3.57
	Mo^{93}	1.51	8.23	0^+(g.s.)	1.91	140±45	130±35	5.40±1.78	6.94±1.84
	Mo^{95}	0.83	8.14	0^+(g.s.)	1.16				
	Mo^{99}	0.44	8.92	0^+(g.s.)	(0.018)	13 UL	27 UL	5.33 UL	15.3 UL
	Sn^{115}	0.506	9.24	0^+(g.s.)	1.65	240±30	160±40	10.73±1.33	9.89±2.45
	Sn^{117}	0.157	9.40	0^+(g.s.)	0.29	40±14	25±13	10.21±3.55	8.77±4.59
	Sn^{119}	0.021	9.66	0^+(g.s.)	0.171	13 UL	13 UL	5.40 UL	7.45 UL
	Sn^{121}	g.s.	9.88	0^+(g.s.)	0.157	25 UL	---	11.77 UL	

*For the Zr^{91} $d_{3/2}$ IAS we have assumed that $G_c = 1$ and used the summed cross sections for decay to both the 0^+ and 2^+. We have further assumed that the $d_{3/2} \rightarrow 2^+$ angular distribution is similar to that of the $d_{3/2} \rightarrow 0^+$ transition.

†From measured total (d,np) cross section.

the m-substate populations of $d_{5/2}$ IAS, has been used in converting the measured values for $\sigma(170°)_{d,np}$ into rough estimates of total (d,np) cross sections for all of our $d_{3/2}$ IAS.

Consideration of this table, the measured excitation functions, and angular distributions lead us to make the following observations:

(1) The enhancement factor F serves as a rough measure of one's ability to detect a particular (d,np) decay. These decay peaks which clearly stand out well above background correspond to transitions for which $F \geq 0.25$. As mentioned earlier the magnitude of F depends critically on whether or not the IAS can decay by neutron emission.

(2) More quantitatively, at high incident energies the values of $\sigma_{sp}(\ell)$, bearing in mind the large uncertainties of the analysis, have essentially the same magnitude for states with a given proton orbital angular momentum, ℓ, independent of A and independent of the behavior of the cross sections at lower incident energy. For that matter, there appears to be little dependence on ℓ in these cross sections. Perhaps the biggest discrepancy concerns the excitation of the $d_{3/2}$ IAS in Nb^{91*}; here, however, our lack of information on the angular distribution for proton decay to the first 2^+ state in Zr^{90} makes the determination of $\sigma_{sp}(\ell)$ very uncertain.

DWBA calculations of the single particle cross sections have been made in which various bound state form factors have been assumed; at these higher energies, agreement of the measured and calculated cross sections has been found to within a factor of 2. In other words it would appear that a direct interaction description of the (d,n) process generally suffices at these higher energies. However, this description does encounter at least one difficulty. Those DWBA calculations which we have carried out so far for the excitation of $d_{5/2}$ IAS have yielded values for the population of the $m = \pm 1/2$ substate varying from 0.50 to 0.8 while the measured values dip to 0.4 at the higher incident energies.

(3) As the incident energy is decreased toward threshold, a more complicated pattern seems to emerge. Particularly in those instances where $\sigma(170°)_{d,np}$ is large, the values of the $\sigma_{sp}(\ell)$ are somewhat larger near threshold than at high energy; in fact these $\sigma_{sp}(\ell)$ show similar behavior throughout the energy range studied. On the other hand, there are several other examples where either $\sigma_{sp}(\ell)$ is measurably less than it is at higher energies or only a small value for the upper limit on this quantity can be established. The rapid increase in cross section near threshold is not characteristic of the DWBA calculations which we have so far performed. Further, the variation in energy dependence is not understood at this time. (J.S. Blair, N. Cue, C. Ling, P. Richard)

---

1. A.I. Yavin, R.A. Hoffswell, and T.M. Noweir, Proceedings of the Conference on Isobaric Spin in Nuclear Physics, edited by J.D. Fox and D. Robson, Academic Press (1966), p. 584.
2. C.F. Moore, C.E. Watson, S.A.A. Zaidi, J.J. Kent, and J.G. Kulleck, Phys. Rev. Letters *17*, 926 (1966).
3. See Section 28, Ref. 3.

4. C.F. Moore, P. Richard, C.E. Watson, D. Robson, and J.D. Fox, Phys. Rev. *141*, 1166 (1966).
5. G. Vourvopoulos and J.D. Fox, Phys. Rev. *141*, 1180 (1966).
6. R.M. Bassel, R.M. Drisko, and G.R. Satchler, Oak Ridge National Laboratory Report ORNL-3240.

---

11. The Spectrum of Alpha Particles Emitted in the (He^3,α) Reaction in Heavy Elements

The observation (see Sec. 8) that highly excited states in residual nuclei are populated with appreciable probabilities in the (α,α') reaction, suggests that corresponding things may be true in other kinds of direct reactions like pickup and stripping reactions.

To avoid confusions from contributions of evaporated particles, it is well (as in the (α,α') studies) to restrict one's attention to heavy targets and to charged particles in the exit channel. For the incoming particle one wants a reasonably high energy and in order to provide for the possibility of high excitation of the residual nucleus, one wants a large positive Q. For these reasons, the reaction chosen for study was the (He^3,α) reaction, with He^3's of 22.5 MeV (the highest energy easily available at the tandem accelerator).The same particle-identification techniques were used as in the (α,α') measurements. The targets chosen for study were Sn^{118} and Au^{197}. For these targets the maximum energy of the emitted α particles is about 35 MeV compared to the 42 MeV in the inelastic scattering studies.

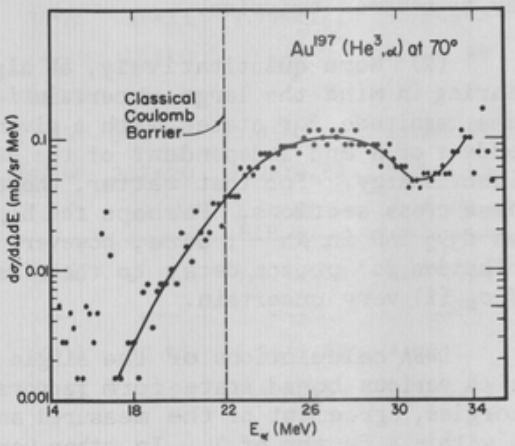

Fig. 11-1. The alpha particle energy spectrum for Au^{197}(He^3,α) at 70° with 22.5 MeV incident He^3 particles. The line through the points is merely to guide the eye.

Qualitatively the results for (He^3,α) resemble those for (α,α'), there being a considerable yield of alpha particles with energies from 35 MeV on down to the Coulomb barrier. (See Fig. 11-1.) Preliminary results suggest some differences between the (He^3,α) and (α,α') results: (1) The (He^3,α) cross-section, in contrast to the (α,α'), decreases with increasing A [the ratio of the Au/Sn differential cross sections at 50° being 0.16 for (He^3,α) whereas it is 1.2 for (α,α')] and (2) The (He^3,α) cross-section decreases for more forward angles instead of increasing as was seen in the (α,α') cross-section. For example, the 50°/70° ratio for Au^{197}(He^3,α) is 0.35 while the 40°/60° ratio for Au^{197}(α,α') is 3. The latter observation perhaps can be explained in part by the lower incoming and outgoing energies in the (He^3,α) reaction. (G. Chenevert and I. Halpern)

12. Studies of (d,He^3) Reactions on Sr^{88}, Y^{89}, and Zr^{90}

The analysis of the work reported last year[1] has been completed and the results have been submitted for publication.[2] (C. D. Kavaloski, J. S. Lilley, D. C. Shreve, and Nelson Stein)

---

1. Nuclear Physics Laboratory Annual Report, University of Washington (1966), p. 22.
2. C. D. Kavaloski, J. S. Lilley, D. C. Shreve, and Nelson Stein, submitted to Physical Review.

---

13. The (d,p) Reaction on Zr^{90}

A study of stripping reactions at incident energies below and above the Coulomb barrier has just been undertaken. Below the Coulomb barrier, such stripping reactions will occur outside the nucleus where nuclear distortions will be of minor importance and compound nuclear contributions will be negligible. This can be assured if the Q value of the reaction is near zero so that the energy of the emitted particle is also below the Coulomb barrier. This implies that for such stripping reactions as (d,p), with a Q value generally about +5 MeV, one should be concerned especially with stripping to highly excited states in the residual nucleus. A comparison of experiments above and below the Coulomb barrier can yield an understanding of DWBA procedures.

A study has begun on the reaction $Zr^{90}(d,p)Zr^{91}$, which has a Coulomb barrier of about 8 MeV. Figure 13-1 shows some preliminary results of angular distributions to the ground and the 1.21 MeV excited state in Zr^{91} for 11 MeV deuterons. Extraction of angular distributions for excitation of higher excited states, theoretical fits to the data, and the extraction of spectroscopic factors have yet to be completed. It is planned to study such a reaction at several energies around the Coulomb barrier, with special emphasis being paid to those reactions leading to highly excited states. Other stripping reactions besides (d,p) will be included in the investigation. (J. Cramer, R. Hinrichs, D. Oberg, and G. Phillips)

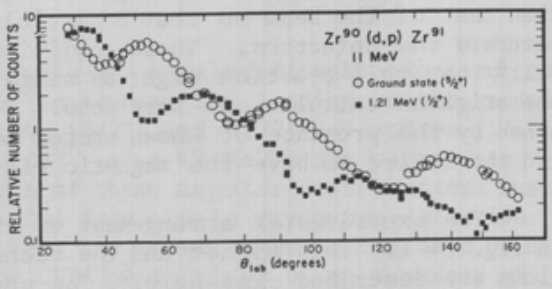

Fig. 13-1. Angular distributions for $Zr^{90}(d,p)Zr^{91}$ to the ground $(5/2^+)$ and 1.21 MeV $(1/2^+)$ states.

---

14. Small Angle J-Dependence of (α,t) Reactions

The J-dependence of stripping reactions at large angles is well established.[1] Nearly all stripping and pickup reactions have angular distributions that are somewhat characteristic of the total angular momentum transfer J as well as the orbital angular momentum transfer ℓ.[2] This dependence has generally been interpreted as arising from a spin-orbit interaction.[1] Unfortunately, detailed anal-

yses of these data are rather difficult due to problems with the distorted wave Born approximation (DWBA) calculations needed at these large angles.

A study of the small angle behavior of the angular distributions for (α, spin 1/2 particle) stripping reactions was suggested by the work of Henley and Kelley.[3] They have shown that if a spin-orbit force is included in a DWBA calculation as a first order perturbation, the angular distributions predicted for transitions leading to states of spin $j = \ell + 1/2$ and $j = \ell - 1/2$ will have different shapes even at very small angles. Using a simple diffraction model and geometrical arguments for a (α,nucleon) reaction, they have deduced that the effect of the spin-orbit interaction will be to increase the cross section for the $j = \ell - 1/2$ state relative to that for the $j = \ell + 1/2$ state. Thus, one might be able to assign spins and determine the strength of the $\vec{\ell}\cdot\vec{s}$ force from the cross sections at small angles. DWBA calculations for (α,p) reactions predict that this small angle J-dependence may be quite large. The experiments reported here were performed to test the predictions of this simple theory.

We made a choice between the various possible (α, spin 1/2 particle) reactions on the basis of experimental convenience. We wanted to detect the out-going particles in silicon detectors of reasonable thickness. This condition favored He^3-ions and tritons over protons and neutrons. Also, since we desired to separate the reaction products from the 42-MeV alpha beam at small angles with a magnet, the magnetic rigidity (proportional to momentum divided by charge) for the beam and the out-going particles had to be substantially different. The magnetic rigidity for protons and α particles of equal energies is the same. It was also convenient to have the magnetic rigidity of the out-going particles greater than that of the beam so that α particles degraded in the collimator would not saturate the detectors. These conditions all favored the (α,t) reaction. It was felt[4] that this reaction might be similar to the (α,nucleon) reaction for which the original calculations were done. The specific reactions studied were determined by the presence of known states of spin $j = \ell \pm 1/2$ in the final nucleus and the desire to have the magnetic rigidity of the tritons as large as possible.

The experimental arrangement of the magnet, detectors, and targets is shown in Fig. 14-1. This magnet and the techniques to measure small angle cross sections are described elsewhere.[5] The counter is mounted behind a collimating telescope which defines the angle of bending in the magnet and which can be pointed away from the center of the magnet to detect particles emitted at small angles. In addition to the particle identification accomplished by the magnet and an energy detector, a standard ΔE-E counter system was used to separate tritons from other particles of the same energy (notably alpha particles) which were scattered into the detector by the telescope apertures. For the large angle region ($\theta > 10$ deg) this same ΔE-E counter system was used in the conventional manner with the targets mounted at the center of the scattering chamber.

The angular distributions for the reaction $Ni^{64}(\alpha,t)Cu^{65}$ leading to the ground state ($3/2^-$) and 0.770-MeV state ($1/2^-$) were measured from 2.5 to 70 deg. and are shown in Fig. 14-2. The curves in Fig. 14-2 are the results of $\ell = 1$ DWBA calculations using two sets of optical model parameters without a spin-orbit potential.[6] The two sets of optical model parameters were obtained by fitting[7] elastic scattering data for $Ni^{60}(\alpha,\alpha)$ at 43 MeV[8] and $Cu^{63}(He^3,He^3)$ at

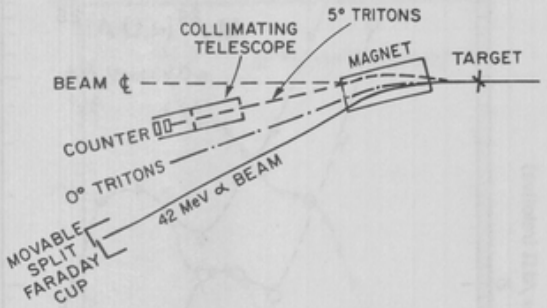

Fig. 14-1. Scattering chamber setup for small angle data. The magnet is at the center of the chamber, with the target in front of it. Trajectories are indicated for the 42-MeV beam alpha particles and for 30 MeV tritons emitted at 0° and some small angle. Note that the counter telescope looks off-center to see the small angle tritons.

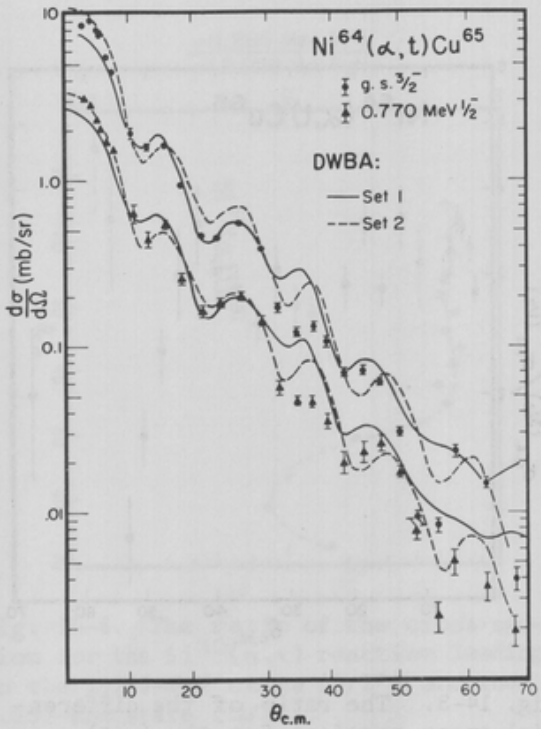

Fig. 14-2. Angular distributions for the $Ni^{64}(\alpha,t)$ reaction leading to the ground state ($3/2^-$) and 0.770-MeV states ($1/2^-$) of Cu^{65} using 42-MeV alpha particles. Both of these angular distributions must be ℓ=1 from simple stripping selection rules. The curves through the data points are DWBA predictions using two sets of optical model potentials (see Table 14-1).

31 MeV[9] with shallow and deep wells respectively. These sets of parameters are given in Table 14-1. The relative spectroscopic factors obtained from this DWBA analysis ($C^2S_{g.s.}/C^2S_{0.770}$ = 1.15 for set 1 and 1.25 for set 2) agree fairly well with those obtained from a study of the (He^3,d) reaction[10] leading to these same states ($C^2S_{g.s.}/C^2S_{0.770}$ = 1.05). This supports the assumption that the (α,t) reaction proceeds by a simple stripping mechanism.

To facilitate comparison of the data a ratio of the (α,t) cross sections for the excitation of these states is shown in Fig. 14-3. As can be seen, there is very little, if any, J-dependence at small angles for this particular reaction.

Investigations of the $Si^{30}(\alpha,t)P^{31}$ and $Mg^{24}(\alpha,t)Al^{25}$ reactions are now under way and preliminary large angle data have been taken. The angular distributions for the $Mg^{24}(\alpha,t)$ reaction leading to the ground state ($5/2^+$) and the 0.95-MeV state ($3/2^+$) of Al^{25} are shown in Fig. 14-4. If one assumes that these transitions proceed by a simple stripping mechanism, then both of the angular distributions should be ℓ = 2. As is seen in Fig. 14-4, there are large differences between these angular distributions. We cannot tell at the present time if

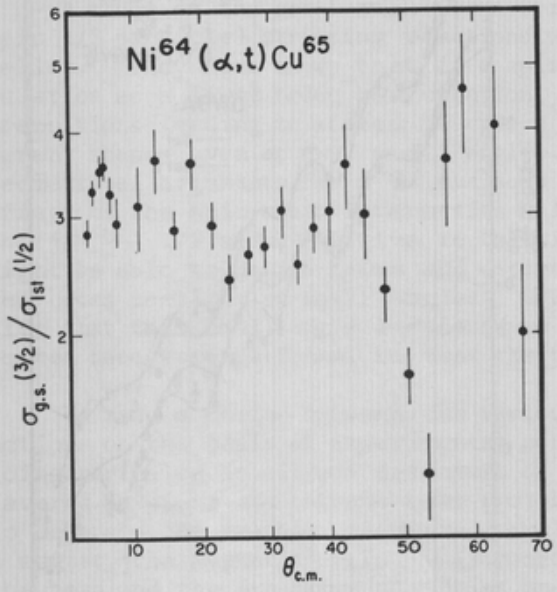

Fig. 14-3. The ratio of the differential cross sections for the (α,t) reactions leading to the ground state ($3/2^-$) and 0.770-MeV states ($1/2^-$) of Cu^{65}.

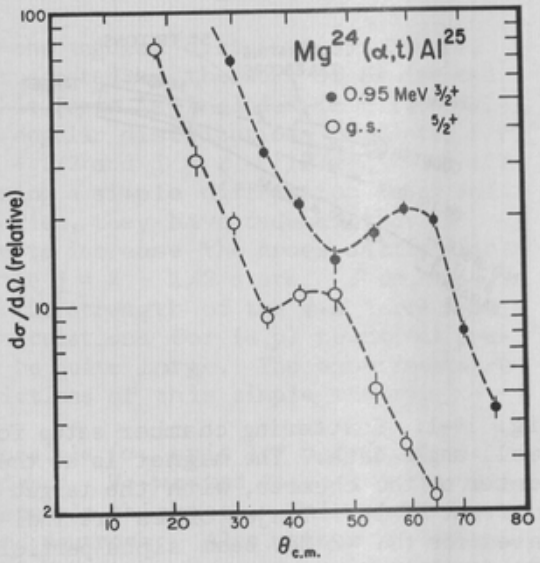

Fig. 14-4. Relative angular distributions for the $Mg^{24}(\alpha,t)$ reaction leading to the ground state ($5/2^+$) and 0.950-MeV state ($3/2^+$) of Al^{25}. The curves are drawn through the points to guide the eye.

these differences are due to a J-dependence or to some other source.

Table 14-1. Optical model parameters used in DWBA analysis of the $Ni^{64}(\alpha,t)Cu^{65}$ reaction. The form of the nuclear optical potential used was

$$U = - V/(1 - e^{x}) - i(W - W' \frac{\partial}{\partial x'})/(1 - e^{x'})$$

where

$$x = (r_0 A^{1/3} - R)/a \text{ and } x' = (r_0' A^{1/3} - R)/a'.$$

Reaction	Set	V (MeV)	W (MeV)	r_0 (F)	a (F)	r' (F)	a' (F)	W' (MeV)
$Ni^{60}(\alpha,\alpha)$	1	199	21.9	1.42	0.56	1.42	0.56	0
	2	44.1	17.4	1.58	0.55	1.44	0.62	0
$Cu^{63}(He^3,He^3)$	1	120	0	1.22	0.81	1.23	0.85	100
	2	21.4	27.0	1.60	0.74	1.56	0.73	0

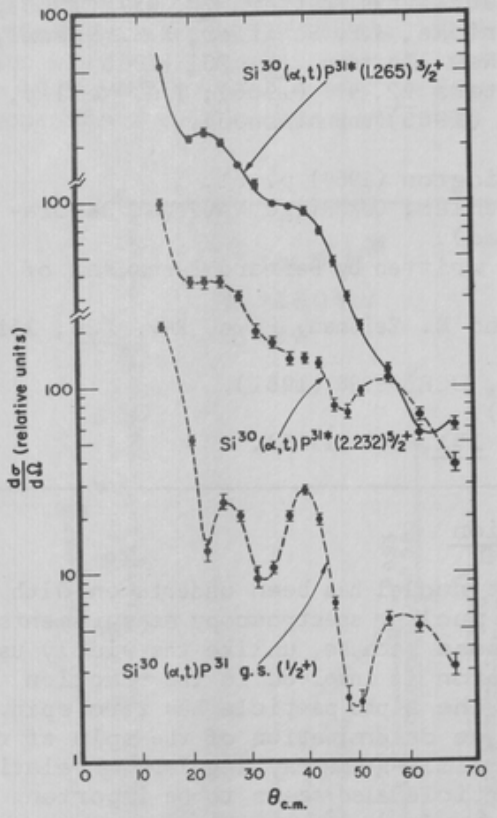

Fig. 14-5. The relative angular distributions for the $Si^{30}(\alpha,t)$ reaction leading to the ground state $(1/2^+)$, 1.265-MeV state (3.2^+) and 2.232-MeV state $(5/2^+)$. The curves are drawn through the points to guide the eye.

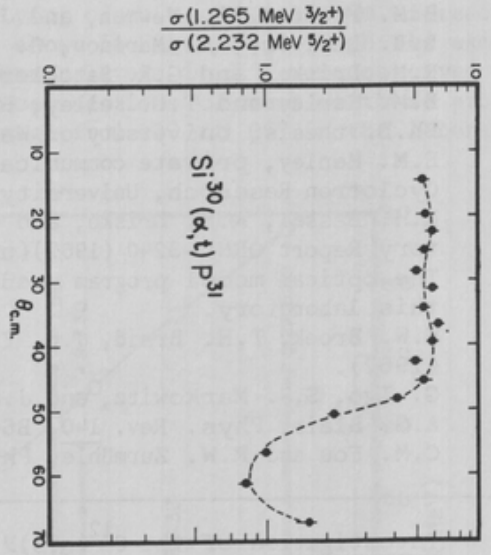

Fig. 14-6. The ratio of the cross section for the $Si^{30}(\alpha,t)$ reaction leading to the 1.265-MeV state $(3/2^+)$ and the 2.232-MeV state $(5/2^+)$.

The preliminary angular distributions for the reaction $Si^{30}(\alpha,t)$ leading to the ground state $(1/2^+)$ 1.27-MeV $(3/2^+)$ and 2.23-MeV $(5/2^+)$ states of P^{31} are shown in Fig. 14-5. The shapes of these angular distributions are very similar to those measured for the (He^3,α) reaction[11] leading to similar states in S^{31}, the mirror nucleus of P^{31}.

In the (He^3,α) case the differences in the shape of the $\ell = 2$ angular distributions for the transitions to the $3/2^+$ and $5/2^+$ states were interpreted as being due to a J-dependence. We might conclude, therefore, that the differences we observe are also due to a J-dependence. The ratio of the cross sections for the transitions leading to the 1.27-MeV $(3/2^+)$ and 2.23-MeV $(5/2^+)$ states of P^{31} is shown in Fig. 14-6.

We plan to continue the study of these latter reactions by taking data at small angles and investigating transitions to other final states.
(P.F. Mizera, D.C. Shreve, and D.W. Storm)

1. L.L. Lee, Jr., J.P. Schiffer, B. Zeidman, G.R. Satchler, R.M. Drisko, and R.H. Bassel, Phys. Rev. *136*, B971 (1964).

2. R.H. Fulmer and W.W. Daehnick, Phys. Rev. Letters 12, 455 (1964); M.K. Brussel, D.E. Rundquist, and A.I. Yavin, Phys. Rev. 136, B838 (1965); B.M. Preedom, E. Newman, and J.C. Hiebert, Phys. Letters 22, 657 (1966); L.L. Lee, Jr., A. Marinov, C. Mayer-Boricke, J.P. Schiffer, R.H. Bassel, R.M. Drisko, and G.R. Satchler, Phys. Rev. Letters, 14, 261 (1965).
3. E.M. Henley and T.G. Kelley, Phys. Letters 22, 495 (1966); T.G. Kelley, Ph.D. thesis, University of Washington (1966)(unpublished).
4. E.M. Henley, private communication.
5. Cyclotron Research, University of Washington (1964) p. 51.
6. R.H. Bassel, R.M. Drisko, and G.R. Satchler, Oak Ridge National Laboratory Report ORNL-3240 (1962)(unpublished).
7. The optical model program used was OP, written by Bernard Fernandez of this laboratory.
8. H.W. Broek, T.H. Braid, J.L. Yntema, and B. Zeidman, Phys. Rev. 126, 1514 (1962).
9. G. Igo, S.S. Markowitz, and J.G. Vidal, UCRL-9996 (1961).
10. A.G. Blair, Phys. Rev. 140, B648 (1965).
11. C.M. Fou and R.W. Zurmühle, Phys. Rev. 151, 927 (1966).

---

15. Investigation of the $C^{12}(\alpha,p)N^{15}$ Reaction

A survey of the (α,p) reaction in light nuclei has been undertaken with the object of investigating its usefulness in nuclear spectroscopy measurements. The (α,p) reaction is attractive for this purpose because, unlike the widely used (d,p) reaction, only the spin (1/2) of the proton is involved in the reaction mechanism and subsequent data analyses, since the alpha particle has zero spin. This feature is extremely important for a unique determination of the spin of the final state, J_f, of the product nucleus by particle-gamma-ray angular correlation measurements.[1] The zero spin of the alpha particle also seems to be important in a study of the angular distributions of the outgoing protons, where a pronounced effect has been observed for direct reactions having the same angular momentum transfer ℓ, but going to final states of different spin $J_f = \ell \pm 1/2$. While the cross sections for the lower J_f exhibit oscillatory behavior with angle, the cross sections for the higher J_f are found to be generally smooth.[2] This behavior can be predicted from DWBA theory, unlike the similar but less pronounced behavior in the (d,p) reaction, which is complicated by the non-zero spin of the deuteron. In spite of the attractive features of the (α,p) mechanism, this reaction has heretofore not been widely studied because of the generally negative Q-values associated with it. Such Q-values make necessary relatively high energy alpha beams with good energy resolution, such as are available from the University of Washington tandem Van de Graaff accelerator.

The $C^{12}(\alpha,p)N^{15}$ reaction was chosen as a test case for the (α,p) studies for several reasons: specifically, the excited levels in N^{15} below 10 MeV are for the most part well-known experimentally and have been extensively interpreted theoretically; furthermore the levels include a wide variety of known spins. However, considerable mystery is still associated with the state at 9.16 MeV excitation in N^{15}. Previous experiments[3] have indicated in fact that this level may be a close-lying doublet with one of the states unaccounted for theoretically.

A 100 $\mu g/cm^2$ carbon target was bombarded with a 22 MeV alpha beam. The reaction protons were separated from elastic and inelastic alpha particles by an E-ΔE counter telescope and an analog multiplying circuit. A spectrum of reaction protons as seen at 20° in the laboratory is shown in Fig. 15-1. With the exception of the 9.05 MeV state, all previously known levels in N^{15} were observed up to 10.71 MeV in excitation. Differential cross sections of each of these proton groups have been measured every 4° over a range from 12° to 96° in the laboratory

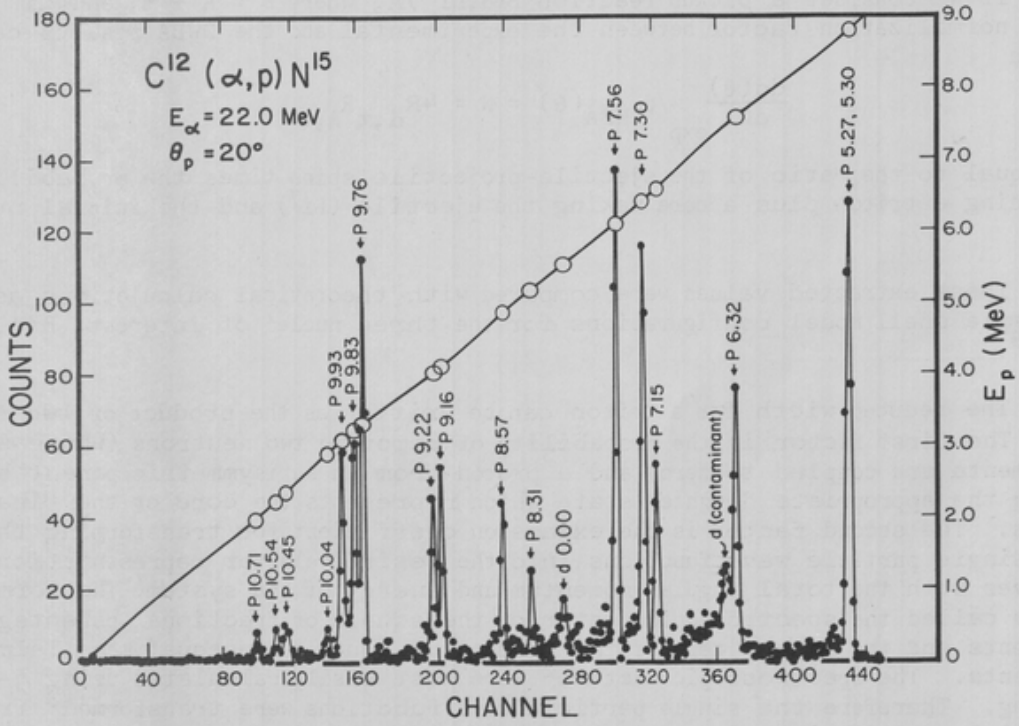

Fig. 15-1. Protons detected at 20° in the laboratory from the bombardment of 22 MeV alpha particles on carbon. The diagonal line shows the energy calibration.

system. These angular distributions are being analyzed in terms of their possible J-dependent character. With the expected increase in the intensity of the available alpha beams, proton-gamma-ray coincidence and angular correlation measurements will be carried out. In addition, investigations are planned of the (α,p) reaction on other targets including Mg^{26}, $Si^{29,30}$, and Ti^{48}. (J. Allen and G. Phillips)

1. A.E. Litherland and A.J. Ferguson, Can. J. Phys. 39, 788 (1961).
2. J.P. Schiffer, BNL 948 (C-46), Vol. 11, p. 455, Brookhaven National Laboratory, 1965.
3. G.W. Phillips, F.C. Young, and J.B. Marion, Phys. Rev. (to be published).

16. Triton Reduced Widths Using the (α,Li^7) Reaction

The results of the DWBA fits to the experimental angular distributions for the (α,Li^7) reaction on B^{11}, N^{15}, and F^{19}, reported last year,[1] have been used to extract relative reduced widths for tritons. The normalization factor between the experimental and theoretical differential cross sections is proportional to this reduced width.

If we consider a pickup reaction $B(\alpha,Li^7)A$, where $B = A + t$, and $Li^7 = \alpha + t$, the normalization factor between the experimental and the DWBA results can be written

$$\left(\frac{d\sigma(\theta)}{d\Omega}\right)_{exp} / \sigma_{DWBA}(\theta) = N = 4R_{\alpha,t}R_{A,t}.$$

N is equal to the ratio of the ejectile-projectile spins times the probabilities of finding a triton plus a core making the ejectile (Li^7) and the initial nucleus (B).

These extracted values were compared with theoretical calculations assuming simple shell model configurations for the three nuclei of interest: B^{11},N^{15}, and F^{19}.

The reduced width for a triton can be written as the product of two factors. The first factor is the probability of removing two neutrons (whose angular momenta are coupled to zero) and a proton from an antisymmetric parent state leaving the appropriate daughter state which represents the core or the final nucleus. The second factor is the expansion coefficient for transforming these three single particle wave functions into the desired cluster representation which conserves both the total angular momentum and energy of the system. The former term is called the spectroscopic factor or the square of fractional parentage coefficients and the latter term is the product of equal and unequal mass Talmi coefficients. The spectroscopic factors[2] were most easily calculated using j-j coupling. Therefore the single particle wave functions were transformed[3] from j-j to L-S coupling in order to use the convenient Talmi coefficient tables[4] for equal mass transformations and formulas[5] for the unequal mass transformations.

The results of these calculations are listed in Table 16-1. The first column shows the assumed shell model configurations for each target nucleus. The next column lists the center-of-mass wave function of the triton relative to the core. This is also the bound-state wave function used in the DWBA form factor. Finally, the last column shows the reduced widths, denoted by θ_t^2.

The calculated widths are compared to the extracted widths by normalizing the results to the B^{11} case, thereby eliminating the triton reduced width for Li^7.

The results of this comparison are shown in Table 16-2. The extracted relative reduced widths for B^{11} and N^{15} would appear to be consistent with a simple shell model description for their respective ground states. However, the extracted value for F^{19} shows a large enhancement of triton clustering when compared with the averaged value of the two dominant shell model configurations. (J.B. Gerhart and P. Mizera)

Table 16-1. Triton Reduced Widths

S = Spectroscopic Factor
X = Transformation Coefficient from jj to L-S Coupling
k_3 = Talmi Coefficient

Target	$\|H^3\rangle_{c.m.}$	$S \cdot X^2$	$k_3^2(\|H^3\rangle)$	$\theta_t^2 = S \cdot X^2 \cdot k_3^2$
$Be^8 + lp^3$	2P	1/3	0.45	0.150
$C^{12} + lp^3$	2P	1/3	0.45	0.150
$C^{12*} + lp^3$	2P	5/6	0.45	0.375
	1F	5/6	0.22	0.183
$O^{16} + 2s^3$	4S	1	0.032	0.032
$O^{16} + ld^2 \cdot 2s$	4S	3/5	0.026	0.016

Table 16-2. Triton Relative Reduced Widths

	θ_t^2(calculated)	θ_t^2(extracted)
$\frac{C^{12} + H^3}{Be^8 + H^3}$	1.0	0.92
$\frac{C^{12*} + H^3}{Be^8 + H^3}$	3.72	3.33
$\frac{O^{16} + H^3}{Be^8 + H^3}$	$\langle 0.16 \rangle_{av.}$	2.17

1. Nuclear Physics Laboratory Annual Report, University of Washington (1966) p. 34.
2. R. Sherr, Direct Interaction and Nuclear Reaction Mechanisms, Padua (1962); ed. by R. Clementel and C. Villi (Gordon and Breach, New York, 1963)p.1027.
3. M. Rotenberg, R. Bivins, M. Metropolis, and J. Worten, Jr., The 3-j and 6-j Symbols (The Technology Press, M.I.T.,Cambridge, Mass. 1959) p.22.
4. J. Brody and M. Moshinsky, Tables of Transformation Brackets for Shell Model Calculations (Monografias Del Instituto De Fisica, Mexico, 1960).
5. Y. Smirnov, Nucl. Phys. 27, 186 (1961).

17. Heavy Ion Transfer Reactions

An investigation has been made of the feasibility of studying heavy ion transfer reactions with the tandem Van de Graaff. It has been proposed that such a study upon medium weight target nuclei at energies below the Coulomb barrier would yield spectroscopic factors which would be more reliable than those obtained from (d,p) work. With heavy ion stripping, such as (N^{14},N^{13}), below the Coulomb barrier, the nuclear force can indeed be called a small perturbation to the Hamiltonian and be accurately treated as such; also compound nucleus contributions to the cross-section with heavy ions would be diminished, as compared to direct interactions; and a non-DWBA analysis (e.g., the Breit-Ebel semi-classical tunneling theory)[1] could be used to obtain the spectroscopic factors.

To study this type of reaction a reliable method of identifying and separating heavy ions is required. The technique using solid-state E and ΔE detectors is unusable here because 25 MeV N^{14} will stop in about 22μ of silicon. Previous methods have used Al foils[2] to detect the β^+ active N^{13}, and also a gas proportional counter to serve as a ΔE-E system.[3] The former method is unable to distinguish between reactions leading to different states in the final nucleus and in the latter the resolution of the proportional counter is insufficient at these energies to resolve the excited states in most final nuclei.

The identification scheme tested here was to use both the energy, E, and the time-of-flight, t, of the reaction particle to generate the function Et^2, which is proportional to the mass, using the SDS 930 computer for a two-parameter analysis. For time-of-flight determination, we had available the buncher-flapper system of the Van de Graaff (see Sec. 48). However, the best time-packet obtainable was about 6 nsec wide. An alternative system detected both the reaction particle and the recoil particle, the former detected at some distance from the target and the latter close up. These signals were then used to generate start and stop pulses for timing. With very good resolution in the timing system, identification could be achieved. For a tandem experiment with O^{16} at 20 MeV, with the second counter a distance of 1 1/2 feet from target, we needed a separation of at least 0.5 nsec to identify the outgoing O^{15}. Resolving times of this magnitude are only possible under the most favorable circumstances; thus this work may have to be done with lighter bombarding particles and more conventional identification techniques. (J. Cramer, R. Hinrichs, D. Oberg, and G. Phillips)

---

1. G. Breit and M.E. Ebel, Phys. Rev. *104*, 1030 (1956).
2. J.A. McIntyre, J.G. Couch, J.C. Hiebert, Phys. Rev. *152*, 883 (1966).
3. C.E. Anderson, D.A. Bromley,and M. Sachs, Nucl. Instr. and Meth. *13*,238 (1961).

III. REACTIONS INVOLVING SPIN FLIP

18. He^3 Spin Flip

An experimental project has been started to study spin flip reactions[1] using He^3 as the incident projectile. The motivation behind this project is to investigate the spin flip reaction as induced by projectiles more strongly absorbed than protons.

There are several difficulties involved in using He^3. First, the He^3 beam intensity obtainable from this laboratory's tandem Van de Graaff is relatively small. Much effort has gone into increasing this beam (Section 47). Second, one must do particle identification in order to separate He^3, deuterons, and protons. For this purpose, a 72μ solid state transmission detector and a 1000μ solid state detector have been purchased. The signals from these two detectors are fed into a multiplier system[2] to accomplish the particle identification. The rest of the electronics consists of a normal fast-slow coincidence which is used to gate a 512 channel analyzer. Since the fast coincidence is often the most difficult to set up, a time-to-pulse height converter has been employed to facilitate this problem. Start and stop pulses are derived from the fast discriminators associated with the particles and gamma rays, respectively. The time spectrum obtained with this arrangement consists of a flat background, corresponding to accidentals, and a peak, corresponding to true coincidences. A slow discriminator window is set around the peak to complete the fast coincidence part of the circuit.

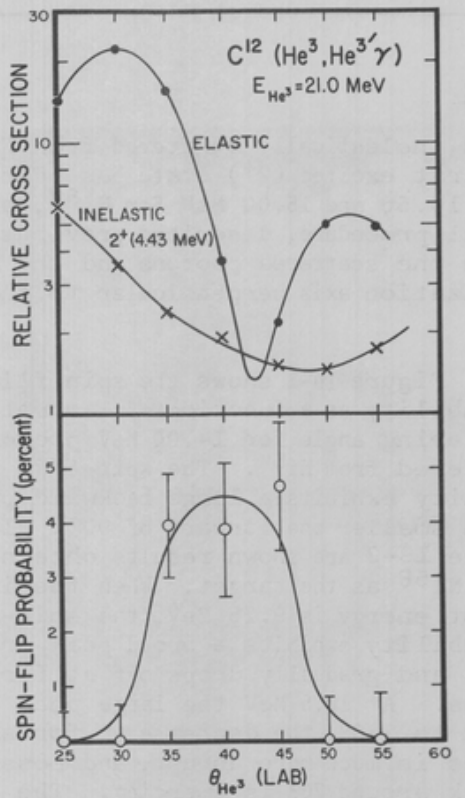

Fig. 18-1. Lower: He^3 spin flip probability in the reaction $C^{12}(He^3,He^{3'})C^{12*}(4.43)$. Upper: Relative differential cross sections for the reactions $C^{12}(He^3,He^3)C^{12}$ and $C^{12}(He^3,He^{3'})C^{12*}$ (4.43), as functions of laboratory scattering angle.

Measurements have been made on the spin flip probability in the reaction $C^{12}(He^3,He^3\gamma)C^{12*}(4.43)$ at 21 MeV. The results are shown in Fig. 18-1. The elastic cross section at 30° is roughly 28 mb/sr, with the main uncertainty due to target thickness. The error bars on the spin flip probability are statistical. Since the relative contributions of the m=±2 and m=0 substates are not known, the data shown assumes equal contribution. If there were no m=±2 contribution, the spin flip probability would be zero for all angles shown. If

there were no m=0 contribution, the maximum spin flip probability would be about 6.5%.

This work is being continued and extended to back angles where proton spin flip measurements have shown large spin-flip probabilities. (J. G. Cramer, T. D. Hayward, W. A. Kolasinski, D. M. Patterson, F. H. Schmidt, and J. Tesmer)

---

1. Nuclear Physics Laboratory Annual Report, University of Washington (1966), p. 59.
2. Nuclear Physics Laboratory Annual Report, University of Washington (1965), p. 76.

---

19. Proton Spin Flip in Inelastic Scattering

The probability for spin flip of protons inelastically scattered from Ni^{58} and Ni^{64} nuclei leaving the latter in their first excited (2^+) state has been measured at incident proton energies of 9.25, 10.50 and 15.00 MeV for Ni^{58}, and 10.50 and 14.00 MeV for Ni^{64}. The experimental procedure, described previously,[1] involves the detection of coincidences between the scattered protons and the de-excitation gamma rays emitted along the quantization axis perpendicular to the scattering plane.

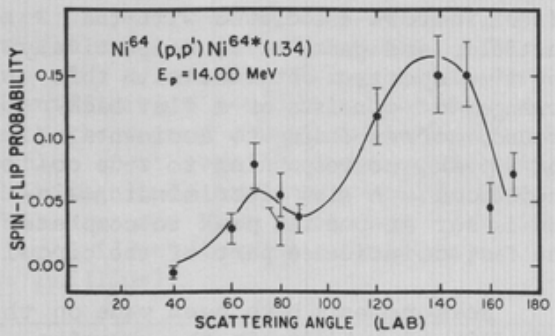

Fig. 19-1. Proton spin-flip probability in the reaction $Ni^{64}(p,p')Ni^{64*}(1.34)$ as a function of laboratory angle.

Figure 19-1 shows the spin flip probability as a function of laboratory scattering angle for 14.00 MeV protons scattered from Ni^{64}. The spin-flip probability exhibits a large backward peak, and a smaller one forward of 90°. In Figure 19-2 are shown results obtained with Ni^{58} as the target. When the incident energy is 9.25 MeV, the spin-flip probability exhibits a broad peak around 100°, and gradually drops off at forward angles. At 10.5 MeV the large peak has moved to 130°, the decrease at forward angles is much more abrupt, and possibly a peak around 70° is emerging. The 15 MeV results show the characteristic angular dependence, with strong backward peaking and very little spin flip at forward angles.

There is considerable evidence[2] that in inelastic scattering of protons from Ni^{58} at incident energies around 10 MeV, the compound-nuclear processes play an important role, while at 15 MeV one might expect the compound-nuclear contribution to be considerably less. The Ni^{58} data could thus be interpreted as showing that both compound-nuclear and direct processes contribute to the probability

for spin flip, the characteristic backward peaked pattern being associated with a direct process. Previously obtained data[1,3] on C^{12} and Ni^{60} seem to support this hypothesis. In the neighborhood of the 10.5 MeV scattering resonance in C^{12} the spin-flip probability rapidly changes its angular dependence and magnitude as the incident proton energy is varied, while between 12 and 15 MeV, where the magnitude of the scattering cross-section changes very slowly with energy, the spin-flip probability maintains its characteristic backward-peaked shape, and shows little change in magnitude. In the Ni^{60} and Ni^{64} results obtained at 10.5 and 14 MeV the spin-flip probability exhibits the characteristic angular dependence. If the above interpretation is correct, this would indicate that here the compound-nuclear contribution is relatively small. (J. G. Cramer, B. Fernandez, W. A. Kolasinski, and F. H. Schmidt)

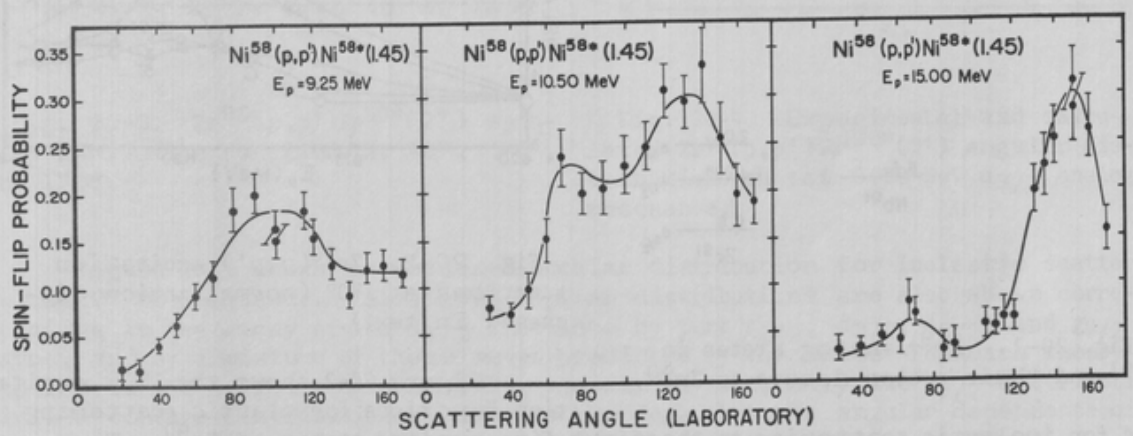

Fig. 19-2. Proton spin-flip probability in the reaction $Ni^{58}(p,p')Ni^{58*}(1.45)$ at 9.25, 10.5 and 15.00 MeV.

---

1. F. H. Schmidt, R. E. Brown, J. B. Gerhart, and W. A. Kolasinski, Nucl. Phys. *52*, 353 (1964).
2. L. W. Swenson and R. K. Mohindra, Phys. Rev. *150*, 877 (1966).
3. Nuclear Physics Laboratory Annual Report, University of Washington (1966), p. 59.

---

20. Proton Spin-Flip and Cross Section Measurements in the $Zr^{90}(p,p')$ Reaction on the $d_{3/2}$ Isobaric Analog Resonance in Nb^{91}

A study of the $d_{3/2}$ analog resonance in Nb^{91} excited by $Zr^{90}(p,p')$ has been made by measuring the cross section and spin-flip[1] excitation functions over the resonance at 90°, 140°, and 170°, and an-on resonance angular distribution of the

differential cross sections and spin-flip probability. Figure 20-1 shows the reaction and analog relations diagramatically.

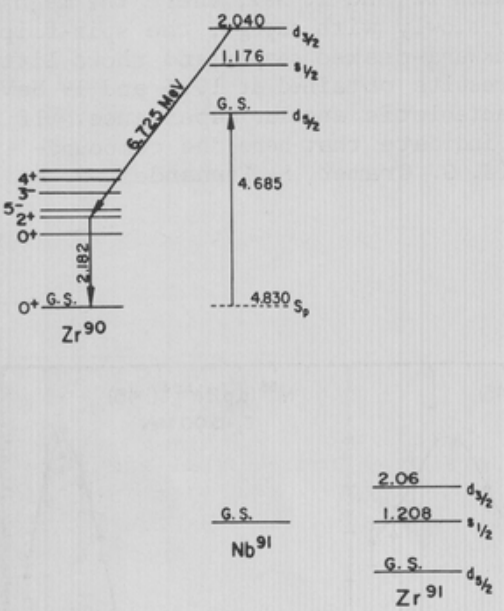

Fig. 20-1. Zr^{91} analog states in Nb^{91} and their proton decays to Zr^{90}.

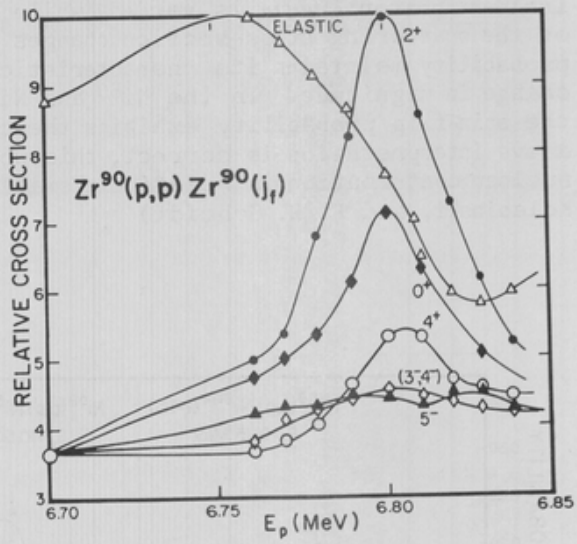

Fig. 20-2. $Zr^{90}(p,p')$ excitation functions at 170° (normalization discussed in text).

Figure 20-2 shows the 170° excitation functions for elastic scattering and for inelastic scattering to the first five excited states of Zr^{90}. The elastic and 2^+ inelastic functions are normalized to 10 at their maximum values, while the other functions are normalized to equal the 2^+ off-resonance at 6.70 MeV, thereby emphasizing the relative strength of the resonance in the various channels. From these data it can be seen that the resonance in the inelastic channels is strongest to the 2^+ state, which rises above off-resonance background by a factor of 2.8, followed by the 0^+ which rises by 2.0, and the 4^+ which rises by 1.5. The odd parity 5^- state and the 3^-, 4^- doublet[2] do not appear to be fed by the resonance.

The strength of the $d_{3/2}$ resonance to the 2^+ state makes this resonance an ideal subject for a spin-flip study because of the large cross section and the relatively high energy (2.18 MeV) de-excitation gamma ray from the 2^+ to the ground state used in the spin-flip correlation measurement.[1] The limitations of the spin-flip measurement technique restricted its application to the inelastic excitation of the 2^+ state. Figure 20-3 shows the spin-flip excitation function at 90°, 140°, and 170°, along with the 2^+ excitation at 170° which is shown for reference. Rather surprisingly, the spin-flip probability for inelastic scattering to the 2^+ state is remarkably constant as a function of energy, in contrast to the cross section. This indicates that the spin-flip and non-spin-flip con-

tributions to the cross section are maintaining an essentially constant ratio even though their magnitudes change by almost a factor of three on the resonance.

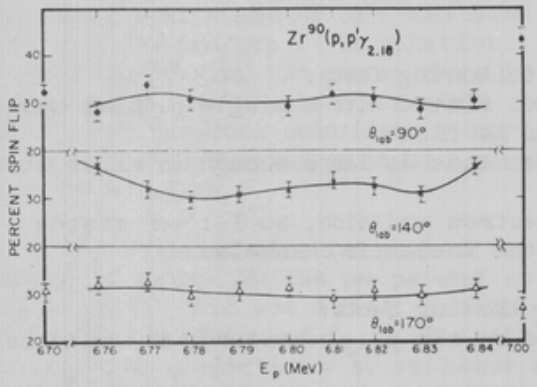

Fig. 20-3. $Zr^{90}(p,p')Zr^{90*}(2^+)$ spin-flip excitation functions at 90°, 140°, and 170°.

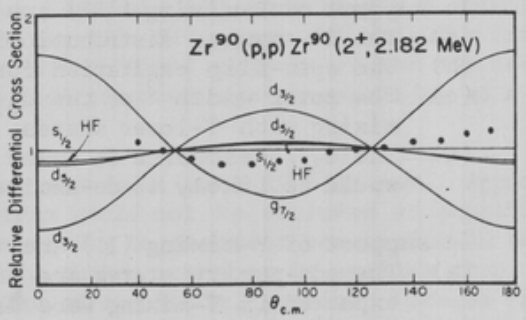

Fig. 20-4. Experimental and calculated $Zr^{90}(p,p')Zr^{90*}(2^+)$ angular distributions on the 6.80 MeV $d_{3/2}$ analog resonance.

Figure 20-4 shows the measured angular distribution for inelastic scattering to the 2^+ on-resonance. Calculated angular distributions are also shown corresponding to the decay of the $d_{3/2}$ resonance by pure $s_{1/2}$, $d_{3/2}$, $d_{5/2}$, and $g_{7/2}$ waves, and by a mixture of these waves predicted by the Hauser-Feshbach theory applied to the outgoing channel only. As can be seen, only the $g_{7/2}$ distribution gives a concave distribution similar to the data, but the angular dependence of the $g_{7/2}$ distribution is much stronger than that of the data.

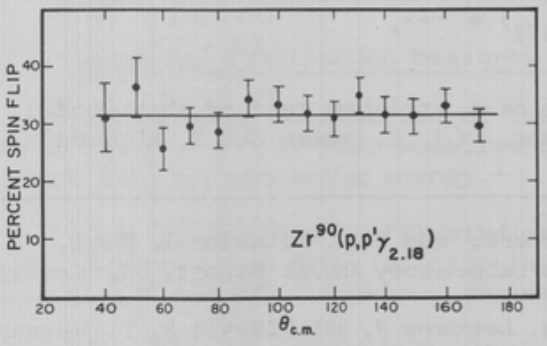

Fig. 20-5. $Zr^{90}(p,p')Zr^{90*}(2^+)$ spin-flip angular distribution on the 6.80 MeV $d_{3/2}$ analog resonance.

Figure 20-5 shows the on-resonance spin-flip probability angular distribution. It is seen that within experimental error there is no strong angular dependence in the spin-flip probability.

In order to understand the decay of the $d_{3/2}$ resonance to the Zr^{90} 2^+ state and its bearing on the configuration of the $d_{3/2}$ state, let us consider the possible ways in which this decay can take place: (I) the $d_{3/2}$ state can decay by a single partial wave; (II) the $d_{3/2}$ state can, because of a mixed wave function, decay by two or more partial waves whose amplitudes will interfere in the differential cross section; (III) the $d_{3/2}$ state, because of its wave

function cannot decay directly to the 2^+ state, can mix with T-lower states of the same spin and parity, and these states can then decay to the 2^+ state.

Possibility (I) may be ruled out at once because the observed angular distribution cannot be fitted by assuming a single partial wave, as was seen in Fig. 20-4.

In support of T-mixing (III) are the following facts:

(a) The 2^+ angular distribution is not fitted with a single partial wave.
(b) The spin-flip excitation function is flat.
(c) The total width [3] of the $d_{3/2}$ resonance is large enough to allow some mixing with T-lower states.
(d) The $d_{3/2}$ resonance is bound to neutron emission, so T-lower states would be likely to de-excite in the inelastic channels.

In support of Ψ-mixing (II) are the following facts:

(a) The odd-parity states are not fed by the $d_{3/2}$ resonance, as would be expected if T-mixing were large.
(b) The 2^+ angular distribution is not fitted with a Hauser-Feshbach mix of the partial waves which would be expected to result from T-mixing.
(c) The 2^+ angular distribution can be fitted by a mixture of the s- and g-wave distributions, in a 2:1 ratio. Since $s_{1/2}$ and $g_{7/2}$ waves cannot satisfy a triangular relationship with the incident $d_{3/2}$ waves, there will be no interference between these two contributions and we may simply add cross-sections. Other combinations of partial waves might also fit the observed 2^+ angular distribution, but these would interfere strongly and would probably produce a non-flat spin-flip angular distribution.

We feel that while T-mixing cannot be eliminated, the preponderance of evidence is on the side of a strong component of the 2^+ plus s and g waves in the $d_{3/2}$ state configuration. If one assumes this to be the case, a rather simple calculation using proton penetrabilities gives a representation of the $d_{3/2}$ wave function of

$$\Psi_{d_{3/2}} \simeq \cdots + \Psi_{2^+}(0.05\ s_{1/2} + 0.95\ g_{7/2}) + \cdots .$$

This rather definite prediction could serve as a stringent test of shell-model calculations in the Zr^{90}+p and Zr^{90}+n systems. (J. G. Cramer and P. Richard)

---

1. F. H. Schmidt, R. E. Brown, J. B. Gerhart, and W. A. Kolasinski, Nucl. Phys. *52*, 353 (1964); Nuclear Physics Laboratory Annual Report, University of Washington (1965), p. 22.
2. D. L. Hendrie and G. W. Farwell, Phys. Letters *9*, 321 (1964); R. T. Wagner, E. R. Shunk, and R. B. Day, Phys. Rev. *130*, 1926 (1963).
3. J. D. Fox, Florida State University (private communication).

IV. PHOTONS FROM NUCLEAR REACTIONS

21. Double-γ Decay of Ge^{72}

The search[1] for a two photon transition between the 0^+ first excited state and the ground state of Ge^{72} has been made by bombarding a thick target of $Ge^{72}O_2$ with 4.8 MeV protons. The relatively long (.3 μs) lifetime of the state was exploited by pulsing the proton beam in 1 μsec intervals and recording γ-γ coincidences only when the beam was off. Two NaI crystals 60° apart and shielded from each other detected coincident γ rays. The pulse-height outputs of the two detectors were connected as inputs to the on-line computer system operating as a 32 × 64 analyzer.

No evidence of a two-photon transition was found in a 12 hour run. Approximately 30 counts in the two parameter spectrum could not be excluded as possible 2-γ events. This set a limit for the ratio of 2-γ to electron conversion in the 0^+ to 0^+ transition of $\Gamma_{2\gamma}/\Gamma_c \leq 6\times10^{-5}$. This number seems to be smaller than theoretical predictions[2] by at least an order of magnitude, possibly because of error in estimating the strength and position of the giant dipole resonance in Ge^{72}. The accuracy of the experiment was limited by positron activity induced in the O^{18} present in the target by the (p,n) reaction, and by neutron-capture γ rays in cascade from $n+Al^{27}$ in the walls of the chamber.

The Ge^{72} target has been reduced to the metallic form and the experimental configuration is being redesigned to eliminate the background from neutron capture γ rays. Another run is planned in the near future. (J. P. Allen, W. J. Braithwaite, J. G. Cramer and C. F. Williamson)

---

1. Nuclear Physics Laboratory Annual Report, University of Washington (1966), p. 44.
2. Most of the theoretical work is summarized in D. E. Albarger and P. D. Parker, Phys. Rev. *135*, B294 (1964).

---

22. Gamma Ray Polarization Measurement

The circular polarization of the gamma rays from the 4.43 MeV 2^+ first excited state of C^{12} is being measured at an alpha scattering angle of 19° (lab) and at 22.5 MeV bombarding energy.[1]

Initial in-plane (α,α'γ) studies in conjunction with previous in-plane angular correlation data[2] indicate that the polarization measurement should be made at 19° and 89° (laboratory angles).

The measurements are being carried out with two liquid nitrogen cooled alpha particle counters,[3] and total alpha particle counting rates as high as 70,000 counts per second have been successfully handled by the electronics; however, alpha beam limitations[4] have prevented us from operating at this level. For the

19° measurement 60 namp of beam on target would satisfy our beam requirement while at 89° we will probably be able to use as much as 200 namp on target.

To make the measurements will require the observation of about 2.5×10^5 true coincidence events between each alpha counter at 19° and the polarization sensitive gamma counter and about 10^5 true events between each alpha counter at 89° and the polarization sensitive gamma counter. At maximum counting rates these measurements should require about seven days and three days, respectively, of continuous data collection. At somewhat less than the maximum data collection rate (the alpha beam current was relatively low) during a ten day run a total of about 1.2×10^5 true events were observed at the 19° point.

The data dumping and analysis is being done by use of the SDS 930 computer and a link tape program[5] which allows greatly enlarged use of the computer by effectively increasing the memory space for program storage. (T. D. Hayward, D. M. Patterson, F. H. Schmidt and J. R. Tesmer)

---

1. Nuclear Physics Laboratory Annual Report, University of Washington (1966), p. 44.
2. W. W. Eidson, J. G. Cramer, D. E. Blatchley, R. D. Bent, Nucl. Phys. *55*, (1964) p. 6B-692.
3. Nuclear Physics Laboratory Annual Report, University of Washington (1966), p. 83.
4. Section 47 of this report.
5. Section 39 of this report.

---

23. Intensity Distributions of Rotational E2 Gamma Rays Following (α,3n) and (α,4n) Reactions

This work is a follow-up of the study of rotational gamma rays following (α,3n) reactions which was presented in last year's annual report.[1] In that study the relative intensities of the rotational transitions gave a picture of the angular momentum distribution in the assembly of residual nuclei toward the end of the particle-photon evaporation cascade. The puzzling result was that the average residual nucleus had much less angular momentum in the late stages of the cascade than any simple theoretical estimate predicted.

It was suggested in last year's study that the angular momentum discrepancy might be explained in part by a systematic error in the assumed detector efficiency. Accordingly, the efficiency of the detector [Ge(Li), 1 $cm^2 \times 4$ mm], was remeasured using a larger number of gamma sources. The sources were standardized with a 3" x 3" NaI crystal whose efficiency is known.[2] This remeasurement confirmed the earlier efficiency measurement.

It was mentioned last year that the low intensities at high J might come about because nuclei of high J tend to emit more photons at the expense of neutrons. Such an effect would make the excitation functions for the (α,3n) reaction

dependent upon the J value of the compound nucleus originally formed in the bombardment. Excitation functions for higher J events would be shifted to higher energies. Such shifts would be reflected in a rapid change of the rotational line intensity pattern with bombarding energy. To test this conjecture, degrader foils were used to vary the cyclotron bombarding energy in 2 MeV steps from 32 to 42 MeV. It was found that the median J in the rotational band increased only about 2% per MeV increase in bombarding energy. This shift is too small to help explain the anomalously low median J at which the cascade enters the rotational band.[3]

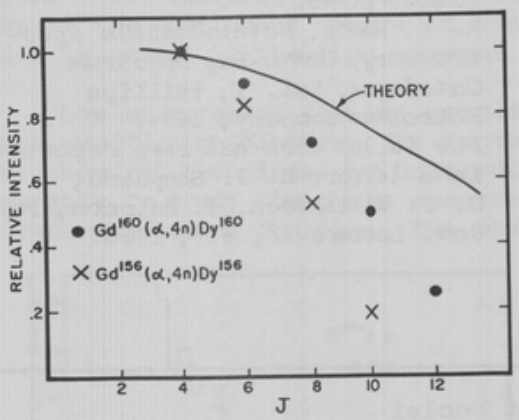

Fig. 23-1. The relative intensities (normalized to the $4^+ \rightarrow 2^+$ transition) of the transitions in the ground state rotational bank of Dy^{160} and Dy^{156}. These nuclei were produced by 42 MeV α bombardment of Gd^{160} and Gd^{156} respectively. The abscissa, J, is the spin of the radiating state. The $2^+ \rightarrow 0^+$ transition is not shown because of uncertainties in internal conversion.

Since the neutrons in the evaporation cascade are known (from their angular distributions) to remove very little angular momentum, the angular momentum loss must occur during the photon cascade which starts after the chain of neutron evaporations and leads finally into the rotational band. To investigate the effect of the length of this photon cascade chain on the final angular momentum distribution, it was decided to compare distributions from some neutron-rich targets with those from targets of isotopes lying close to the stable valley. The isotope pairs chosen for study were (Ge^{156}, Gd^{160}), (Er^{166}, Er^{170}) and (Yb^{172}, Yb^{176}).

In the bombardment of the neutron-rich isotopes the predominant reaction at the maximum α particle energy of our cyclotron (42 MeV) is the (α,4n) reaction. Intensities of rotational lines out to the $12^+ \rightarrow 10^+$ transition were measured and it was found (Fig. 23-1) that the intensity pattern was essentially the same as that for the (α,3n) studies of odd A targets reported last year.

With the stable-valley isotopes the resulting gamma-ray spectra are much more complex than for the neutron-rich isotopes. The (α,4n) rotational lines must be sorted out from a large number of as yet unidentified lines. These other lines are probably due to (α,3n) reactions going to odd A isotopes; see, for example, Fig. 23-2. The complexity of these spectra makes it difficult to determine the intensities of the various lines because of uncertainties associated with background subtraction. An attempt is being made to develop a better data analysis program than we now have. However, it was possible tentatively to identify rotational lines resulting from the (α,4n) reactions in the bombardment of Gd^{156} and Yb^{172}, and to measure their relative intensities. It was found in these preliminary data that the intensities fall off somewhat faster with increasing J for the stable-valley targets than they do for the neutron-rich targets. This implies that the average photon cascade is

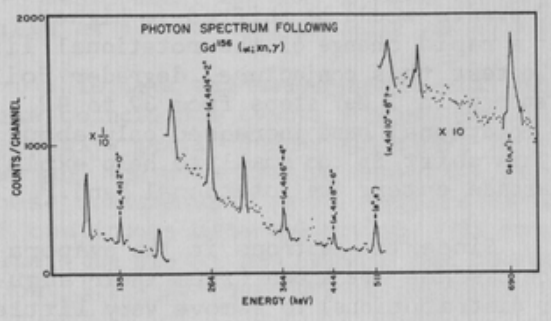

Fig. 23-2. Photon spectrum following bombardment of Gd^{156} with 42 MeV α particles. The spectra were measured with a 1 $cm^2 \times 4$ mm Ge(Li) Solid State detector. The solid line is intended only to guide the eye. A tentative identification of the lines in the ground state rotational band of Dy^{156} is indicated.

longer for the stable valley targets. We have not yet attempted to use the data on the J distributions to obtain quantitative estimates of effective photon chain length. (S. Ferguson, I. Halpern, and C. F. Williamson)

---

1. Nuclear Physics Laboratory Annual Report, University of Washington, (1966) p. 49.
2. R. L. Heath, *Scintillation Spectrometry, Gamma-Ray Spectrum Catalogue*, Vol. 1, Phillips Petroleum Company, 1964.
3. The (α,3n) work has been reported in a letter: B. J. Shephard, C. F. Williamson, I. Halpern, Phys. Rev. Letters *17*, 806, 1966.

---

24. Studies of Radiations from Medium Weight Nuclei

An investigation has been started of the radiations which are strongly excited in the bombardment of certain isotopes in the A=100 region by 42 MeV α particles. A Ge(Li) detector is being used and an energy range up to about 1 MeV is being explored. The purpose of this study is two-fold. First, residual nuclei can be produced whose low lying level structure has not been studied before and one can hope to provide some new spectroscopic information for species away from the stable valley. Second, the relative intensities of lines proceeding between states of known J may yield additional insight into the question discussed in the previous section, namely the way in which angular momentum is removed from a cooling nucleus by a photon cascade. To complement these studies, work has also begun on an investigation of the photon spectrum emitted by some of the targets up to energies of 10 MeV. For this purpose a NaI detector is being used.[1]

So far, the targets that have been bombarded include rhodium, niobium, Cd^{113}, and nine tin isotopes. Some vibrational states in tellurium isotopes which are produced by (α,3n) and (α,4n) reactions on tin have been identified. Many other states have been seen but have not yet been identified. The analysis is continuing. (S. Ferguson and I. Halpern)

---

1. See Section 25 of this report.

---

25. High Energy Photons Emitted from Nuclei

Last year[1] and the year before[2] we reported measurements of high energy (∿15 MeV) photons which were observed from both heavy and light element targets. Typically a heavy target gave a measurable yield of such photons only at the highest excitation energies that were reached at our accelerators (e.g. in bombardments with 42 MeV α particles at the cyclotron or 21 MeV He^3 particles at the tandem). The heavy element photon spectra were continuous. The spectra from lighter targets consisted of discrete lines and were observable even at lower bombarding energies. Much of the year was spent in improving the photon detector system - for example, the reduction of pileup which interferes with the observation of the continuous spectra in heavy elements and the improvement in resolution which is useful in the light element studies (see Sec. 36).

One measurement that was carried out during the year was a study of the (p,γ) reaction on bismuth. The capture cross-section had been measured with radiochemical techniques for bombarding energies, E_p, from 6 to 150 MeV[3] and we were able to study the photon spectrum at E_p=15 and 16 MeV (near the peak of the capture excitation function. The observed spectra are shown in Fig. 25-1 and 25-2.

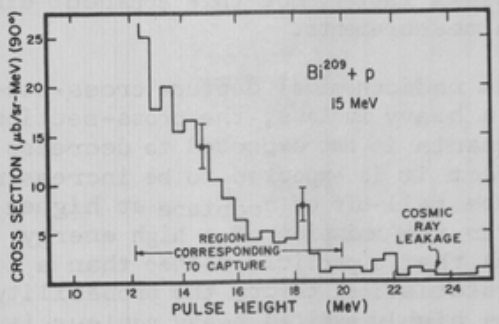

Fig. 25-1. High energy gamma ray spectrum from 15 MeV proton bombardment of Bi^{209}.

By integrating these spectra between the maximum possible photon energy and an energy lower than this by the binding energy of a neutron to the compound nucleus, one can judge whether the capture may be accounted for by the prompt emission of primary quanta to states from which particle emission is not possible. Last year a similar comparison of integrated photon yields and measured capture cross-sections was reported[1] for alpha particle capture in Sn^{112} and it was found that the two cross-sections were in reasonable accord. However the number of counts in the photon spectra was small and the statistical accuracy

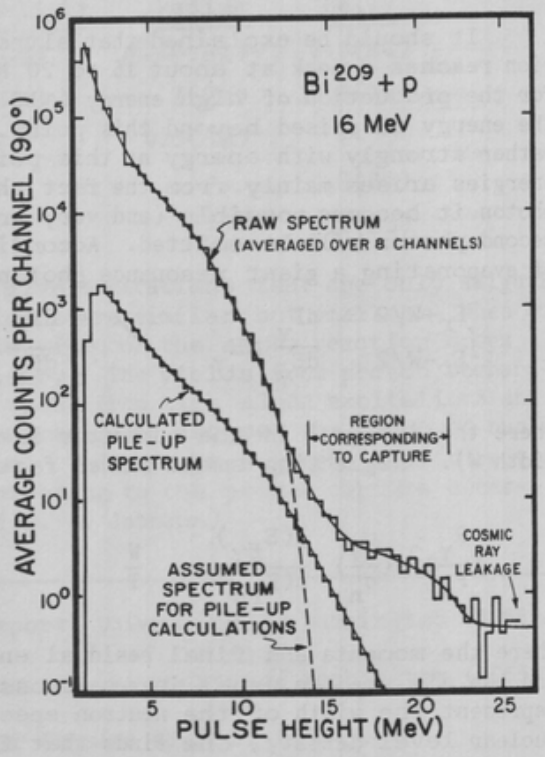

Fig. 25-2. Total gamma ray spectrum from 16 MeV proton bombardment of Bi^{209}.

of the comparison was consequently poor. The counting rates in the $Bi^{209}(p,\gamma)$ study were much better.

To determine the photon yield cross section in $Bi^{209}(p,\gamma)$ a rough efficiency of 20% and isotropic emission were assumed. In previous measurements of high energy spectra the effect of pileup had been assumed to be negligible. To test this assumption an approximate calculation of the pileup spectrum was made using the data from the 16 MeV proton bombardment. This calculation, though rough, showed that the fraction of high energy pulses due to pileup was not negligible. The results of the capture cross-section comparisons are shown below:

Proton Energy (MeV)	Radiochemical Cross-section (mb)	Photon Yield Cross-section (mb)	
		No Correction	With Pileup Correction
15	0.65	0.64	----
16	0.85	1.17	0.98

It is seen that within about 20% the radiochemical and photon-yield cross-sections agree. The energy dependence of the latter seems faster, but this apparent difference may arise in part from errors in both measurements.

It should be explained that although the radiochemical capture cross-section reaches a peak at about 15 to 20 MeV in a heavy nucleus, the cross-section for the production of high energy (~15 MeV) quanta is not expected to decrease as the energy is raised beyond this point. In fact it is expected to be increasing rather strongly with energy at this point. The fall-off of $\sigma_{capture}$ at higher energies arises mainly from the fact that after the emission of a high energy photon it becomes possible (and very probable) that a particle rather than a second photon will be emitted. According to statistical theory the probability of evaporating a giant resonance photon from a highly excited heavy nucleus is

$$\int_{E_r-W/2}^{E_r+W/2} \frac{d\Gamma_\gamma}{dE_\gamma} dE_\gamma \Big/ \int_0^\infty \frac{d\Gamma_n}{dE_n} dE_n$$

where the integral in the numerator is across the giant resonance (energy E_r, width W). Neglecting small number factors, this ratio is

$$\left(\frac{P_\gamma}{P_n}\right)^2 \left(\frac{\sigma_\gamma}{\sigma_n}\right) \frac{\rho(E_{f\gamma})}{\rho(E_{fn})} \cdot \frac{W}{T}$$

where the momenta and final residual energies E_f are appropriate average values, and the σ's are the usual inverse cross-sections. The temperature T is meant to represent the width of the neutron spectrum. Using for ρ the popular Fermi gas nuclear level density, one finds that for a heavy nucleus excited to 40 MeV, the chance of evaporating a giant resonance photon is about 0.1%. This estimate is in good accord with our earlier measurements.[1] At an excitation energy of 30 MeV the probability is about 3 times smaller and at 20 MeV it is over 30 times smaller. The reason for the rapidly increasing probability to evaporate giant

resonance quanta at higher energy arises because the inhibition against their emission is in part energetic. If $\Delta=E_R-E_n$ is the average energy it costs to evaporate a giant resonance quantum in place of a neutron, then the ratio of level densities appearing above involves the Boltzmann factor $e^{-\Delta/T}$. At higher excitations T increases and this exponential factor decreases rapidly. Our object in studying the emission of high energy quanta from heavy nuclei is in part to see to what extent their yields and spectra are in accord with expectations based on elementary statistical theory.

If we examine some of our previous data we find that, in general, statistical theory seems to describe the dependence of cross-section on energy. The most recent data on proton capture do not, however, fit the general pattern. Table 25-1 gives the 90° photon yield at 16 MeV for the various previous experiments including the yields from 15 MeV proton bombardment of Ho^{165} and Bi^{209} measured this year.

Table 25-1. Cross-sections (μb/sr-MeV) for photon emission from a number of target elements under a variety of bombarding conditions.

	Target Mass Number		
Projectiles	Medium-light	Medium	Heavy
42 MeV α	15(Co)	10(Ag)	2.5(Au)
21 MeV He^3	8(Co)	7(Sn)	≤0.3(Au)
18 MeV α	--	0.5(Sn)	--
15 MeV protons			7(Bi)
			12(Ho)

One notes that since 21 MeV He^3 particles give excitations that are only slightly lower than those from 42 MeV alphas the yields are similar but smaller. When one lowers the excitation energy to ∿20 MeV the yield of the alpha reaction drops drastically as predicted by statistical theory. The yields from proton bombardments at 15 MeV are however comparable to those from high alpha excitations and seem not to fit into the statistical framework if one assumes the compound nucleus formation cross sections are about the same. This result suggests that direct or so-called semi-direct capture may be contributing to the proton capture cross-section. (S. M. Ferguson, I. Halpern, and D. L. Johnson)

---

1. Nuclear Physics Laboratory Annual Report, University of Washington (1966), p. 53.
2. Nuclear Physics Laboratory Annual Report, University of Washington (1965), p. 55.
3. P. J. Daly and P. F. D. Shaw, Nuclear Physics *56*, 322 (1964).

V. COMPOUND NUCLEAR REACTIONS

26. Investigation of the $O^{16}(O^{16},\alpha)Si^{28}$ Reaction

The study of this reaction, initiated last year,[1] has been continued. The initial goal of studying the energy dependence at 54 MeV (which corresponds to formation of the S^{32} compound nucleus with the same excitation energy as in the reaction of Si^{28} with 42 MeV alphas) has been abandoned due to the very small cross section and the small beam currents presently available at this energy. Current emphasis is on measurements of the coherence width of the compound nucleus and measurement of the average cross section and angular distribution for 36 MeV O^{16} ions. These measurements will enable characterization of the nuclear level density of S^{32} at high excitation energy and high angular momentum. These results will enable interesting comparisons with similar work in progress elsewhere[2] involving lower energies and angular momentum.

Oxygen-16 ions were produced in the negative ion source of the University of Washington tandem Van de Graaff accelerator using a source mixture of hydrogen and oxygen gases and a BaO coated Pt mesh filament. The accelerated beam was magnetically analyzed to select the charge state +5 or +6, depending on the energy desired. The beam was then directed into the 60 inch scattering chamber. The following targets were used: 1) a self-supporting NiO target (150 $\mu g/cm^2$) for "thick" target excitation functions, 2) a target of WO_3 (305 $\mu g/cm^2$) evaporated onto Au foil (850 $\mu g/cm^2$) for "thick" target angular distributions, 3) a target of WO_3 (29 $\mu g/cm^2$) evaporated onto Au foil (850 $\mu g/cm^2$) for "thin" target excitation functions.

Reaction product alpha particle energies were measured using lithium-drifted and surface barrier detectors. A position-sensitive detector was also used in measuring angular distributions. The detector signals were amplified and presented either to a conventional pulse height analyzer or to the on-line computer operated in a real-time mode as a series of 256 channel pulse height analyzers. The computer was also used on-line as a two parameter pulse height analyzer for signals from the position sensitive detector.

The following measurements were made: 1) thick target excitation functions determined in 1 MeV increments from 31.6 MeV to 36.6 MeV excitation energy. Energy resolution was 0.73 MeV to 0.67 MeV. 2) thick target angular distributions determined at 34.6 and 35.6 MeV. Energy resolution was 0.95 MeV. 3) thin target excitation functions determined in 50 keV increments for the compound nuclear excitation energy from 34.1 MeV to 35.6 MeV. Energy resolution was 60 keV. In each case, alpha particles corresponding to formation of the residual Si^{28} nucleus in the 0^+ ground state and the 1.78 MeV 2^+ excited state were completely resolved; and it is to these two states that the remainder of the discussion refers.

The thick target excitation function was measured over an energy span larger than that covered in the fluctuation studies to determine if the average cross section was dependent on energy. There was no evidence from these measurements for a significant change in the average cross section as the excitation energy was increased from 31.6 MeV to 36.6 MeV.

The thick target angular distribution for the ground state reaction at 34.6 MeV excitation energy is illustrated in Fig. 26-1. The solid curve is the square of the Legendre function for L=12. This comparison indicates that the cross section for the ground state reaction involves primarily J=12 spin states in the compound nucleus. Only even spin compound states are formed, since the target and projectile are identical bosons. The analysis of the angular distribution measurements at 35.6 MeV has not been completed.

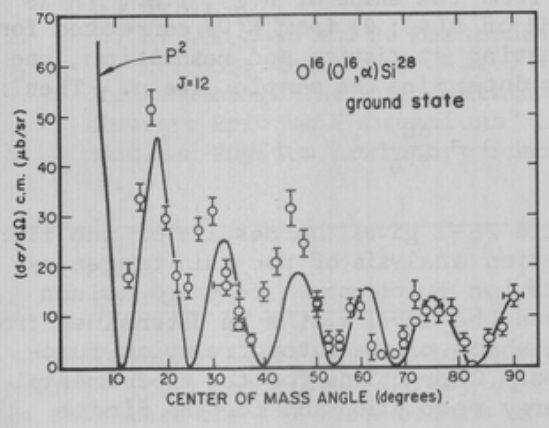

Fig. 26-1. The experimental angular distribution at 34.6 MeV excitation energy compared with that expected (solid line) if the compound spin state were J=12.

The narrow energy width for the thin target data should permit the observation of compound nuclear statistical fluctuations.[3] The thin target excitation functions for the ground and first excited states at 26° c.m. are shown in Fig. 26-2. The thin target excitation function data were treated according to the methods of Gibbs[4] to extract compound nuclear level widths.

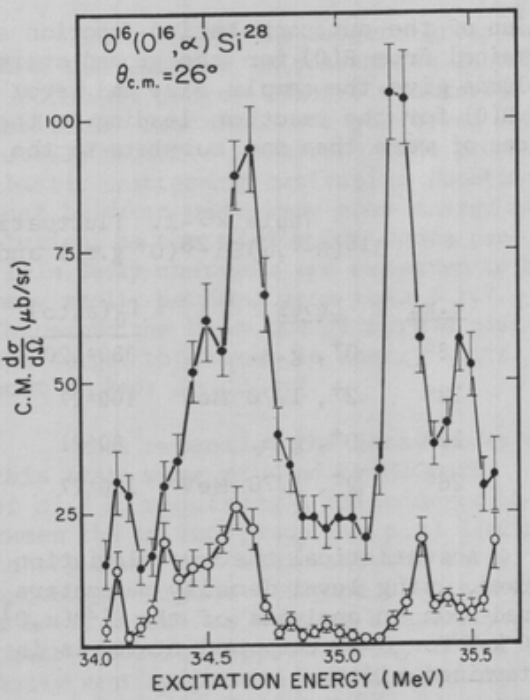

Fig. 26-2. The open circles are the experimental cross sections for the reaction $O^{16}(O^{16},\alpha)Si^{28}(0^+,g.s.)$ at an excitation energy of 34.6 MeV. The full circles are the cross sections for the 2^+ first excited state.

The autocorrelation function $R(\varepsilon)$ may be defined as:

$$NR(\varepsilon)=\frac{\langle(E+\varepsilon)\sigma(E)\rangle-\langle\sigma(E)\rangle^2}{\langle\sigma(E)\rangle^2}=\frac{1}{1+\frac{\varepsilon^2}{\Gamma_0^2}}$$

where $\sigma(E)$ is the cross section for one given reaction exit channel at the excitation energy E, ε is a variable energy increment, Γ_0 is the compound nuclear level width, and N is the number of independent states for the exit channel of interest. An autocorrelation function for the ground state reaction at 26° c.m. is shown in Fig. 26-3. R(0) has been corrected for experimental counting statistics.

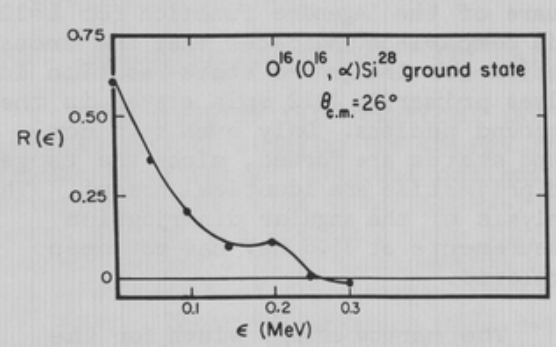

Fig. 26-3. The auto correlation function for cross sections measured between 34.1 and 35.6 MeV excitation energy as discussed in the text.

One may determine Γ_0 in two ways from the auto correlation functions: 1) from the shape of $R(\varepsilon)$, i.e., Γ_0 is FWHM of $R(\varepsilon)$; 2) from $R(0)$ corrected for counting statistics and resolution, one may determine the sample size n. Then[4]:

$$n = \frac{\Delta E}{\pi \Gamma_0} + 1$$

Table 26-1 gives the results of the fluctuation analysis of the thin target excitation functions. The third column gives the level widths as determined from the shape of the autocorrelation function. Corrections for the experimental energy resolution and for the finite sample size have been included. The uncertainty is due to the uncertainty associated with the small sample size. The fourth column gives the experimental value of the autocorrelation function at $\varepsilon=0$. An estimate of n and of Γ_0 can be obtained from $R(0)$ for the ground state reaction since N=1. The fifth and sixth columns give the sample size and level width deduced from $R(0)$. The low values of $R(0)$ for the reaction leading to the 2^+ excited state may be due to contributions of more than one substate to the measured cross section.

Table 26-1. Fluctuation Analysis of Reactions $O^{16}(O^{16},\alpha)Si^{28}(0^+$ g.s.) and $O^{16}(O^{16},\alpha)Si^{28}(2^+, 1.78$ MeV)

c.m.	Level	Γ_0(auto)	R(0)exp	n(R(0))	Γ_0(R(0))	Γ_0(theor)
13°	0^+, g.s.	330±120	0.71	5	120	110
13°	2^+, 1.78 MeV	100±27	0.20			110
26°	0^+, g.s.	80±21	0.63	4.5	130	110
26°	2^+, 1.78 MeV	100±27	0.32			110

A statistical theory calculation of the total level widths has been performed, using level density parameters (a=A/7 and $\mathcal{I}/\mathcal{I}$ rigid=1) which were determined from an analysis of the $Si^{28}(\alpha,O^{16})O^{16}$ reaction.[5] The calculated value of 110 keV for J=12 compound states is in good agreement with the experimentally determined widths.

Statistical model calculations of the average differential cross sections are in progress, and will enable further tests of the level density expression. (C. J. Bishop, J. Norman, R. W. Shaw, and R. Vandenbosch)

1. Nuclear Physics Laboratory Annual Report, University of Washington (1966), p. 64.
2. R. B. Leachman and P. Fessenden, Bull. Am. Phys. Soc. *12*, 206 (1967).
3. T. Ericson, Ann. Phys. (N.Y.) *23*, 390 (1963).
4. W. R. Gibbs, "The Interpretation of Nuclear Excitation Functions at High Energy: Ericson Fluctuations" LA-3266 (1965).
5. Nuclear Physics Laboratory Annual Report, University of Washington (1966), p. 63.

27. Search for a T=2 State in $Mg^{24}(T_z=0)$ *via* Proton Induced Resonances

Several 0^+, T=2 states in $T_z=0$ nuclei have been observed in the isospin allowed (p,t) reaction by Garvey *et al.*[1] $Mg^{26}(p,t)Mg^{24}$ is one example of these. In this case the T=2 state occurs at an excitation energy of 15.43±.07 MeV in Mg^{24}. This puts the state above the proton and alpha separation energy, but still below the neutron separation energy. However, decay by proton emission requires ΔT=1 or 2 and alpha decay is twice T-forbidden (ΔT=2).

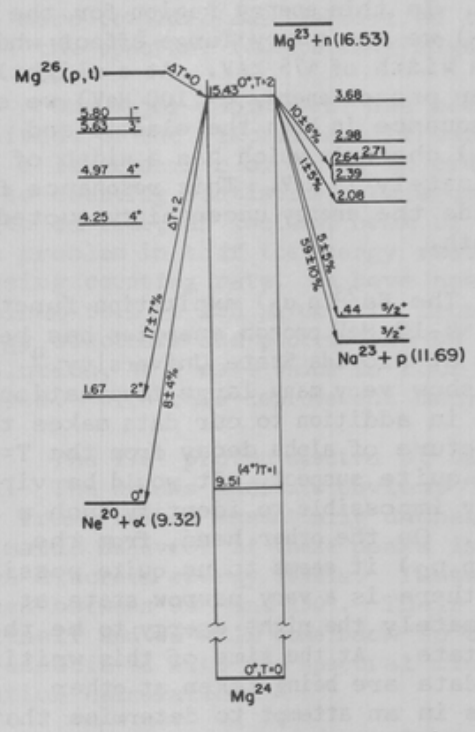

Fig. 27-1. Level scheme of Mg^{24} demonstrating the observed decay of the T=2 state at 15.43 MeV.

A search by the Rutgers group to find these states as resonances in twice T-forbidden proton elastic scattering excitation functions was performed with totally negative results.[2] The proton elastic scattering excitation functions must be taken with very good energy resolution, as the widths for these particle decay channels are expected to be very small, perhaps less than 5 keV. Therefore the beam energy spread plus the target thickness in energy units must be kept to ≤1 keV.

More recently, the decay modes of this state were studied by McGrath *et al.*[3] by requiring a coincidence between the triton group in (p,t) leading to the 15.43 MeV state and the decay protons or alphas. Figure 27-1 contains a level scheme as well as a summary of their results. Approximately 60% of the decay went by proton emission to the ground state (3/2+) of Na^{23} and approximately 5% to the first excited state (0.44 MeV, 2^+) of Na^{23}. A surprisingly large alpha decay (∿8%) to the ground of $Ne^{20}(0^+)$ was found and an even larger decay (∿17%) to the first excited state (1.63 MeV, 2^+) of Ne^{20}.

McGrath *et al.* calculated that this implies that the reduced width for alpha decay is approximately one half that for proton decay, which is rather large when one considers that proton decay can go via T-mixing requiring a minimum of $\Delta T=1$, whereas the alpha decay requires $\Delta T=2$. In their discussion they do not rule out the possibility that the alpha decay eminates from a T=0 (normal state) which is essentially degenerate with the T=2 isobaric analog state.

We have thus undertaken an experiment to remeasure the proton elastic scattering excitation function on Na^{23} at the appropriate energy for this T=2 state in Mg^{24}. In addition we have taken at the same time the (p,α_0) excitation function. The experimental set up consists of a thin ΔE detector (50 micron silicon transmission detector) followed by a 1000 micron E detector. The alpha groups were studied by using the ΔE spectrum with all pass-through particles being gated out and at the same time the $E+\Delta E$ signals were used for the proton spectrum. The data were taken at 170° in the lab.

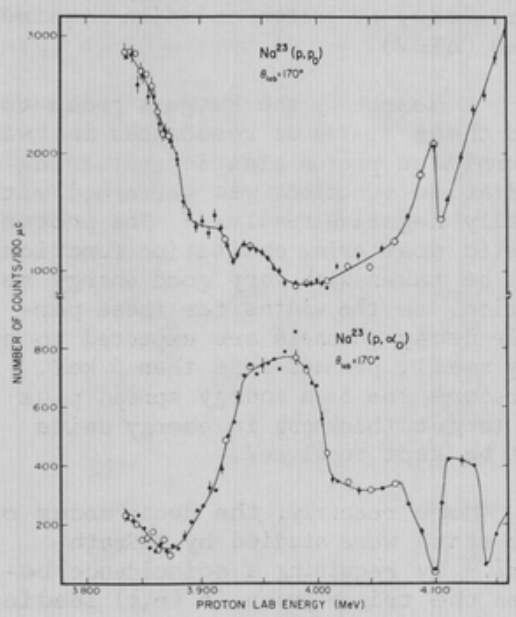

Fig. 27-2. Excitation functions of $Na^{23}(p,p_0)$ and (p,α_0) in the vicinity of the expected T=2 resonance energy (E_p=3.90 .05 MeV).

The results of this experiment are shown in Fig. 27-2. At the expected proton lab bombarding energy of 3.90±.05 MeV we see a very small and narrow (∿8 keV) dip in the proton elastic function. In this energy region for the (p,α_0) we see a very large effect which has a width of ∿75 keV. At a slightly higher proton energy (4.100 MeV) we see a resonance in both the elastic and (p,α_0) channels which has a width of approximately 15 keV. This resonance falls outside the energy uncertainty quoted by McGrath.

The $Na^{23}(p,\alpha_0)$ excitation function from ∿4-12 MeV proton energies has been taken at Florida State University.[4] The data show very many large fluctuations which in addition to our data makes the conjecture of alpha decay from the T=2 state quite suspect. It would be virtually impossible to identify such a state. On the other hand, from the $Na^{23}(p,p_0)$ it seems to us quite possible that there is a very narrow state at approximately the right energy to be the T=2 state. At the time of this writing more data are being taken at other angles in an attempt to determine that there definitely is a state and that it corresponds to an $\ell=2$ (0^+ to $3/2^+$) proton decay. (J. G. Cramer and P. Richard)

1. G. T. Garvey, J. Cerny, and R. H. Pehl, Phys. Rev. Letters *12*, 726 (1964).
2. D. J. Bredin, O. Hansen, G. M. Temmer and R. Van Bree, in *Isobaric Spin in Nuclear Physics*, edited by J. D. Fox and D. Robson (Academic Press, Inc. New York, 1966), p. 472.
3. R. L. McGrath, S. W. Cosper, and J. Cerny, Phys. Rev. Letters *18*, 243 (1967).
4. Adams, Fox, Heydenburg, and Temmer, Bull. Am. Phys. Soc. *6*, 250 (1961).

28. Spectral Fluctuations in the $Al^{27}(d,p)$ Reaction Proceeding to the Continuum

As was discussed in some detail in the 1966 Annual Report,[1] an attempt has been made to study fluctuations in cross sections attributable to overlapping levels at high excitation energies in the residual nucleus. These fluctuations are to be distinguished from the more commonly studied variety of Ericson fluctuations due to overlapping levels in the compound nucleus and, in what follows, they will be referred to as spectral fluctuations. The particular process chosen for study has been the $Al^{27}(d,p)Al^{28}$ reaction. Since the last report, we have acquired more extensive data on this reaction and thereby have been enabled to make more complete calculations of the pertinent correlation functions through which the spectral fluctuations might be identified.

One major improvement has been made in the experimental setup. Since the magnitude of the fluctuations is expected to be small, it is necessary to accumulate a large number of counts in order to reduce the contribution to the structure due to counting statistics. To accumulate the desired number in a reasonable length of time, an incident beam of high intensity is required. But this leads to a problem in that the energy resolution of the detector deteriorates with increasing counting rate. We have now reduced this difficulty by placing a thin aluminum foil ($\sim$ 130 $\mu g/cm^2$) in front of the detection system to eliminate low energy electrons and photons and we can now count, without sacrificing energy resolution, at a rate which is four times faster than that possible when no foil is used. With this improvement many earlier runs have been repeated.

The 170° proton spectra at various incident energies are displayed in Fig. 28-1. The arrows indicate obvious "spurious" peaks whose energies in the laboratory frame remain essentially unchanged at all incident energies shown. The kinematic behavior of these peaks is characteristic of secondary emission between discrete energy levels. These pronounced peaks are not seen at laboratory angles between 90° and 150°. Their origin is, of course, an interesting problem in itself and we will come back to this point later. It is clear that they are not associated with the spectral fluctuations and must be excluded from any correlation calculations.

As is typical of other fluctuation studies, the analysis of our data is couched in terms of the properties of various correlation functions. The most general correlation function with which we shall be concerned may be written as

$$C(\delta,\varepsilon;\theta,\theta',U_{CN}) \equiv \left(\frac{\sigma(U_{CN},U_R,\theta)}{\bar{\sigma}(U_{CN},U_R,\theta)} - 1.0\right)\left(\frac{\sigma(U_{CN}+\delta,U_R+\varepsilon,\theta')}{\bar{\sigma}(U_{CN}+\delta,U_R+\varepsilon,\theta')} - 1.0\right)_{U_R} \qquad (1)$$

where δ and ε are increments in the excitation energies of the compound system, U_{CN}, and of the residual nucleus, U_R, respectively; the variables following the semi-colon are considered to be fixed. Correspondingly, the subscript U_R following the brackets indicates that the average is to be taken over that quantity. With this notation, the self-correlation coefficient at fixed incident energy, SC, would be $C(0,0;0,0,U_{CN})$, while the angle cross-correlation coefficient at fixed incident energy, $AXC(\theta,\theta')$, would be $C(0,0;\theta,\theta',U_{CN})$.

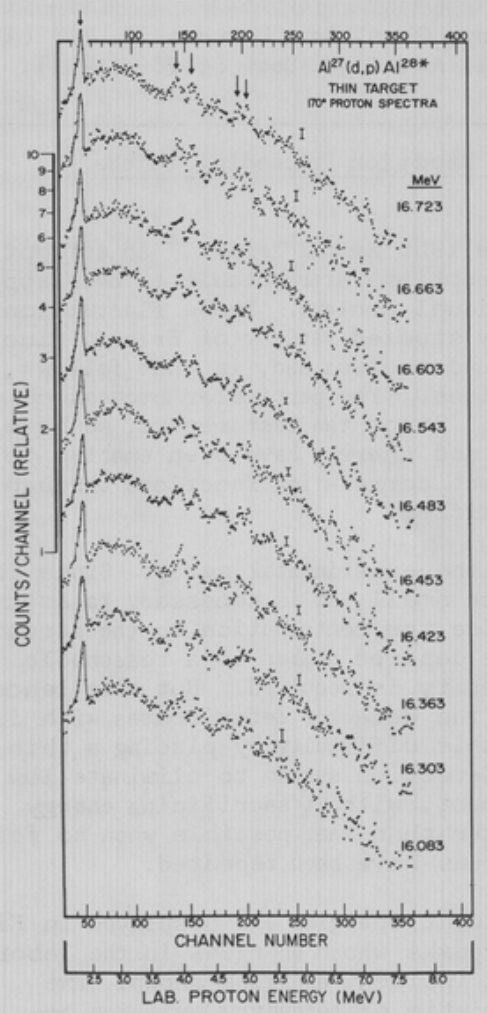

Fig. 28-1. Proton spectra from d + Al^{27} reactions observed at 170° in the laboratory frame. The corresponding laboratory incident energies are indicated. The typical errors due to counting statistics are shown. The arrows indicate the obvious "spurious" peaks whose energies in the laboratory frame remain essentially unchanged at all incident energies.

If the structure observed in the proton spectra is to be attributed to spectral fluctuations, the various correlation functions must have the following properties: (1) the self-correlation coefficient at fixed incident energy, SC, should fall off smoothly as the observation angle is changed from 180° to 90°, where there will be more magnetic substates contributing incoherently to the cross section; (2) similarly, the angle cross correlation coefficient at fixed incident energy, $AXC(\theta,\theta')$, should fall off smoothly as $(\theta - \theta')$ is increased; an angular correlation width α should characterize this behavior.

Further restrictions can be placed on the correlation functions,[2] when the S-matrix is assumed to be a sum of products of Breit-Wigner terms with random partial widths for both the compound and residual system, that is

$$S(U_{CN},U_R) = \sum_{\beta}\sum_{\lambda} \frac{a_{\alpha\lambda}}{(U_{CN} - U_\lambda + i\Gamma/2)} \times \frac{a_{\lambda\beta}}{(U_R - U_\beta + i\gamma/2)} \qquad (2)$$

where α labels the incoming state, while

λ and β refer to the C.N. and residual states with total widths Γ and γ, respectively. These restrictions are: (3) the auto-correlation function at a fixed incident energy, $AC(\varepsilon) \equiv C(0,\varepsilon;\theta,\theta,U_{CN})$, should have a Lorentzian shape, that is be proportional to $[\gamma^2/(\gamma^2 + \varepsilon^2)]$; (4) the energy cross correlation function,[3] $XC(\delta) \equiv C(\delta,0;\theta,\theta,U_{CN})$ should be proportional to $[\Gamma^2/(\Gamma^2 + \delta^2)]$; (5) finally, the general energy correlation function when both δ and ε are different from zero should be proportional to the product of Lorentzian factors, *i.e.*,

$$C(\delta,\varepsilon;\theta,\theta,U_{CN}) \propto \left(\frac{\Gamma^2}{\Gamma^2 + \delta^2}\right)\left(\frac{\gamma^2}{\gamma^2 + \varepsilon^2}\right). \qquad (3)$$

A plot of Eq. (3) with $\Gamma = 2\gamma$ is shown in Fig. 28-2.

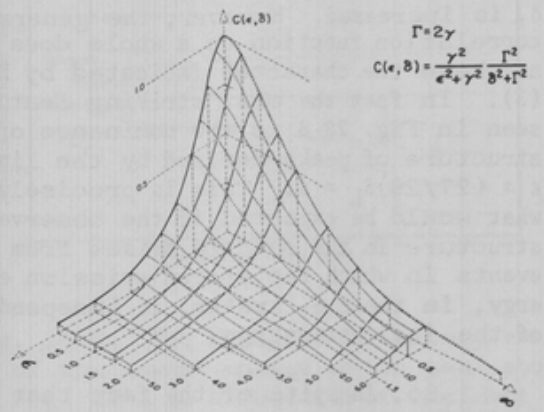

Fig. 28-2. The product of Lorentzian factors is shown as a function of two independent variables, ε and δ. This is the expected shape for the general energy correlation function when computed from spectra exhibiting spectral fluctuations.

In the analysis of the experimental data all correlation functions were calculated with aid of an electronic computer. The functional form of the average cross section was computed for each spectrum by forming the convolution of the spectrum with a Gaussian weighting function. The FWHM of the Gaussian function was taken to be 500 keV, which is roughly 14 times the observed energy resolution. By this method, the local fluctuations will be averaged out, leaving the coarser structure unchanged. The energy interval over which averages have been calculated was chosen to extend from U_R = 13.3 MeV to U_R = 17.3 MeV. As mentioned before, the pronounced "spurious" peaks indicated in Fig. 28-1 were excluded from the calculations by omitting the surrounding energy region from the analysis.

The contribution due to counting statistics is expected to affect only the self-correlation coefficient, since the random statistical fluctuations will average out in the calculation of a cross correlation function. Because of the energy dependence of the average cross section and the small magnitude of observed structure, the contribution to the self-correlation coefficient from counting statistics is difficult to estimate. We circumvented this difficulty by performing a cross correlation calculation on two identical spectra taken at different times; the resulting coefficient can be regarded as the true self-correlation coefficient. Since the correlation coefficients and correlation functions are not strongly dependent on incident energy, we have frequently averaged these quantities over the incident energy.

The results of these calculations are consistent with the conditions (1) through (4) listed above and, in themselves, would be suggestive of spectral fluctuations. In particular, the self-correlation coefficient falls off as the

observation angle is changed from 170° to 90°. The angular cross-correlation coefficient also decreases as $\theta - \theta'$ is increased, where θ was taken to be 170°.

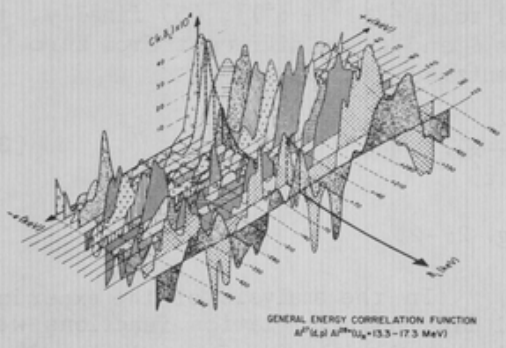

Fig. 28-3.
The general energy correlation function computed from the spectra shown in Fig. 28-1 where the energy regions surrounding the "spurious" peaks indicated by arrows were omitted from the calculations. ε is the incremental change in the residual excitation energy, while δ_L is the incremental change in the laboratory incident energy (the incremental change in U_{CN} is then $\delta = (27/29)\delta_L$). Each curve in the plane perpendicular to the δ_L - axis is an average of several cases with the same δ_L.

The general energy correlation function is displayed in Fig. 28-3. (Here the axis labeled δ is the incremental change in the incident laboratory energy and is equal to $(29/27)\delta_L$.) By looking at the $\delta_L = 0$ plane, it is seen that the auto-correlation function has the expected fall-off as the residual energy increment, ε, is increased; similarly, by examining the $\varepsilon = 0$ plane it is seen that the energy cross-correlation function has the expected fall-off as the compound excitation energy increment, δ, is increased. However, the general correlation function as a whole does not have the character indicated by Eq. (3). In fact the most striking feature seen in Fig. 28-3 is the dominance of a structure of peaks defined by the line $\varepsilon = (27/29)\delta_L = \delta$. This is precisely what would be expected if the observed structure in the spectra arises from events in which the proton emission energy, in the c.m. system, is independent of the incident energy.

So, in spite of the fact that conditions 1-4, necessary for the existence of spectral fluctuations have been met, we are led to a surprising conclusion that the observed structure, in the part of the spectrum remaining after explicit exclusion of the pronounced "spurious" peaks, is still dominated by events similar to those excluded. The reasons why these events satisfy conditions 1-4 will be deferred for the moment.

We now turn to the origin of these "spurious" protons. The conclusion that they are emitted from a state of well-defined energy in the (first) residual nucleus to a discrete final state was mentioned earlier. The energetics of all the possible reaction channels following the formation of a Si^{29} compound nucleus at $U_{CN} = 32.7$ MeV, together with the measured lab energy of the pronounced peaks in Fig. 28-1, suggest that the most probable sequence is one in which states in Si^{28} with excitation energies $\geq$ 14.3 MeV are formed by the $Al^{27}(d,n)$ reaction and the observed protons are emitted from these Si^{28} states.

If this identification is correct, we still have to explain why at this high an excitation energy, where the states are presumably dense although not necessarily overlapping, a relatively few states are preferentially populated by the (d,n) reaction. This circumstance is not easily understood in the context of the statistical model. A possible explanation is that these states are the iso-

baric analogues (IAS) of excited states ($E_x^* > 5.14$ MeV) in Al^{28}. Since it is known that there is sharp structure in the $^{x}(\bar{d},p)$ spectra corresponding to excitation energies up to 10 MeV, it may be expected that similar structure will appear in the (d,n) spectra corresponding to higher excitation energies. This explanation is supported by the fact that isobaric analogues of low-lying states ($E_x^* < 5.14$ MeV) in Al^{28} have been observed,[5] and that proton decay from IAS formed in the $Zr^{90}(d,n)Nb^{91*}$ reaction has recently been reported.[6]

To verify this identification in detail for at least one state, we have measured the threshold of the strongest peak ($E_p = 2.40$ MeV) shown in Fig. 28-1. In Fig. 28-4, the observed laboratory energy of this peak is shown as a function of incident energy together with the calculated energy limits for proton decay to the ground state of Al^{27} from IAS (whose parent analogues are the known levels in Al^{28}) formed in the $Al^{27}(d,n)Si^{28*}$ reaction. From this comparison we can identify this transition as the decay from the isobaric analogue of the 5.14-MeV level in Al^{28} to the ground state of Al^{27}. It is then not unreasonable to assume that much of the rest of the structure in the proton spectra is due to proton decay from other IAS formed in the reaction $Al^{27}(d,n)Si^{28*}$.

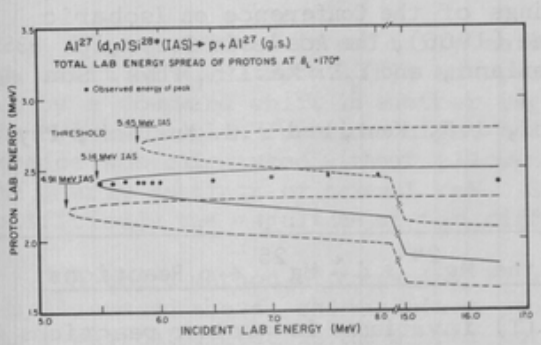

Fig. 28-4. The measured laboratory energy of the lowest energy proton peak shown in Fig. 28-1 as a function of incident deuteron energy. The smooth curves (both solid and dashed) are the calculated energy limits within which the proton decay to the g.s. of Al^{27} from the isobaric analogues of three known levels in Al^{28}, following the $Al^{27}(d,n)Si^{28*}$ reaction, can lie. These three levels have the largest reduced widths among the many levels near $\sim$ 5 MeV of excitation energy.

It yet remains to explain why the pronounced peaks are not seen at angles between 90° to 150° (in contrast to 170°), and why the self-correlation coefficient decreases from 170° to 90°. From the kinematics of these two-step processes, it can be shown that if the (d,n) angular distribution is forward peaked (so that the recoiling Si^{28*} nucleus is backward peaked), the laboratory energy distribution of protons from a given transition is broadened as the angle of observation is changed from 180° to 90°. For the bombarding energies of this experiment, this broadening at 90° is sufficient to bury these peaks in the background. We also note that the fall-off of the auto-correlation function, $AC(\varepsilon)$, and of the energy cross correlation function, $XC(\delta)$, is qualitatively consistent with secondary emission between states of well-defined energy, again because of the broadening effects of recoil upon otherwise narrow peaks.

In conclusion it is clear that if the existance of spectral fluctuations is to be tested, it is necessary to avoid reactions which strongly excite isobaric analogue states (or, in principle, any other limited group of intermediate states). A further outcome of this work has been the suggestion that isobaric analogues of relatively highly excited states can be readily formed in (d,n) re-

actions; of course, isobaric analogues of low-lying states have been observed in many reactions. A more positive confirmation of the nature of the intermediate states excited in the present experiment is now being undertaken, although detailed studies of proton decay from IAS formed in (d,n) reactions are in progress with a different emphasis.[7] (J.S. Blair, D. Bodansky, N. Cue, and C.D. Kavaloski)

1. Nuclear Physics Laboratory Annual Report, University of Washington (1966), p. 65.
2. R.O. Stephen, private communication.
3. Eq. 3 of Ref. 1.
4. T. Ericson, Ann. Phys. (N.Y.) *23*, 230 (1963); D.M. Brink and R.O. Stephen, Phys. Letters *5*, 77 (1964).
5. A.A. Jaffe and M. Harchol, "Proceedings of the Conference on Isobaric Spin in Nuclear Physics", Tallahassee (1966), The Academic Press, p. 835; J.M. Clavert, A.A. Jaffe, A.E. Litherland, and E.E. Maslin, Phys. Soc. *A68*, 1008 (1955).
6. C.F. Moore, C.E. Watson, S.A.A. Zaidi, J.J. Kent, and J.G. Kulleck, Phys. Rev. Letters *17*, 926 (1966).
7. See Sec. 10.

29. Test of Time-Reversal Invariance in the $Mg^{24} + d \rightleftarrows Mg^{25} + p$ Reactions

An experiment to test time-reversal (T) invariance in nuclear reactions is now essentially complete. This experiment, which has been described previously,[1,2] involves measuring the cross section ratio $R(E) = \sigma(E,\theta_2)/\sigma(E,\theta_1)$, for the $Mg^{24} + d \rightleftarrows Mg^{25} + p$ reactions, where E is the excitation energy in the Al^{26} system and θ_1 and θ_2 are (c.m.) angles corresponding to maxima in the angular distribution. The test of T invariance comes in testing the equality of R_d, the ratio measured in the (d,p) reaction, and R_p, the ratio measured in the inverse (p,d) reaction.

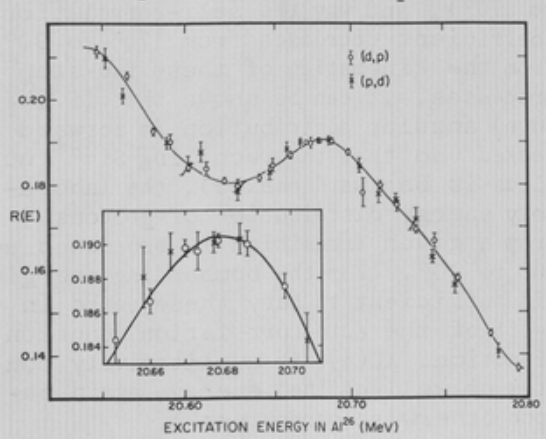

Fig. 29-1. Excitation functions for the cross section ratios R_d and R_p. The solid curve is an eight term Fourier cosine series fitted to the data. The indicated uncertainties include both statistical and systematic contributions.

The principal data of this experiment consist of excitation functions for $R_d(E)$ and $R_p(E)$, which are shown in Fig. 29-1. There are several ways in which a comparison between R_d and R_p can be made. The simplest quantitative way is to use the accurate points nearest the peak: R_d at E = 20.679 MeV and R_p at E = 20.678 MeV. These ratios, $R_d = 0.1902 \pm 0.0004$ and $R_p = 0.1901 \pm 0.0006$, were found to agree to within 0.4 percent (standard deviation).

However, this simple method does not take advantage of all the available information, since only two data points are used. One way of comparing all the data is to fit a function $R_c(E)$ to all the data points of $R_d(E)$ and $R_p(E)$, taken together. Then the difference be-

tween the average deviations of $R_d(E)$ and $R_p(E)$ from $R_c(E)$ is

$$\varepsilon = \overline{R_d(E_i) - R_c(E_i)} - \overline{R_p(E_j) - R_c(E_j)},$$

where E_i and E_j are the energies at which the (d,p) and (p,d) measurements were made. (Note that the introduction of the function $R_c(E)$ is necessitated in this method by the fact that the sets of energies, E_i and E_j, are not identical.) The function $R_c(E)$ was chosen to be an eight term Fourier cosine series fitted to all the data points. This function is shown in Fig. 29-1, where it can be seen to give a reasonable, smooth fit to the data. The resulting ε was found to be 0.0002 ± 0.0005. When expressed as a fraction of the mean value of R, over the energy interval considered, this is a difference of $(0.1 \pm 0.3)\%$.

This procedure is not fully satisfactory because it measures only an average shift of $R_d(E)$ from $R_p(E)$; an upward shift in one energy region could be offset by a downward shift in another region, giving a zero value for ε even though the two excitation functions might not be identical. Furthermore, the mean difference was calculated without allowance for the possibility of fluctuations in the energy settings of several keV. Such fluctuations would tend to increase artificially the magnitude of the difference, ε.

A third method of comparing R_d and R_p is a compromise between the two methods discussed above, and minimizes the difficulties in these methods. A value for ε was calculated in the manner outlined above and with the same function $R_c(E)$, but using only the seven (d,p) data points and the five (p,d) data points which lie nearest the peak in R(E) at 20.68 MeV. The difference found for this limited region was $\varepsilon = -0.0001 \pm 0.0006$ or $(-0.06 \pm 0.3)\%$. The data near the peak were taken with the smallest statistical errors and with the greatest care in studying systematic errors. Therefore it is reasonable to depend on these data alone, using the data at other energies primarily as evidence that the energies in the (d,p) and (p,d) reactions are properly matched. Thus the result of this last method is taken to be the most appropriate measure of the agreement found in the present experiment. It is quite close to the results of the other methods. Thus it is concluded that there is no evidence for a violation of T invariance in the present study; the (d,p) and (p,d) results agree within an experimental uncertainty (standard deviation) of 0.3%.

The important information about T invariance is obtained by relating this upper limit on the agreement between the cross section ratios to an upper limit on the average fraction, F, of the reaction amplitude which is odd with respect to time reversal and, eventually, by relating it to an upper limit on the fraction $\mathcal{F}$ of the interaction Hamiltonian which is odd with respect to time reversal. This procedure is conveniently carried out by first relating ε to F, and then relating F to $\mathcal{F}$.

It is relatively straightforward to obtain an approximate relationship between ε and F. Considerations discussed in Ref. 2 suggest that F is probably less than the experimental uncertainty in ε, i.e., $F < 0.3\%$.

It is more difficult to relate F and $\mathcal{F}$. For reactions proceeding by the by the compound nucleus mechanism, such as $Al^{27}(p,\alpha)Mg^{24}$, estimates of the ratio

F/$\not{T}$ range from 1 to 6.[3,4] On the other hand, Robson[5] has shown that certain direct reactions may not be sensitive to T violations at all, *i.e.*, F/$\not{T}$ << 1.

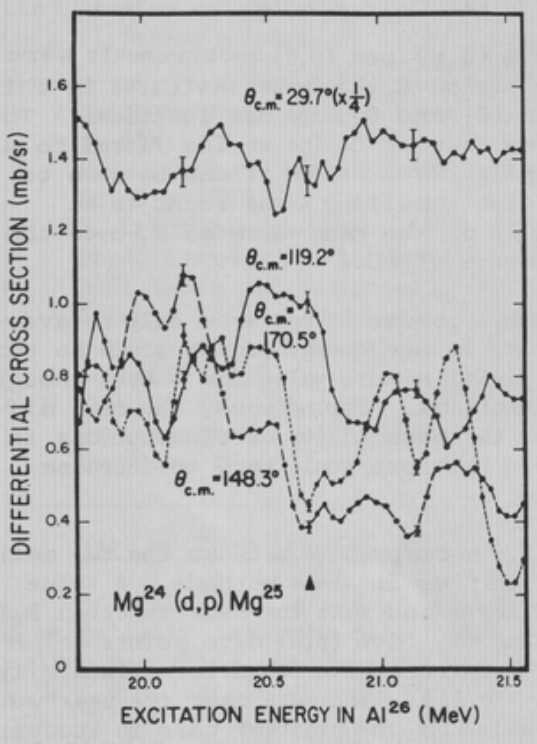

Fig. 29-2. Excitation function for the $Mg^{24}(d,p)Mg^{25}$ differential cross section at several (c.m.) angles θ. Typical relative uncertainties are 5%; the absolute cross section has an uncertainty of 10-20%.

These considerations led us to an investigation of the reaction mechanism involved in the $Mg^{24}(d,p)Mg^{25}$ reaction and its inverse. The excitation functions shown in Fig. 29-2 were taken with this in mind. These data exhibit the energy fluctuations characteristic of reactions in which there is a substantial contribution from compound nuclear mechanisms.

A quantitative estimate of the fraction y_d of the reaction which proceeds by the direct mechanism can be made by using the relation[6]

$$(\overline{\sigma^2}/\bar{\sigma}^2) - 1 = (1 - y_d^2)/N$$

where N is the effective number of independent amplitudes that enter into the reaction. If we assume that N is the number of possible combinations of magnetic substates of the particles involved, application of this relation to the data of Fig. 29-2 indicates that the reaction is primarily direct, but as much as 1/5 of the cross section at the back angles is attributable to a compound nuclear mechanism.

Were one to assume that the direct part of the reaction is insensitive to a T non-invariance, the numbers given above would imply an upper limit on $\not{T}$ of about 2 percent. However, it is probable that the direct part of the reaction is at least partially sensitive to a T violation. Robson's argument requires that the reaction be explainable by the distorted wave Born approximation (DWBA) with a cut-off outside the nuclear radius, but for the $Mg^{24}(d,p)Mg^{25}$ reaction it has proven difficult to find a good DWBA fit, especially at angles as large as 120°.[7] Thus this limit for $\not{T}$ is probably unnecessarily high.

If the ratio F/$\not{T}$ for the direct part of the reaction were as large as 1/2, the upper limit on $\not{T}$ would be about twice the uncertainty in ε, *i.e.*, $\not{T} < 0.6\%$, which at present is the best available estimate. This estimate must be accepted with the realization that it could be in error by a factor of 10 in either direction.

Work at present is directed toward obtaining improved estimates of F/$\not{T}$ and

completing a paper describing the experiment in detail. (D. Bodansky, W.J. Braithwaite, D.C. Shreve, D.W. Storm, and W.G. Weitkamp)

1. Nuclear Physics Laboratory Annual Report, University of Washington (1966) p. 39.
2. D. Bodansky, W.J. Braithwaite, D.C. Shreve, D.W. Storm, and W.G. Weitkamp, Phys. Rev. Letters *17*, 589 (1966).
3. T.E.O. Ericson, Phys. Letters *23*, 97 (1966).
4. C. Mahaux and H.A. Weidenmüller, Phys. Letters *23*, 100 (1966).
5. D. Robson, private communication.
6. T. Ericson and T. Mayer-Kuckuk, Ann. Rev. Nucl. Sci. *16*, 183 (1966).
7. W.R. Smith and E.V. Ivash, Phys. Rev. *131*, 304 (1963).

VI. NUCLEAR FISSION

30. Isomeric Yields of Nb^{95} from Proton Induced Fission of U^{235}

The relative independent yields of the high and low spin isomeric states produced in fission can be used in deducing the initial average angular momentum of the primary fission fragments. A recent experiment[1] yielded a value of $\sigma_g(I=9/2)/[\sigma_g(I=9/2) + \sigma_m(I=1/2)]$ of 0.06 for the $Nb^{95g}(I=9/2)$ - $Nb^{95m}(I=1/2)$ isomeric pair obtained from proton induced fission of uranium. This surprisingly low ratio implies a much smaller initial average angular momentum than indicated by other experimentally determined isomeric ratios.[2,3]

A target of U^{235} was chosen to determine the relative yields of the niobium isomers. A preliminary experiment with a U^{238} target indicated that the independent yield was too small to determine for this neutron-rich target. In the present experiment 100 mg of U^{235} foil, surrounded by very pure one-mil aluminum catcher foils, was bombarded with 35 μamps of 10 MeV protons for two hours in the 60-in. cyclotron. Only the catcher foils were used to insure that no zirconium impurities in the U^{235} foil would interfere in the determination of the isomer ratio by participating in (p,xn) reactions. Previous experiments[4] had indicated that there was a high activity of Nb^{92} contaminant when a bombarded uranium oxide target had been analyzed. The estimated range of these spallation products is much shorter than that of the fission fragments, so that only a small fraction recoil out of the uranium into the catcher foils.

One hour after bombardment the catcher foils were dissolved in acid. Niobium oxide was precipitated using 20 mg of niobium carrier, in the presence of 5 mg each of zirconium, molybdenum, and tellurium holdback carriers. Radiochemical purification was achieved by successive $BaZrF_6$ and sulfide precipitations. The chemical yield was about 60%. The sample was mounted on a thin mylar film for counting.

The yield of the Nb^{95g} isomer was determined by measuring the 768 keV γ ray with a Harshaw integral Line Assembly 3"×3" NaI(Tl) crystal; while the Nb^{95m} isomer, which decays almost exclusively by internal conversion to the ground state, was determined by measurement of the K x-ray with a 1"×1/32" NaI(Tl) crystal.

As the calculated independent yield of Nb^{95} from the fission of U^{235} is hundreds of times smaller than the cumulative yield of its β-unstable parent Zr^{95}, a correction was made for the amount of Nb^{95g} produced by the decay of 65 day Zr^{95} during and after bombardment but prior to the first chemical separation. The growth rate of Nb^{95} from Zr^{95} decay was obtained by milking niobium from the original target solution 9 days after bombardment. The niobium sample was purified and counted in the same manner as the primary separation. The correction for growth prior to the first chemical separation was about 30% of the total γ ray count of the initial sample.

A blank run was performed on the aluminum catcher foils to insure that no radiochemical interferences would come from possible impurities in the foils. No interferences were seen.

An isomer ratio of $\sigma_g(I=9/2)/[\sigma_m(I=1/2) + \sigma_g(I=9/2)]$ of $0.96^{+0.01}_{-0.02}$ was obtained. The large uncertainty was due mainly to the low counting rate for the x-ray.

A statistical model calculation to predict the isomer ratios as a function of the assumed initial root-mean-square angular momentum of the primary fragments was performed. The results are shown in the following table. It can be seen

Table 30-1. Isomer ratios of Nb^{95} calculated from a statistical model for several assumed initial rms angular momenta of the primary fragments.

$\sqrt{\overline{J^2}}$	$\frac{\sigma_g}{\sigma_m + \sigma_g}$
7.4	0.88
10	0.92
12	0.96
experiment	$0.96^{+0.01}_{-0.02}$

that the new experimental ratio is consistent with appreciable angular momentum in the primary fragment, in agreement with observations for other isomeric pairs. (C. Rudy and R. Vandenbosch)

1. E. Hagebø, J. Inorg. Nucl. Chem. *25*, 1201 (1963).
2. D.G. Sarantites, C.D. Coryell, and G.E. Gordon, Phys. Rev. *138*, B353 (1965).
3. H. Warhanek and R. Vandenbosch, J. Inorg. Nucl. Chem. *26*, 660 (1964).
4. Nuclear Physics Laboratory Annual Report, University of Washington (1965) p. 60.

31. Competition between Neutron Emission and Fission at Moderate Excitation Energies

Work is continuing on the experiment initially discussed in the 1966 Annual Report.[1] The major portion of the past year has been spent on assembling and testing instrumentation which will be needed for the experiment.

In order to test the entire system a preliminary experiment using a natural uranium target was performed. Protons of 11 and 15 MeV were used as bombarding particles. We measured the angular distribution and pulse-height spectra of neutrons emitted in coincidence with fission fragments by the time-of-flight method in an effort to deduce the fraction of neutrons emitted prior to fission. The detection of a fission fragment in a counter close to the target was used as the start pulse in the time-of-flight system. The anode signal from a conventional neutron scintillation counter, which incorporates a plastic scintillator coupled

to an XP1040 photomultiplier, was used as the stop pulse. An unsaturated signal from the 11th dynode of the phototube was presented to a discriminator and coincidences between it and fission fragments were used to gate a multichannel analyzer, which recorded the neutron time spectrum. Time-of-flight spectra at 90° and at 180°+0° with respect to the fission counter were taken at the two bombarding energies.

The results, shown in Fig. 31-1, have been converted to neutrons/fission fragment *vs.* neutron energy (laboratory system). Qualitatively the results are as expected. The 180°+0° yield is larger at both bombarding energies. The 15 MeV yield is larger at both angles. This is to be expected since the higher excitation energy allows either the possibility of emission of an extra neutron prior to fission, or an increase in the average number of neutrons after fission. The dotted spectra have included a correction for the efficiency of the neutron counter. This efficiency was calculated by observing a Cf^{252} neutron spectrum and using the neutron densities determined by Bowman, *et al.*[2] The sharp rise of the corrected spectra below 0.75 MeV is not expected and it was suspected that it is due to poor energy resolution of the neutron detection system, particularly at low energies. At these energies the efficiency corrections are quite large and the neutron yield is small. Several tests were undertaken to determine the energy resolution of the neutron counter.

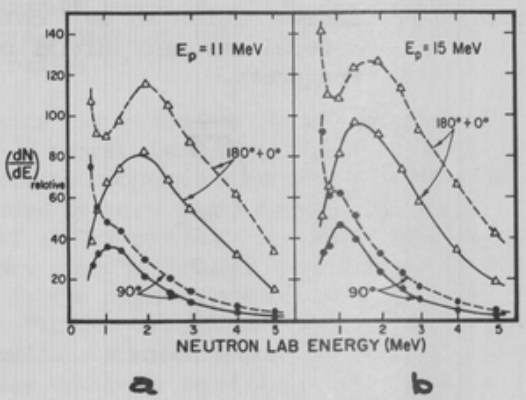

Fig. 31-1. Relative neutron yield/fission fragment at 90° and 180°+0° with respect to the fission counter at proton energies of (a) 11 MeV and (b) 15 MeV. The dotted curves were obtained after incorporating the neutron counter efficiency.

By using the buncher-flapper system[3] on the tandem Van de Graaff and (p,n) reactions on light nuclei we could obtain mono-energetic neutrons to use in conjunction with our time-of-flight system. The unsaturated dynode signal of the neutron counter was presented to a discriminator which was used as a gate for a multi channel analyzer. The start pulse for the neutron time-of-flight spectrum was provided by the phototube anode and a signal from the buncher-flapper was used as the stop pulse. A time spectrum obtained with a Be^9 target is shown in Fig. 31-2. Other targets which would be useful in (p,n) studies of this type are B^{10} and C^{13}.

Graphs of the number of counts in the ground state peak as a function of discriminator setting showed considerable high energy tailing beyond the expected bias cutoff -- an indication of poor resolution.

Further tests of the scintillation counter using sources of alpha particles and conversion electrons indicated that the energy resolution was greater than 40%. It is desirable to have a resolution on the order of 15% for the experiment. A considerable amount of work has been done since then in attempting

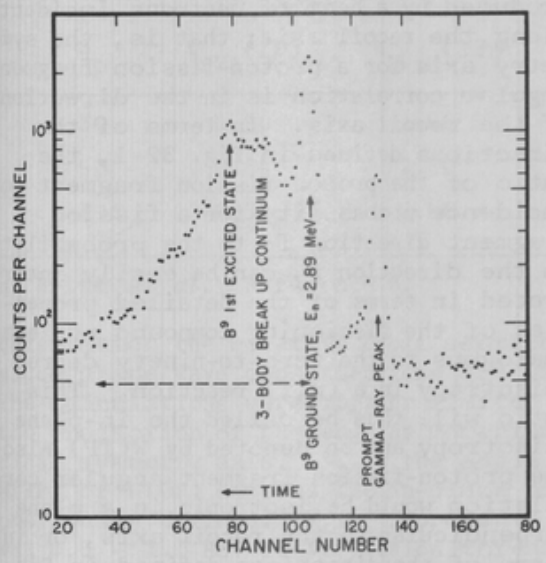

Fig. 31-2. Neutron time-of-flight spectrum for the $Be^9(p,n)B^9$ reaction. Flight path=100 cm; neutron detector angle=90°; proton bombardment energy= 5.7 MeV.

to identify and correct the cause of the poor resolution. Some improvement has been attained by increasing the efficiency of light collection, accomplished by resurfacing the crystal face and using a bright aluminum reflector.

Another project undertaken during this past year has been the data acquisition package. The final experiment will involve simultaneous measurement of two fission fragment energies and the neutron flight time. A three-parameter program has been written for on-line data acquisition utilizing our SDS 930 computer. The information from each event is packed into a single computer word, stored in a temporary buffer region in memory, and finally recorded on magnetic tape in blocks of 1000 events. Live-time display of the time-of-flight spectrum and of the fission mass-yield curve is provided. (C. J. Bishop, I. Halpern, R. Shaw, and R. Vandenbosch)

---

1. Nuclear Physics Laboratory Annual Report, University of Washington (1966) p. 70.
2. H. R. Bowman, S. G. Thompson, J. C. D. Milton, and W. J. Swiatecki, Phys. Rev. *126*, 2120 (1962).
3. See Sec. 48 of this report.

---

32. Angular Correlations in the $Pu^{239}(d,pf)$ Reaction

This experiment is a continuation of previous work[1,2] and uses the same kind of experimental apparatus described earlier.[2] New measurements have been performed with a Pu^{239} target.

This report is primarily concerned with a comparison of the experimentally determined (d,pf) angular correlations with those calculated using distorted wave theory.

Fission fragments in coincidence with protons were measured in the (d,p) reaction plane and out of that plane. The geometry, including the three fission fragment directions that are of principal interest, is illustrated in Fig. 32-1. Although data were taken at some intermediate fission fragment angles, no additional conclusions can be reached from these data.

The significance of measuring fission fragments in the three directions specified is made evident by first discussing the predictions of a plane wave approximation for the (d,p) reaction. This approximation results in a fission

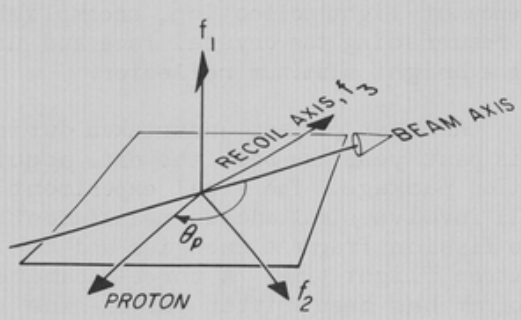

Fig. 32-1. The geometry of the experiment showing the angles of interest. The proton angle, θ_p is 140° from the beam axis; f_1, f_2, and f_3 are the most important fission fragment directions. f_1 is perpendicular to the (d,p) reaction plane, f_2 is in that plane but perpendicular to the recoil axis, and f_3 is along the recoil axis.

fragment distribution analogous to that produced by a beam of neutrons incident along the recoil axis; that is, the symmetry axis for a proton-fission fragment angular correlation is in the direction of the recoil axis. In terms of the directions defined in Fig. 32-1, the ratio of the proton-fission fragment coincidence probability for a fission fragment direction f_3 to the probability in the direction f_2 can be easily interpreted in terms of the detailed properties of the fissioning compound nucleus, analogous to the zero-to-ninety degree anisotropy in a (n,f) reaction. This ratio will thus be called the in-plane anisotropy and be denoted by W(IP).Also, the proton-fission fragment angular correlation would be isotropic in a plane perpendicular to the recoil axis, or in terms of the directions defined in Fig. 32-1, the ratio of the coincidence probability in the direction f_2 to that in the direction f_1 should be equal to one. This ratio will be called the out-of-plane anisotropy, W(OP).

Distorted wave Born approximation (DWBA) theory predicts that the angular correlation will be more complex than that calculated by the use of plane waves. The angular momentum transfer from the stripping process no longer necessarily results in orbital angular momentum vectors aligned in the plane perpendicular to the recoil axis. In general the angular momentum vectors have a smeared directional distribution, with an average direction described by a symmetry axis differing from the recoil direction. Strictly speaking, there may be no symmetry axis at all. For each value of orbital angular momentum of the captured neutron, the correlation function contains statistical tensors, each rank of which contains, in general, a number of terms. Each of these latter terms may have a different symmetry axis.[3] But when one adds all these terms and averages over the many values of orbital angular momentum that can contribute, an average symmetry axis can usually be defined.

The in-plane fission fragment anisotropy may be considerably different from that predicted by a plane wave approximation, even if DWBA theory is used to calculate the relative cross sections for each value of angular momentum transfer, as in Britt *et al.*[4] The in-plane anisotropy may be damped due to the smeared distribution of the angular momentum vectors, even in cases where the average symmetry axis coincides with the recoil axis.

Table 32-1 gives a brief comparison of anisotropies calcluated for a specific case using plane wave and distorted wave approximations to generate the statistical tensors describing the transferred angular momentum. Angular momentum transfers of from zero to three units were taken into account. In the plane wave

Table 32-1. Calculated and experimental anisotropies for 15 MeV deuterons.

θ_p	$W_{PWA}(IP)$	$W_{DWBA}(IP)$	$W_{EXPT}(IP)$	$W_{DWBA}(OP)$	$W_{EXPT}(OP)$
50	3.90	1.90	1.42±0.11	4.47	1.35±0.15
90	3.64	2.80	1.71±0.10	1.57	1.12±0.05
140	3.54	3.46	2[a]	1.04	0.98±0.05

a) Britt *et al.*, Reference 5.

calculation the relative cross sections were taken from the DWBA calculations since plane wave cross sections are usually in poor agreement with experiment. The calculations were further limited to fission through a K = 0 band, where K is the projection of the angular momentum of the Pu^{240} compound nucleus on the nuclear symmetry axis. θ_p is the angle of the coincident proton from the beam axis. W(IP) or W(OP) denotes the in-plane or out-of-plane anisotropy, respectively, as previously defined. W_{EXPT} represents the measured anisotropy in an energy interval 0.5 - 1.5 MeV above fission threshold.[5] All data were taken at an incident deuteron energy of 15.0 MeV.

The measured anisotropy is much smaller than the calculated value, presumably because fission is also occuring through transition states with non-zero K values. But if one assumes that low values of K dominate in this energy region, the dependence of the anisotropy on proton angle calculated using distorted wave theory is the same as that seen experimentally. That is, the in-plane anisotropy decreases and the out-of-plane anisotropy increases as one goes to forward proton angles. These trends in the angular correlations extend over a broad range of excitation energies as can be seen in Fig. 32-2.

It can be seen that the plane wave calculation does not predict a fall-off for the in-plane anisotropy at forward proton angles, even though DWBA relative cross sections were used in the calculation. Also, in a plane wave description of the (d,p) reaction the out-of-plane angular distribution is always isotropic, which clearly differs from the experimental results at a proton angle of 50° and to a lesser extent at 90°. At 140° this distribution was found to be isotropic over the measured range of excitation energy, as predicted by both plane and distorted wave theories.

One must conclude that the DWBA calculations agree reasonably well with experiment; that is, the variation in the angular correlation with proton angle follows the general predictions of distorted wave theory.

Optical model parameters were obtained by measuring the elastic scattering of 15.0 MeV deuterons and 13.0 MeV protons on Pu^{239}, and fitting these data with an optical model search routine.[6] The DWBA reaction amplitudes were calculated using T-SALLY.[7] The DWBA angular correlations are surprisingly insensitive to the form of the absorptive potentials. Both volume and surface absorption potentials give very similar angular correlations, as long as the potentials chosen

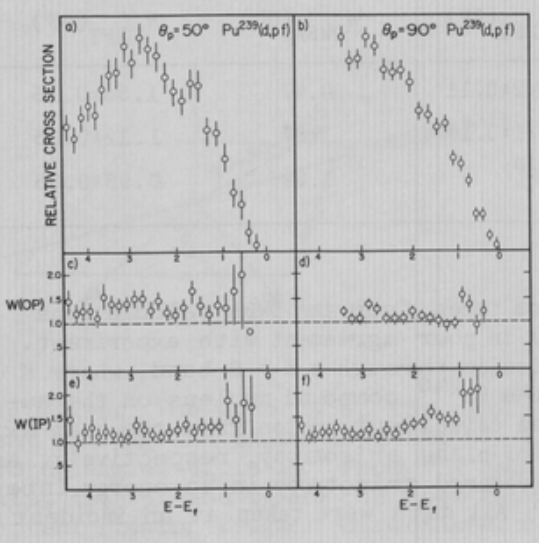

Fig. 32-2. The abscissa in these plots is the excitation energy of the compound nucleus above the fission threshold[5] for Pu^{240}. The ordinates in (a) and (b) are the relative cross sections in a fission fragment direction previously denoted by f_2, which is 90° to the recoil axis and in the (d,p) plane. W(IP) and W(OP) are the in-plane and out-of-plane anisotropies defined in the text. W(OP) was measured at a proton angle of 140° and was found to be isotropic over the energy range shown above.

are adjusted to fit the elastic scattering in the entrance and exit channels. (R. Vandenbosch and K. Wolf)

---

1. Nuclear Physics Laboratory Annual Report, University of Washington (1965) p. 22.
2. *ibid.* (1966), p. 61.
3. W. Tobocman and G.R. Satchler, Phys. Rev. *118*, 1566 (1960).
4. H.C. Britt, W.R. Gibbs, J.J. Griffin, and R.H. Stokes, Phys. Rev. *139*, B354 (1965).
5. We are referring to the first threshold at 4.8 MeV as identified by Northrop, Stokes, and Boyer, Phys. Rev. *115*, 1277 (1959).
6. The optical model search routine was obtained from B. Fernandez, University of Washington.
7. R.H. Bassel, R.M. Drisko, and G.R. Satchler, Oak Ridge National Laboratory Report ORNL-3240.

---

33. Doubly Charged Particle Emission During Nuclear Fission

Studies of fission accompanied by the emission of a third small fragment, almost always an alpha particle, have continued.[1,2] In order to obtain a higher coincidence counting rate we now use a position-sensitive α particle detector subtending a (planar) angle of ∿60° relative to the target. With this arrangement we are able to obtain information on the angle of emission of the alpha particle relative to the two heavy fragments; the kinetic energies of the two heavy fragments and the alpha particle are measured also, enabling the mass division to be determined, and thus the angular correlation of the emitted alpha particle relative to either fragment.

The energy and position information is fed into the SDS 930 computer for analysis and storage, event by event, on magnetic tape. Testing of the system and the computer programs was accomplished using a Cf^{252} on a thick backing. In this configuration only one fission fragment and the coincident alpha particle could be measured. The results agreed closely with those of Atnoesen and Thomas.[3]

The first experiment will repeat the earlier measurement[1] on U^{235}. Some data were obtained in a short run, but the statistics are not good enough to draw any definite conclusions. (A.W. Fairhall, J. Gonyeau, and D.G. Perry)

1. Nuclear Physics Laboratory Annual Report, University of Washington (1966) p. 76.
2. *ibid.* (1965), p. 57.
3. R.A. Atneosen and T.D. Thomas, Phys. Rev. *139*, B307 (1965).

VII. MISCELLANEOUS RESEARCH PROJECTS

34. Total Body Neutron Activation for Determination of Body Calcium

Certain elements in the human body may be quantitated by exposing man to neutrons and then detecting the induced radioactivity. This procedure was attempted by Anderson et al.[1] after exposing two subjects to 0.1 rad of 14 MeV neutrons. By total body counting and gamma ray spectrometry they estimated the amounts of sodium and chlorine in the body by detecting the Na^{24} and Cl^{38} produced by the capture of neutrons thermalized in the body. An accurate measurement of calcium might be made if the irradiation time and the interval between irradiation and counting could be made short, since the half life of the induced Ca^{49} is only 8.8 minutes.

A quantitation of total body calcium would be a valuable aid to the study of bone demineralization which takes place:

1. in the aging process
2. as a side effect of certain drug therapies
3. during periods of weightlessness.

Measurements with a tissue-equivalent ion chamber placed 16 ft. from the target box indicated that the cyclotron delivered 0.1 rad in 20 seconds when a thick beryllium plate was bombarded with 15 microamperes of 22 MeV deuterons. Measurements with a graphite-walled ion chamber showed that about 30% of this dose was due to gamma rays and 70% was from neutrons.

The uniformity of the neutron field was measured by the thermal (n,γ) reaction of Mn^{55}. Capsules of MnO_2 were irradiated in jugs of water 6" in diameter, then counted with a NaI crystal. These measurements showed that at 16 ft. from the target the neutron flux varied only 4% over a vertical distance of 6 ft. The neutron distribution measured by the activation of Na^{24} in the $Al^{27}(n,\alpha)$ reaction (effective threshold 7.5 MeV) varies by 32% in the same region. However, the manganese experiment is probably a better approximation to the anticipated thermal reaction in an hydrogenous medium.

MnO_2 capsules were used to measure the thermal neutron distribution in a model of the human body (Remab skeletal phantom). The ratio of the highest to lowest thermal neutron fluxes was 1.24. Since knowledge of this flux distribution is important to an understanding of the variability of the calcium determination, the flux distribution will be measured in a human cadaver, which should provide a more realistic approximation to the human body.

A human cadaver was exposed to 0.14 rad under the same conditions as the ion chamber experiment and was counted in a whole-body counter consisting of six 9" × 4" NaI crystals arranged in a ring through which the cadaver was moved on a special bed. The rate at which the bed moved was decreased exponentially to compensate for the decay of Ca^{49}. In 12.4 minutes 14,000 counts were obtained in the Ca^{49} photopeak which rises prominently above other radiation components at 3.1 MeV (Fig. 34-1). Thus adequate statistical precision may be obtained at moderate radiation exposures.

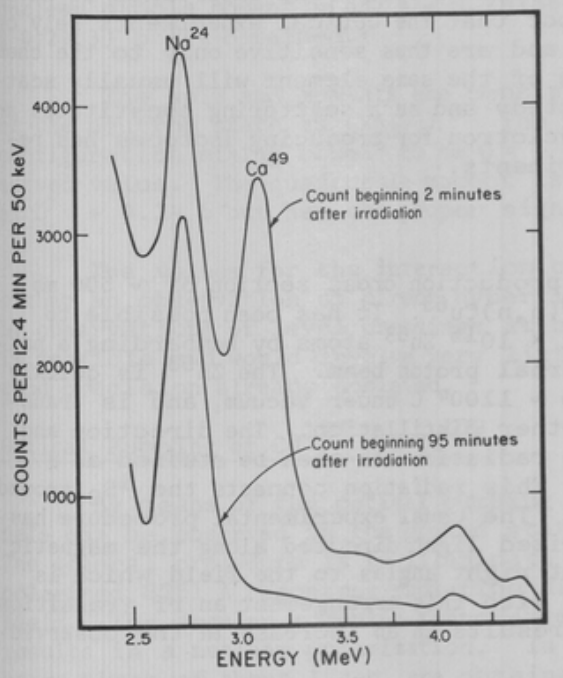

Fig. 34-1. Gamma ray spectrum observed with a whole-body counter of a cadaver exposed to 0.14 rad of neutrons.

In conclusion, it appears feasible to make a statistically precise measurement of total body calcium. It remains to make this method quantitative by chemical analysis of cadavers after they have been studied by this method, by development of secondary standards, by evaluation of corrections for gammas from Na^{24}, Cl^{38} and S^{37} (product of the reaction Cl^{37} (n,p)), and by assessment of the variability due to body size, positioning and cyclotron operation. (W. A. Nelp, Medicine and Radiology).

---

1. Anderson, *et al.* Lancet, December 5, 1964, p. 1201.

---

35. Studies of Nuclear Spins and Moments by Optical Pumping Techniques

For many years the atomic beams magnetic resonance method[1,2] has been used to determine the spins and static moments of long-lived nuclear states. The method, as applied to radioactive nuclei, has been used for a large number of cases and is characterized by both high sensitivity and high precision. It also suffers from some important limitations. The atomic state of the system of which the nucleus is a part must be sufficiently long-lived to survive during a transit through an apparatus. In practice this has largely restricted the experiments to atoms in their ground state or in metastable states which can be easily populated. In all cases the desired nuclear property is inferred from the electron-nucleus or hyperfine interaction. Since the interactions in an atomic state with total angular momentum J are restricted by symmetry to those with nuclear multipoles of order $n \leq 2J$, the beams method will often not yield information about the higher order multipoles. The limitation is particularly clear in the large class of atoms with diamagnetic J = 0 ground states. It also applies to another important group with J = 1/2 ground states in which no quadrupole interaction is possible.

Within the last few years a number of experiments with radioactive atoms have been carried out using the related techniques of optical pumping, optical double resonance and optical level-crossing spectroscopy.[3,4] These methods, like atomic beams, are capable of high precision and high sensitivity. Unlike atomic beams they can be used to make measurements in excited atomic states. Since the optically accessible states include ones with higher angular momentum than the ground state, hyperfine interactions of higher multipolarity can be observed.

Cyclotron-produced nuclides are especially desirable in the optical experiments since they can often be obtained carrier-free. The importance of having carrier-free isotopes is related to the fact that the optical experiments rely on optical resonance fluorescence scattering and are thus sensitive only to the chemical nature of the sample. Other isotopes of the same element will usually scatter equally as well as the isotope under study and such scattering constitutes an undesirable background. The use of the cyclotron for producing isotopes has resulted in several successful optical experiments.

Optical Double Resonance Studies of Zn^{63}

Thirty-eight min. Zn^{63} has a large production cross section of $\sim$ 500 mb for 10.5 MeV protons via the reaction $Zn^{63}(p,n)Cu^{63}$. It has been possible to produce an equilibrium quantity of about 1×10^{15} Zn^{63} atoms by bombarding a natural copper foil target in a 170 μamp external proton beam. The Zn^{63} is quickly distilled from the target by heating it to $\sim$ 1100° C under vacuum, and is transferred to a quartz resonance cell by a further distillation. The direction and polarization of scattered 3076 Å resonance radiation can then be studied as a function of applied static and rf fields. This radiation connects the $^1S_0$ ground state and the excited $^3P_1$ state at 3.8 ev. The usual experimental procedure has been to illuminate the sample with unpolarized light directed along the magnetic field and to detect that light scattered at right angles to the field which is linearly polarized parallel to the field. With this arrangement an rf transition between Zeeman sublevels of the $^3P_1$ state results in an increase in the observed light scatter.

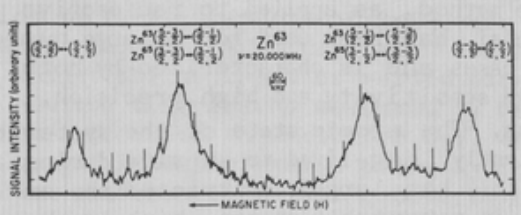

Fig. 35-1. Zeeman spectrum used in the determination of the nuclear spin of Zn^{63}. The fractions in parentheses indicate the quantum numbers for each of the transitions.

A total of five different Zeeman transitions were observed in magnetic fields up to 120 gauss. From these observations it is possible to deduce the spin, magnetic moment, and quadrupole moment of Zn^{63}. The spin I = 3/2 follows from the observation of four resonances equally spaced about a magnetic field corresponding to a g-factor of $g_F = 3/5$ (Fig. 35-1). In this case the identification is somewhat complicated by overlapping resonances from Zn^{65}. However, the observation of a two-quantum transition at a field appropriate to a $(F = 5/2, m_F = 5/2) \leftrightarrow (F = 5/2, m_F = 1/2)$ transition definitely establishes the presence of the overlapped resonances in Zn^{63}.

The isotopic identification can be made by following the decay of the amplitude of an individual resonance. For example, the observed half-life of the resonance decay, 38.4 ± 1.6 min., agrees closely with the accepted half-life for Zn^{63}, 38.3 min.

A least squares fit of the fields and frequencies of fourteen resonances to a modified Breit-Rabi Hamiltonian yields the hyperfine interaction constants in the $^3P_1$ state. The magnetic dipole interaction constant A = - 326.57(4) MHz

and the quadrupole interaction constant B = 34.46(3) MHz. If these values are compared to those measured[5] for Zn^{67} in the same atomic state then values for the nuclear dipole moment $\mu(63) = -0.28156(5)\ \mu_N$ and the quadrupole moment Q = + 0.29(3) b are obtained.

The spin and moments are consistent with the usual shell model assignment of the neutron state as $(2p_{3/2})$.[3] The magnitude of the moment is predicted by a configuration mixing model[6] to be $\mu = -0.268\ \mu_N$ in good agreement with the observed value. The quadrupole moment is somewhat larger than the predicted value of Q = + 0.14 b but has the proper sign for the assigned configuration.

The values for the interaction constants can be considerably improved by either an observation of direct hyperfine transitions at low magnetic fields or by observations of level crossings at higher fields. Either type of experiment is feasible and would involve very little search effort in view of the reasonably good precision already achieved.

Optical Pumping of Cd^{107} and Cd^{109}

By means of the optical pumping technique nuclear magnetic resonance signals can be observed in the ground state of diamagnetic atoms such as cadmium. The general procedure is to illuminate a vapor sample of cadmium with circularly polarized 3261 Å resonance radiation directed parallel to an applied magnetic field. The angular momentum transferred to the sample by the optical absorption results in a nuclear polarization. In the case of cadmium reasonably long relaxation times of about 1 sec. are obtainable. As a result, a relatively high degree of polarization (50%) and narrow resonance lines are observed.

The two cadmium isotopes are produced in the cyclotron by the reactions $Ag^{107}(p,n)Cd^{107}$, $Ag^{109}(p,n)Cd^{109}$ in a natural silver target. The cadmium activity can be distilled into an absorption cell in a manner similar to that used for zinc. Strong resonance signals have been observed for both isotopes. The resonance frequencies are compared to the proton frequency in a mineral oil sample or to the resonance frequency of Cd^{111} in the same sample cell. The results to date give:

$$\nu_{107}/\nu_{109} = .7429588\ (3)$$
$$\nu_{107}/\nu_{111} = .20678088\ (10)$$
$$\nu_{109}/\nu_{111} = .27832081\ (12)$$
$$\nu_{107}/\nu_{H'} = .04379263\ (10)$$
$$\nu_{109}/\nu_{H'} = .05894356\ (12).$$

The incentive for making measurements of this precision is to obtain information about the distribution of magnetism in the nucleus. The measure of the distribution obtained is the "hyperfine structure anomaly". For a point dipole nucleus the magnetic dipole interaction constant obtained from the hyperfine structure and the nuclear g-factor should be strictly proportional. In practice the finite nuclear size results in a deviation from the expected proportionality. For medium weight to heavy nuclei the effect is of the order of 1%. In order to

avoid the difficult problem of calculating atomic wave functions to this accuracy a differential hyperfine anomaly is defined which is

$$A_1{}^{\Delta}A_2 = \frac{A_1/A_2}{g_1/g_2} - 1.$$

A_1 and A_2 are the dipole constants for the lighter and heavier of two isotopes of the same element respectively, and g_1 and g_2 are the corresponding nuclear g-factors.

If our moment measurements in cadmium are combined with earlier measurements[7] of the dipole constants we then find the following anomalies:

$$^{107}\Delta_{111}(^3P_1) = + .096(2)\%$$
$$^{109}\Delta_{111}(^3P_1) = + .090(2)\%.$$

The anomaly can also be calculated using the same configuration mixing model wave functions which give good values for the nuclear moments. The results of such a calculation are:

$$^{107}\Delta_{111}(^3P_1) = + .030\% \qquad ^{109}\Delta_{111}(^3P_1) = - .024\%.$$

The cause of the poor agreement is not known at present and further theoretical work is being undertaken.

This research is supported by Grants GP 3490 and GP 6436 from the National Science Foundation. (R. Chaney, N. Laulainen, M.N. McDermott, P. Spence, Department of Physics).

1. H.A. Shugart, "Direct Measurements of Spins of Radioactive Nuclei", pp. 5-30 in *Nuclear Spin-Parity Assignments*, N.B. Gove, Ed. (Academic Press, New York 1966).
2. W. Nierenberg, Ann. Rev. Nucl. Sci. *7*, 349 (1957).
3. M.N. McDermott and R. Novick, Phys. Rev. *131*, 707 (1963).
4. G. zu Putlitz, Ergeb. Exakt. Naturw. *37*, 106 (1965).
5. A. Lurio, Phys. Rev. *126*, 1768 (1962).
6. N. Noya, A. Arima, and H. Horie, Progr. Theoret. Phys. (Kyoto) Supple. *8*, 33 (1958).
7. P. Thaddeus and M.N. McDermott, Phys. Rev. *132*, 1186 (1963).

VIII. INSTRUMENTATION FOR RESEARCH

36. Technical Improvements in the Detection System for High Energy Photons

The measurements of high energy photon spectra which were reported last year[1] and this year (Sec. 25) point to a number of ways in which our detection system might be improved. We briefly discuss some of these detection system problems and attempted solutions.

1. Improvement of Resolution: One expects the resolution, R, of a NaI spectrometer to improve with increasing photon energy, E_γ, roughly as given by[2]

$$R = \alpha+\beta E_\gamma^{-1/2}$$

where the second term is due to the statistics of the number of photo-electrons produced and the first represents the sum of all the energy-independent more or less intrinsic sources of line spread. Measurements of line widths in our spectrometer (Fig. 36-1) show that for energies above 5 MeV, the resolution departs significantly from the above relationship. For example, for 15.1 MeV photons the resolution (∿10%) is about three times worse than one would expect from an extrapolation of low energy measurements. It should be emphasized here that the measured lines do not include first and second escape peaks, which are eliminated by the anticoincidence annulus. This loss in resolution at higher energies is not due to the phototube itself. Using a light pulser to produce pulses equivalent to those from a 15 MeV γ ray, one obtains a line whose width is only 0.7%. Thus the 10% width measured for the actual photons must have something to do with the interaction of high energy photons in the NaI. The most plausible cause for the resolution loss would seem to be the leakage, from the far end of the crystal, of soft radiations which are produced in the shower initiated by the incident photon. Such leakage can significantly effect the response function of a crystal as Zerby and Moran[3] and others have pointed out. These observations suggest that it may pay to improve the anticoincidence shield (at present a hollow cylinder) by plugging its back end with a NaI detector as is done by Bostrom and Draper.[2]

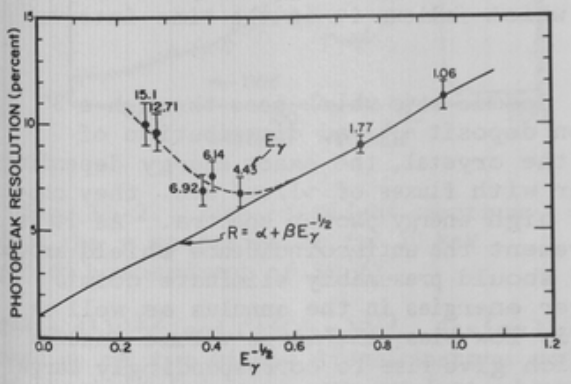

Fig. 36-1. Photopeak resolution versus $E^{-1/2}$ for the present detector system.

2. Gain Stabilization: A NaI spectrometer designed for studies of high energy photons should not be run at the same high voltages used in low energy spectrometry because 1) very large pulses in phototubes are likely to produce fatigue, feed back and other troubles and 2) in order to obtain a useful rate of high energy events one must generally perform a measurement at very high total counting rates (of mostly low energy photons). However, just lowering the voltage on a NaI spectrometer phototube in order to do higher energy measurements, introduces

time walk and noise problems. It is desirable to maintain normal voltages between lower dynodes but to decrease voltages in upper dynodes. A new base circuit was designed to convert our low energy NaI spectrometer into a high energy spectrometer. With this circuit counting rate gain shifts remain below 1% up to rates of several thousand per second. The pulse height versus energy relation also appears to remain linear to the largest pulses of interest.

3. Pile-up Rejection: Because of the high counting rate of low energy photons that generally accompanies a measurement of a high energy photon spectrum, it is necessary to eliminate spurious high energy pulses that arise from the piling up of low energy pulses in the pulse height analyzer. This is especially true on studies of high energy spectra from heavier targets because these spectra are generally structureless. It is therefore not possible with such spectra to recognize the onset of pile-ups by characteristic changes in spectral shape. As shown in Sec. 25 of this report the pile-up contribution is large and difficult to calculate accurately. A system has been developed which uses double-delay-line shaped pulses and rejects those for which the time between the start and cross-over points does not fall within preset limits. This system has not been thoroughly tested but preliminary tests indicate that it will reject a pulse when it is followed by another of the same height which follows it in the time interval of 0.1 to about 1.4 μsec.

4. Rejection of Cosmic Ray Pulses: Cosmic rays which pass through a 3" diameter NaI detector at minimum ionization deposit a broad distribution of energies in the neighborhood of 25 MeV in the crystal, the exact energy depending on the path. Since such cosmic rays appear with fluxes of $\sim 1/cm^2$ sec. they constitute a serious background in studies of high energy photon spectra. As it is normally used for response-function improvement the anti-coincidence shield around the NaI detector is biased at $\sim$0.2 MeV and should presumably eliminate cosmic rays since these deposit considerably larger energies in the annulus as well as the main detector. Unfortunately, with this low bias, the large volume annulus typically has counting rates of 10^5 c/s which give rise to correspondingly large dead times ($\sim$10%) in the anticoincidence circuitry. (See Fig. 25-1 and -2 of this report for views of cosmic ray leakage.) To insure the rejection of cosmic ray pulses by the anticoincidence shield, an auxiliary anti-coincidence circuit was placed in parallel with the usual one. This one is biased at 5 MeV and consequently has negligible dead time. With the full anti-coincidence circuitry in operation, cosmic ray pulses were found to be virtually eliminated from the main detector.

5. Elimination of Neutron-Induced Pulses: It was shown in last year's progress report[4] that in a typical bombardment at the tandem Van de Graaff, neutrons from the target are responsible for about as many pulses in a nearby NaI spectrometer as photons from the target. These neutrons presumably make interactions in the NaI or in the surrounding shielding which lead to pulses. This neutron background can be eliminated by time-of-flight techniques now that the Van de Graaff beam can be bunched (see Sec. 48). Figure 36-2 shows the time spectrum of pulses in a NaI crystal at 110 cm from the target when Sn^{124} was bombarded with 10 MeV protons. The necessary stop pulses were provided by the beam bunching system. The prompt γ ray peak here is 14 ηsec. wide and it should be possible to narrow it considerably. But even at this width it is now possible

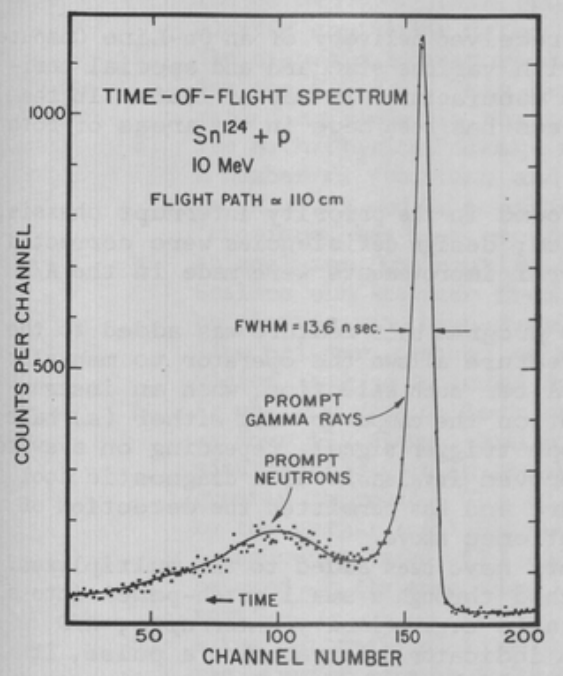

Fig. 36-2. Time-of-flight spectrum from the γ spectrometer for 10 MeV proton bombardment of Sn^{124}.

to measure photon spectra which are produced in nuclear reactions without serious contamination from neutrons produced in the same reactions. (S. M. Ferguson, I. Halpern, and D. L. Johnson)

1. Nuclear Physics Laboratory Annual Report, University of Washington, (1966) p. 53.
2. C. O. Bostrom and J. E. Draper, Rev. Sci. Instr. *32*, 1024 (1961).
3. C. D. Zerby and H. S. Moran, ORNL-3169 (1962).
4. Nuclear Physics Laboratory Annual Report, University of Washington, (1966) p. 102.

37. Particle Identification by Pulse Shape Discrimination

An attempt has been made to separate protons and deuterons using pulse shape discrimination.[1] The experiment was done using 13 MeV deuterons from the laboratory's Van de Graaff accelerator. The reactions considered were $C^{12}(d,d')C^{12}$ and $C^{12}(d,p)C^{13}$. Basically, the particle identification system was made up of two window discriminators and a time-to-pulse height converter. One of the discriminators was set just above the noise level and was used to generate the "stop" pulse for the time-to-pulse height converter. The other discriminator was set at a level which corresponded to about 50% of the pulse height of interest and it was used to generate the "start" pulse for the time-to-pulse height converter. It was necessary to use leading edge discrimination so that the timing between the two signals would be related to the shape of the leading edge of the pulse. From previous calculations,[1] it was expected that the pulses from protons and deuterons of the same energy would have a time difference in crossing the two discriminators of about 20 ns. It was found that the time jitter associated with the leading edge discrimination was about 10 ns. As a result, no definite separation was found. This project has been dropped for the present. If time allows, it might be interesting to try the system again with some modifications in conjunction with a two-parameter analyzer. (T. D. Hayward and D. M. Patterson)

1. Nuclear Physics Laboratory Annual Report, University of Washington (1966), p. 82.

38. On-Line Computer System

In December of 1965, the laboratory received delivery of an On-Line Computer System consisting of an SDS 930 computer with various standard and special peripherals. The system was accepted from the manufacturer in May of 1966. In the year since acceptance of the system, progress has been made in the areas of both hardware and software (programming):

A. Hardware

1. Several missing wires were found in the priority interrupt chassis, and these flaws were corrected; design deficiencies were corrected in the multiplexer, and several improvements were made in the A/D converters.
2. A P-Stop or absolute address program halt feature was added to the computer main-frame. This feature allows the operator to manually specify a memory location. After such selection, when an instruction is taken from this location the computer will either (a) halt or (b) produce an oscilloscope trigger signal, depending on a switch setting. This feature has proved invaluable as a diagnostic tool for both hardware and software and has permitted the detection of many of the design flaws mentioned above.
3. System Status Indicator Lights have been added to the multiplexer. These indicators can be patched through a small patch-panel into a variety of system status signals e.g. priority interrupts, A/D ready signals, etc. When an indicator unit receives a pulse, it will light a colored indicator light on the panel; depending on a switch setting, the light either holds until reset or holds for about 1/10 sec before resetting. Six such indicator units have been built and incorporated in the system. These have greatly reduced experimental setup time and provided convenient monitoring of the operation of an experiment.
4. Pulse-Height Analyzer Dump Capabilities have been provided for the Nuclear Data analyzers in counting rooms 3 and 4. This has made possible the dumping of a complete 512 channel spectrum from one of the multichannel analyzers to the computer memory in approximately 1 second. The computer can then operate on or store the data in a variety of ways, depending on the requirements of the experiment. The counting room scalars have also been wired into the computer so that they can be read directly by the computer. These capabilities have substantially increased the data-collection efficiency of experiments which do not directly require the computer as an on-line data collection device.
5. A replacement for the SDS 9150 card reader is being built. The initial design of the card handler and interfacing logic is completed and the handler fabrication is approximately 60% completed. The new reader uses photo-electric sensing of card punches, and will operate at a speed between 100 and 400 cards per minute.

B. Software

The number and variety of programs written in the past year is too large to be intelligently discussed here. Below are some of the more important software additions.

1. An Optical Model Code with automatic search has been written for the 8K SDS 930. This program allows the analysis and fitting of elastic scattering data.
2. The standard laboratory kinematics program HEEWEE has been recoded for the SDS 930. This permits rapid calculation of reaction kinematics as needed in the course of an experiment.
3. The Math/Physics Package which includes subroutines for calculating a number of functions and coefficients including Clebsch-Gordan, Racah, X, Z and Z1 coefficients and Legendre, Gamma, and Bessel functions, has been recoded to operate on the SDS 930.
4. An analyzer Dump routine has been written which reads out the Scalers and Analyzer from either counting room. The data may then be plotted with high-density plotting symbols (18 × 20/inch) on the line printer, punched on cards, or written on magnetic tape. Provision is also included for reading a data block from magnetic tape.
5. An on-line data collection program allows the computer to function as four 512 channel analyzers. Thus four detectors can be used simultaneously in an experiment, or data-collection efficiency greatly improved. The size of the data array is at present limited by the rather small 8K memory of the system. A routing system now being constructed will allow an even larger number of detectors to be used at the same time. Output of data is similar to the dump routine.
6. A two parameter on-line data collection program allows the use of the system as a 64 × 32 channel analyzer, or with a position-sensitive detector as 16 angular regions of 128 channels each or 8 angular regions of 256 channels each. Output of data is similar to the dump routine.
7. A data analysis program which permits analysis of an analyzer spectrum with the light pen has been written. Data is read in from cards or magnetic tape, and displayed on the CRT screen on a logarithmic scale. A background may then be drawn in with the light pen. This background is subtracted and the difference spectrum is displayed. The lower and upper limits of peaks to be analyzed are then specified with the light pen and the peaks are integrated. Following analysis, an optional plot of the data and background is plotted with high-density plotting symbols on the line printer.

(N. Cheney, J. G. Cramer, B. Fernandez, and D. Perry)

---

39. FORTRAN Linking as Used for Computer Associated Experiments

A. Description of the System

In using the SDS 930 computer, acquired last year by this laboratory,[1] for computer associated experiments, it has been found that in many applications the 8,192 words of core memory are not sufficient. One way to effectively expand the size of core memory for some applications is to use FORTRAN linking, which was included in the software package received with the computer. In using FORTRAN linking, previously compiled FORTRAN programs are loaded from magnetic tape in such a way that the system run-time and common storage areas of memory are not

affected. Thus one can pass information from one program to the next through common storage. The order in which the programs are loaded from magnetic tape is under operator and/or program control. A program which is much too large to fit into the computer can be broken up into self contained sections and run in sequence. The only limitation on total program size, other than the time required to load the linked programs from magnetic tape, is the amount of core memory available for common storage. One still needs a larger core memory for applications which require storing large arrays of data, as in using the computer as an on-line two-parameter analyzer.

B. Purpose of the Programs

FORTRAN linking is especially useful in applications where extreme speed is not essential. Reduction and analysis of data is one such application. To this end, programs have been written and are being written which allow an experimentor to quickly transfer data from the 512 channel analyzers and scalers in the Van de Graaff counting area to the computer; store these data on magnetic tape; produce a hard copy print-out and plot of these raw data; determine peak and background areas; analyze the peaks of interest; print and plot the results; and calculate and display such things as scaler ratios used for consistency checks. Thus, one can obtain an analysis of a spectrum as well as various consistency checks within several minutes after a spectrum has been collected. By having this information available during a data collection run, the experimenter is in a much better position to guide the course of the experiment and to discover and correct mistakes and malfunctions. Thus one can make more efficient use of data collection time.

C. Description of Finished Programs

1. Analyzer Dump Program. This program is used for the initial handling of the data. With it, one can quickly transfer data from any of the 512 channel analyzers and the scalers in the Van de Graaff counting area into the computer. This frees the analyzer so that additional data may be collected while the previous data are being handled by the computer. The program stores the data on magnetic tape, produces a tabular print out, and plots the data. It will also reproduce the data on punched cards if they are desired. Along with the print out of the data, the program also prints the scalers and ratios of selected scalers. The program has the added feature that it can find and load into core memory any specified block of data previously written on the data tape.

2. Peak Finding Program. This program is used to roughly determine the height, width, and position of peaks and shoulders in a raw spectrum. It also makes a rough fit to a fifth order polynomial background function. The program first finds obvious peaks and regions of clean background. The background regions are fitted to a fifth order polynomial using matrix inversion methods. The peaks are assumed to have the same width and a Gaussian shape. The peaks and background found on the first pass are subtracted from the raw spectrum and another pass is made. In this way the program can usually pick up shoulders and peaks sitting on top of a high background. The program prints the parameters it has found and makes an overlapped plot on the raw data and the rough fit.

3. Non-Linear Least-Squares-Fit Program. This program fits the raw data

to a fifth order polynomial background and skewed Gaussian peak shape. The program can handle up to 20 peaks at a time. At present all peaks are fitted with the same width and skewness parameters, but allowances have been made so that another independent width and skewness parameter can easily be included in the future. The initial values of the parameters are obtained from the rough fit program described above. The program uses a method of steepest descent to find a χ^2 minimum.[2] The output from the program consists of the final parameters, the initial parameters, the difference and percent differences of the initial and final parameters, and an overlapped plot of the raw data and the functional fit to the data. The program takes about 2 minutes to run with 10 peaks. It might be noted that the search program proper, with no input/output included in it, uses all but about 300 words of core storage. Thus it would be impossible to conveniently run this program on a small computer without resorting to something like FORTRAN linking.

Some of the programs above have been used as linked programs, in an experimental project (Sec. 22), and have proven to be a valuable asset. Two data analysis programs to be used in conjunction with this non-linear least squares fit program are nearly finished. Programs are also being written to kinematically keep track of peaks of interest for analysis purposes and to display various results for quick inspection on the oscilloscope display unit associated with the computer. It is felt that FORTRAN linking has proven its usefulness and that this mode of operation will become much more widely used in computer oriented experiments in the future. (J. G. Cramer, T. D. Hayward, and D. M. Patterson)

---

1. Nuclear Physics Laboratory Annual Report, University of Washington (1966), p. 79.
2. D. W. Marquardt, J. Soc. Indust. Appl. Math. *11*, 431 (1963).

---

40. Liquid Nitrogen Cooled Holder for Lithium-Drifted Germanium Detectors

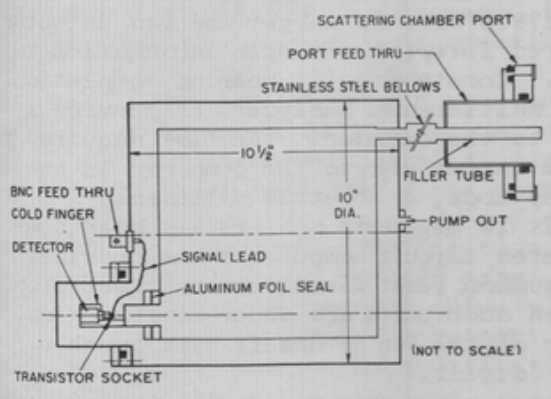

Fig. 40-1. Cross section of the liquid nitrogen cooled holder for lithium-drifted germanium γ ray detectors.

Prior to July, 1966, a Joule-Thomson cryostat system had been used to cool our Ge(Li) γ ray detectors.[1,2] However, on several occasions, the cryostat clogged up, probably due to moisture condensation, requiring a time-consuming partial warm-up of the detector before the cryostat could be made to function again. Therefore, it was decided to build a detector holder cooled by liquid nitrogen.

A detector holder was built which can be used either in air or inside the evacuated 60-inch scattering chamber (Fig. 40-1). It consists of two co-axial stainless steel cylinders which form a crude Dewar. The insulating vacuum be-

tween the two cylinders is maintained by a mechanical pump. The detector is held on a removable cold-finger attached to one end of the inner cylinder by a flange gasketed with an aluminum foil. The aluminum gasket is easy to make and provides a reliable vacuum seal down to liquid nitrogen temperatures. Changing the cold-finger is a relatively simple task.

The inner cylinder can be filled with liquid nitrogen from outside the scattering chamber through a pair of long, flexible stainless-steel bellows. The main problem in filling a Dewar inside a scattering chamber is to avoid freezing any rubber vacuum gaskets. This problem was solved by the use of a filler tube feed-through in a standard observation port which provides a long heat path between the liquid nitrogen tubes and the O-ring gaskets in the port. This technique was developed for a system designed to cool charged particle detectors.[3]

One filling of nitrogen lasts for ten to twelve hours. The nitrogen can be emptied and the detector warmed up in about twenty minutes by blowing compressed air through the filler bellows.

This system is much simpler to operate than the Joule-Thomson cryostat and has been used successfully in all of our more recent experiments. (S. Ferguson and C. F. Williamson)

---

1. Nuclear Physics Laboratory Annual Report, University of Washington (1965) p. 70.
2. C. F. Williamson and J. Alster, Nucl. Inst. and Meth. *46*; 341 (1967).
3. Nuclear Physics Laboratory Annual Report, University of Washington (1966) p. 83.

---

41. Design and Construction of Electronic Equipment

Major programs pursued during the last year include the following:

a. The angle encoder system for the 24 inch scattering chamber; the completed readout provides 0° to ±179.9° for the target and two detector arms. The design for the buffered interface of angle information to the computer has been completed. Construction is nearing completion.
b. Modification of the CR3 and CR4 multichannel analyzers to provide a fast dump mode of data transfer to the computer: the time required to dump a 512 channel spectrum from an analyzer to the computer is one cycle of the oscilloscope display mode, or about 50 millisec.
c. Design and development of 8 digit 15 megahertz scalers has been completed. The design uses integrated circuit components and provides data transfer to the computer, common reset lines, remote start stop, and built in discriminators. Ten such units are under construction.
d. Further testing and modification of the Van de Graaff beam buncher system (see Sec. 48 for further details.)
e. Design and construction of a router-mixer unit to provide for the use of eight detectors as multicounter experiments into a single analog-to-digital converter of the computer. The unit is expandable to provide 16 or 32 counter facility.

IX. ACCELERATOR RESEARCH AND DEVELOPMENT

45. The Three-Stage Van de Graaff Accelerator

Factory tests of the injector stage of the three-stage system were completed during June, 1966. Shipment of the injector components was started in July, 1966 but accidental damage to the pressure tank during the early stages of the shipment combined with a later derailment of the railroad train carrying the tank delayed the delivery of the tank to the laboratory until early October. The assembly of the injector was carried out as rapidly as possible following the arrival of the tank. Operation of the tandem stage of the accelerator system was limited whenever necessary during the installation process to particles, energies and beam intensities which would not prohibit the presence of personnel in the accelerator tunnel in the injector area.

By early January, 1967, the injector assembly had progressed to a point such that power to some of the components would soon be required in order to proceed efficiently. The tandem stage of the accelerator was therefore shut down on January 11 in order to connect the injector stage of the system and to install the integrated three-stage control system and control console. This installation included the revision and replacement of many of the tandem control components and the associated interconnecting wiring.

The change-over was completed and tandem operation was resumed by February 14, although much trouble shooting and debugging of the new and revised equipment remained to be done at that time.

The injector stage vacuum systems were tested during February, 1967, and preliminary operational tests of the ion source and beam neutralizing system were satisfactorily completed in early March. Final assembly of the system before the start of full operating tests was completed by the end of March. The first beam was obtained from the injector stage on April 14, 1967.

During the above mentioned shut down of the tandem accelerator several modifications and improvements were made, including the following:

1. New-type springs for connecting the accelerating tube and column field planes were installed.
2. Lucite rod controls to the terminal for positive operation of the stripper gas metering valve, stripper canal position, foil stripper (when installed), terminal lights, etc. were installed. These rods are operated from outside the tank and replace the string controls formerly used.
3. The alignment of the negative ion source, 20° inflection magnet, both einzel lenses, stripper canal, object slits, analyzing magnet and image slits was checked and adjusted where necessary. The injector system was also aligned with respect to the tandem at the same time.

Other major changes and modifications made to the tandem system during the year include:

1. Movement of the negative ion source to a position 62" farther from the tank to make room for the beam buncher (Sec. 48) and the 5" einzel lens.

2. The beam buncher and 5" einzel lens were installed.
3. A vacuum lock and new filament holder have been installed on the ion source to allow filament changes without letting air into the ion source.
4. A system has been designed and partially installed which will salvage and store the nitrogen gas which boils off in the liquid nitrogen traps. The use of this system will reduce the cost of the insulating gas to a value low enough to permit dumping of the gas from the tank, if desired, in order to eliminate most of the long pump out time now required before entering the tank for repairs.

The Van de Graaff tank has been opened ten times in the last year for the following reasons:

1. 5/11/66 - To replace the thermistor in the lower bearing of the drive motor.
2. 5/15/66 - To repair a pressure seal in the electrical feed-through bushing in the low energy end base plate.
3. 6/28/66 - To replace the belt drive motor which was burned out by a surge caused by a tank spark.
4. 7/1/66 - To replace a resistor and tighten the ring supports to improve voltage holding characteristics.
5. 9/5/66 - To repair the belt drive motor, burned out due to protective circuit failure.
6. 9/9/66 - To replace the belt which was damaged by hitting part of the terminal frame.
7. 9/16/66 - To investigate the cause of poor beam transmission. A loose column spring was replaced and the belt system was moved closer to the end of the tank.
8. 10/16/66 - To check for the cause of beam instability and test for suspected leaks in cooling water lines.
9. 1/11/67 - Planned shut down for modifications and improvements while connecting the injector stage to the new control console.
10. 3/3/67 - To investigate sparking caused by two defective resistors and a loose column spring.

Table 45-1 summarizes the statistics of Van de Graaff operation during the period from May 16, 1966 to April 15, 1967. (J. Heagney, T. Morgan, J. Orth, and G. Rohrbaugh)

Table 45-1. Statistics of Van de Graaff Operation During the Period from May 16, 1966 to April 15, 1967

Division of Van de Graaff Time Among Activities:

Activity		Time (hrs.)	Per Cent
Normal Operation:	Research	4174	77.0
	Machine & Component Tests	153	2.8
Scheduled repairs, modifications, & maintenance		758	14.0
Unscheduled repairs (incl. going into tank)		96	1.7
Experimenter's set-up time		252	4.6
	Total	5433	100.0

Division of Beam Time Among Projectiles:

Protons	1544	38.9
He^4	660	16.6
Deuterons	1192	30.0
O^{16}	374	9.5
He^3	199	5.0
Total	3969	100.0

---

46. Calculations of the Tandem Accelerator Beam Tube Optics

The acceleration tubes are one of the most expensive and vulnerable parts of a tandem accelerator. In an accelerator using straight tubes, a faulty tube section can be shorted out without greatly impairing the operation of the accelerator. However, with inclined-field tubes,[1] such as those used in the University of Washington three-stage tandem accelerator, shorting a tube section can radically alter the trajectory of particles through the accelerator and the performance of the machine. For this reason it is of vital interest to any tandem laboratory to understand the optics of the accelerator in general, and of inclined-field beam tubes in particular.

A simple expression has been derived for the position and inclination $(x_1,\dot{x}_1)$ of a charged particle emerging from an inclined-field tube section, in terms of the entrance position and inclination (x_0,x_0), the entrance and exit potentials of the tube section V_0 and V_1, the length L of the section, and the inclination angle θ of the electric field in the tube section:

$$x_1 = x_0 + L[(2\dot{x}_0'/(1+R)) + \tan\theta]$$

$$\dot{x}_1 = \frac{\dot{x}_0' \cos\theta + R \sin\theta}{R \cos\theta - \dot{x}_0' \sin\theta}$$

where

$$\dot{x}_0' = \frac{\dot{x}_0 \cos\theta - \sin\theta}{\dot{x}_0 \sin\theta + \cos\theta}$$

= inclination with respect to the field symmetry axis

and $R = \sqrt{V_1/V_0}$.

These expressions, along with other beam optics relations including the focusing properties of quadrupole, einzel, and aperature lenses, have been incorporated into a FORTRAN II computer program which calculates and plots the beam trajectory through our accelerator under a variety of terminal voltages and operating conditions. Figure 46-1 shows such a plot of the position and inclination of proton trajectories through the machine at a terminal potential of 5.46 MV.

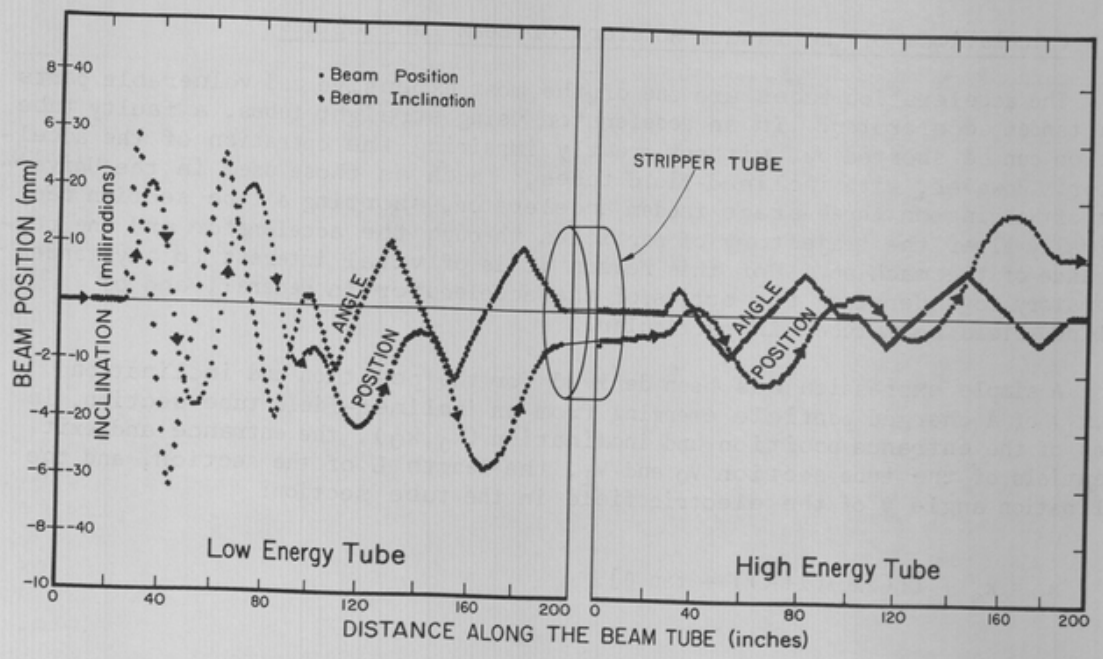

Fig. 46-1. Trajectory of a proton beam through the tandem accelerator at a terminal voltage of 5.46 MV. The beam enters on-axis and parallel to the axis.

The speed of a calculation of this type is limited primarily by the time required for the plot, and takes less than one minute on the laboratory SDS 930 computer.

An interesting effect has been noted in using the tube optics program. If a set of rays are traced from the stripper tube backwards down the low energy tube of the accelerator, it is found that an image of the stripper tube is formed just outside the entrance to the low-energy acceleration tube. If the beam entering the accelerator passes through the image-stripper it is essentially guaranteed to pass through the real stripper tube and presumably through the whole accelerator. Figure 46-2 shows the image of the stripper for a terminal potential of 5.46 MV and 60 keV protons entering the machine. The position of the image-stripper depends, of course, on the terminal potential of the accelerator and the energy of the accelerated particles as they enter the accelerator. The image position shown is fairly typical, however, and provides a clear idea of the requirements on the ion-source optics to achieve maximum transmission through the machine. (J. G. Cramer)

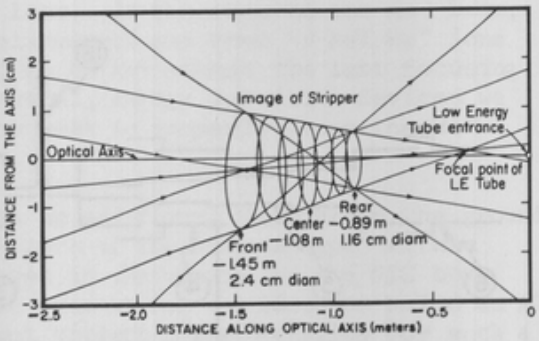

Fig. 46-2. The image of the stripper which is found just in front of the low energy tube. The beam must pass through this image without hitting an edge if it is to pass through the stripper tube.

---

47. Tandem Van de Graaff Negative Ion Source Alpha Beam

During the last year a large number of modifications have been made in the negative ion source (NIS) of the tandem Van de Graaff accelerator. These modifications have been aimed at increasing the alpha and He^3 beams from the machine. The primary interest in these beams has been generated by the need for more beam on target in the gamma-ray polarization measurements[1] and in the He^3 spin flip measurements.[2]

As an introduction to this work we shall briefly explain the operation of the NIS, excluding the theory of the operation of the duoplasmatron.

A beam of positive ions is extracted from the duoplasmatron (Fig. 47-1) (8) through a 13 mil aperture (7) (at ground potential) by the extraction electrode, (1) which rides at -40 kV. The extracted beam is then focused on the exchange canal (3) by an Einzel lens. (The lens is composed of the extraction, focus (2) and exchange electrodes.) A small amount of gas (hydrogen) is allowed to flow into the exchange canal where a portion of the extracted positive beam picks up two electrons from the exchange gas and becomes negative. This negative beam, upon leaving the exchange canal, is then accelerated by the ground electrode (4). It is also focused in its passage between the exchange canal and ground electrode. The effect of this last lens is hard to calculate because it falls between the category of an Einzel lens type gap, where it is assumed that the beam of ions

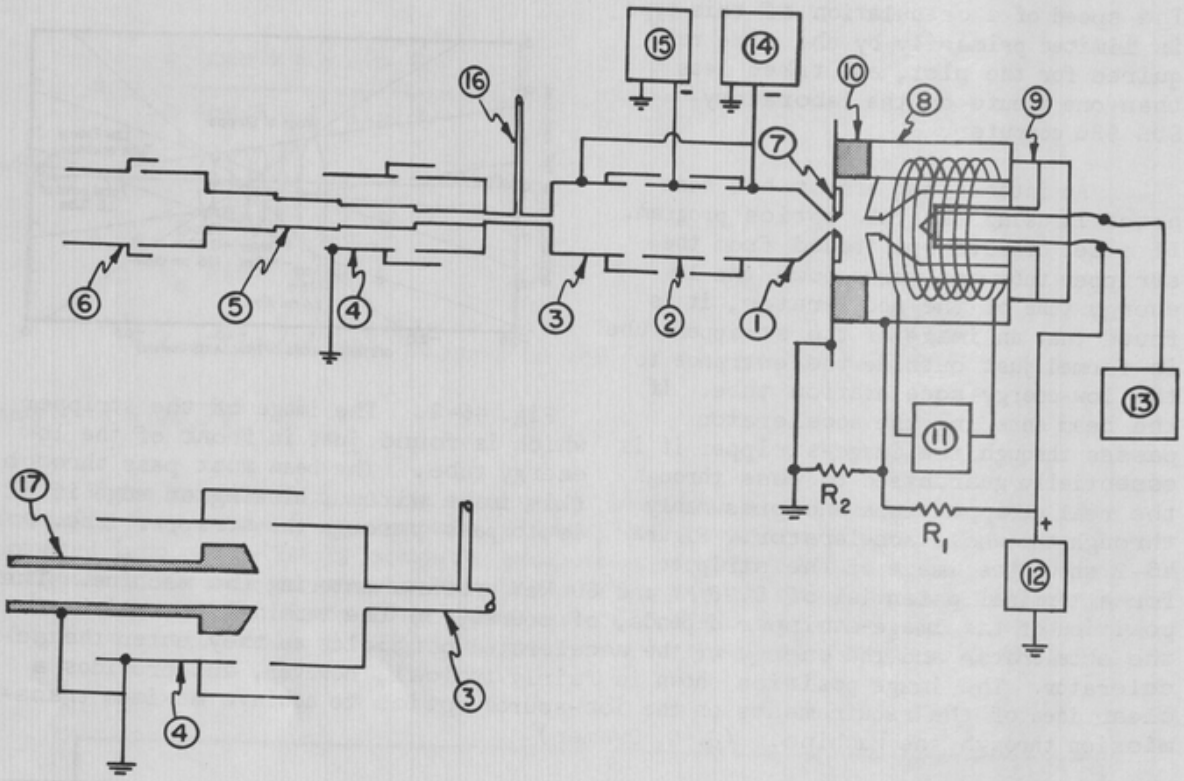

Fig. 47-1. Schematic diagram of the negative ion source: (1) extraction electrode (2) focus electrode (3) exchange canal electrode (4) ground electrode (5) exchange canal extension (6) exchange canal extension ground electrode (7) 13 mil aperture disc (8) duoplasmatron (9) filament lock and filament rod (10) insulator (11) duoplasmatron bottle magnet power (12) filament bias supply (13) filament current supply (14) 50 kV, 50 mA exchange and extraction power supply (15) 10 kV, 10 mA focus power supply (16) exchange gas supply line (17) lens strengthening ground electrode.

has an energy large when compared to its change in energy upon traversing the gap, and the field immersion type lens, where it is assumed that all of the beam energy is acquired in crossing the focusing gap. One can, however, draw certain qualitative conclusions by considering the operation of the source.

The NIS was designed originally to produce H^- ions and it has produced in excess of 60 microamps of H^- beam. This beam is originally extracted from the duoplasmatron as H_3^+ molecular ion with approximately 40 keV of energy at the exchange canal. At this point the molecular ion breaks up by collision with the exchange gas and each proton has roughly 13.3 keV of energy. It should be noted that this places the proton at an energy just above the charge exchange resonance for H^+ in hydrogen going to H^- but still near the maximum of the exchange cross section.[3]

Thus we see that 13.3 keV protons leave the exchange canal and are accelerated to 53.3 keV across the last focusing lens. In the case of the He^- beam, however, we extract 40 keV He^+ from the duoplasmatron and thus 40 keV He^- ions leave the exchange canal and are accelerated to 80 keV across the last focusing lens. Since electrostatic lenses are, in general, energy sensitive devices we see that the last lens of the NIS must be too weak to properly focus the He^- beam.

For this reason it was decided to place an additional lens after the ground electrode. As a result, the quadrupole (AG) lens of the biased type[4] with a water cooled drift tube, was built to be placed in the vacuum of the NIS box, immediately behind the ground electrode. The reasons for deciding to build an AG lens were that 1) we could build the constant current power supplies for such a lens in the laboratory, whereas we did not have the capability to build the power supply for an Einzel lens, and 2) with the biased type AG lens it would be possible to steer the beam out of the source and through the small exit of the NIS vacuum box.

The lens was installed and tested during July, 1966 and found to increase the beam at the high energy end of the tandem by a factor of from 1.5 to 2. About 30% of the improvement could be attributed to improved transmission of the beam through the machine by the use of the steering properties of the biased AG lens. Unfortunately the AG lens suffers from severe aberration when the separation of the two lens segments is comparable to the distance from the lens to the object, which it is. It was noted at the time that the AG lens was tested that it had a negligible effect on the H^- beam. As a result the AG lens was removed and the last lens of the source was strengthened by placing a grounded 3/4 inch diameter stainless steel tube through the center of the ground electrode to the middle of the gap between the exchange and ground electrodes (Fig. 47-1). This moves the ground plane, strengthening the electric field near the axis of the lens and thus strengthening the lens.

This new lens configuration seemed to work as well as the AG lens, with the possible exception of the loss of steering which was attainable with the biased AG lens.

The next attempt to improve the He^- beam was to install what has become known in the laboratory as the "wobble plate". The "wobble plate" is a standard aperture plate (in which the 13 mil aperture mounts and to which the duoplasmatron is attached) that has been modified in such a way that it allows one to move the 13 mil aperture and duoplasmatron around in front of the extraction electrode, and thus optimize the extraction from the duoplasmatron during operation. The source is extremely sensitive to the position of the "wobble plate", but the maximum He^- beam output was not increased by this modification, and it is now believed that this explaines our lack of previous success with the so-called plasma expansion cup.[5,6] We now believe that the plasma expansion cup only makes the alignment of the aperture to the extraction electrode less critical, and that since our source was quite well aligned, its addition made very little change in the source output.

The next change in the source was to add a filament lock to the duoplasma-

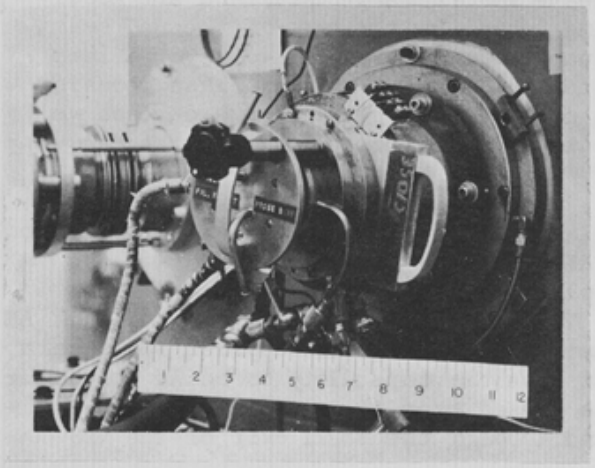

Fig. 47-2. Filament lock and filament rod shown in position on the duoplasmatron source.

tron (Fig. 47-2). This allows changing the filament without losing the source vacuum. This is desirable because it has been observed that the He^- output is reduced by as much as a factor of 2 when the source is let up to air and requires as long as 2 to 3 days to recondition. These figures are extremes and represent conditions when the source is let up to air for an extended period of time (1/2 hour), rather than for a standard filament change; however, they do point to the need for keeping gases other than He out of the source during an alpha run.

The filament lock and filament rod are designed such that the filament rod is completely free when it is removed from the lock, *i.e.* the rod "unplugs" from the filament current, filament bias and air cooling as it is retracted from the filament lock. This facilitates filament changing and allows the complete replacement of the filament rod should it become damaged. The filament rod clamps the filament with tantalum finger clamps which greatly simplify filament replacement.

The filament design has also been changed to simplify fabrication. The new filaments consist of a 1 inch long 30 mil tungsten wire bent smoothly in the middle at a right angle. The filament is then mounted by clamping the two ends with the bend forming the point of the filament. The new design easily reduces fabrication time by a factor of 10, and since the new filaments are shorter, and thus have less resistance, they allow us to run with higher arc currents (which seem to be required for maximum He^- output) and still remain within the range of the arc current regulator.

The filament lock and rod also reduce the time required for a filament change by a factor of about 6 and when spare rods are fabricated it will probably reduce this time by another factor of 3.

Another change has been to return to the use of apertures with tantalum inserts. These apertures have a longer life than the standard copper apertures and thus reduce the number of times that the source vacuum must be broken. It has also now been established as a routine, when an aperture must be changed during an alpha run, that the source is let up to He rather than air or dry nitrogen. This has proven to almost completely eliminate the conditioning time of the source.

It should be noted that at about this time the tandem was shut down for the control console change,[7] and that during this time the ion source and tandem were aligned. As a result of this the alpha particle transmission through the machine was increased from between 15 and 20 percent to between 30 and 40 percent and,

therefore, increases the amount of beam available on target.

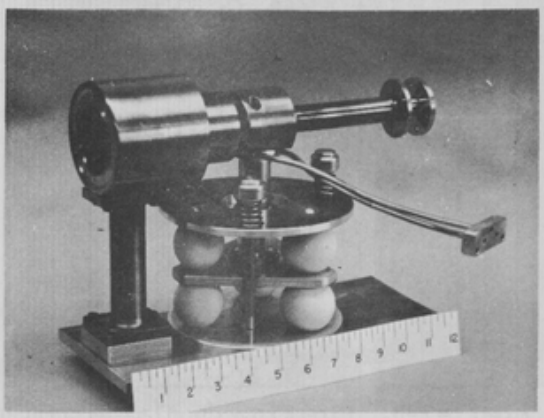

Fig. 47-3. Exchange canal extension assembly showing extension, ground electrode, and dielectric-cooled insulator.

As a result of communications with the University of Pennsylvania[6] it was decided to extend the exchange canal from its original 2 inches to 10 inches (Fig. 47-3). This permits a lower exchange gas flow into the source for optimum source output and thereby reduces the pressure in the source and low energy tube extension. The lower pressure reduces the chance for collision of ions in the He^- beam with background gas in the drift tube. Such collisions inevitably result in the loss of He^- ions from the beam.

In order to maintain the additional focusing in the lens between the exchange canal extension (5) and the new ground electrode (6), the lens gap has been made variable and is presently set at 1/4 inch rather than the original 1/2 inch.

The exchange canal extension has been initially tested and appears to increase the alpha beam on target by as much as a factor of 2. The source pressure with the exchange canal extension operates slightly above one half the pressure which it previously required, as would be expected from the pumping speed of such an exchange canal.

The next modification which is under way but has not as yet been completed is an attempt to increase the energy of the extracted He^+ beam toward the charge exchange resonance in hydrogen. This resonance lies at about 135 keV,[3] and while this is outside the range of the present work we hope to move from our present exchange energy (45 keV) to about 85 keV and thus increase the output by a factor of 2 to 3.

The installation of the present exchange and extraction system is not sufficient to withstand such an increase in voltage and so it is planned to float the duoplasmatron and aperture plate to a positive 40 kV. Such a plan requires an insulator on which to mount the aperture plate, and a highly modified aperture plate as well. These have been constructed and are shown in Figs. 47-4 and 47-5. The insulator was cast and machined from a glass filled epoxy. It is mounted on an aluminum "wobble plate" which in turn mounts on the present NIS. The modified aperture plate consists of a cylindrical steel body with a steel base at one end. This steel base holds the aperture and contains cooling passages to cool the plate. The cylindrical steel body is supported by a brass collar about halfway up its side. This collar seals against the top of the epoxy insulator and provides a plate to which the duoplasmatron is bolted. In order to align the duoplasmatron when an aperture is replaced the duoplasmatron has been placed on

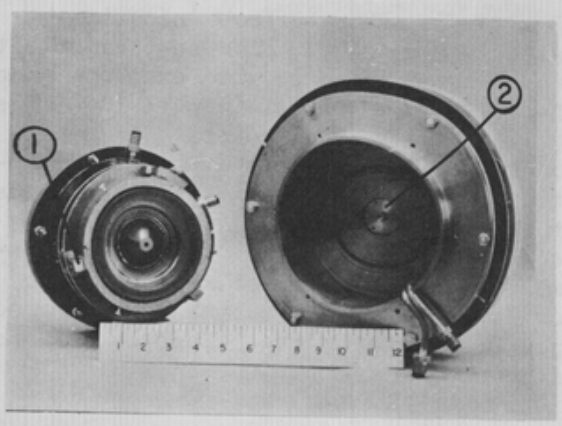

Fig. 47-4. Floating duoplasmatron and its aperture plate. The duoplasmatron (extreme left) is seen from the probe end and one can see the rollers (1) which allow it to be positioned in front of the 13 mil aperture. The insulated aperture plate with an installed 13 mil aperture (2) is seen at the right. Lines at lower right provide dielectric cooling of the aperture plate which floats to positive high voltage with the duoplasmatron.

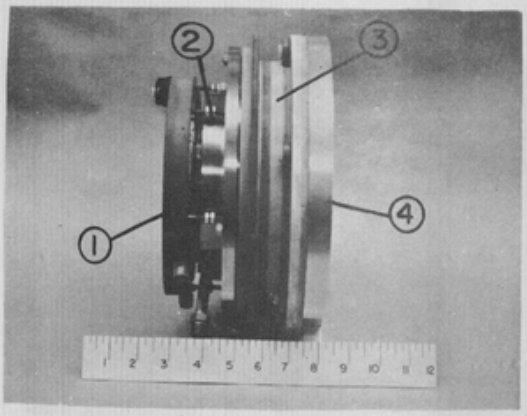

Fig. 47-5. Floating duoplasmatron insulator. The duoplasmatron (1) is shown installed inside the aperture plate cavity (2), which is supported by an epoxy insulator (3). The insulator is mounted on an aluminum transition plate (4) which allows the mounting of the insulator on the present ion source.

small rollers so that it can roll on the inside cylindrical surface of the new aperture plate.

It should be pointed out that there are certain problems with such a plan. These include the necessity to float the power supplies for the duoplasmatron. Such supplies have been built and a 1:1 insulation transformer with a 25 amp, 110 V secondary and 100 kV insulation is on order. It is also necessary to provide dielectric cooling for both the duoplasmatron and the aperture plate, and it is anticipated at this time that this can be provided by the present dielectric cooling used to cool the extraction and exchange electrodes.

The insulated duoplasmatron has been designed in such a way that should it be necessary to go to an alkali metal exchange system[8] the insulator will be adequately shielded from metal contamination.

In conclusion it should be pointed out that at the time this work was started, typical beams of alphas on target were of the order of 2 to 5 ηamp.; they have presently reached in excess of 40 ηamp., with an anticipated future yield of approximately 100 ηamp. (T. D. Hayward, D. M. Patterson, and J. R. Tesmer).

1. Sec. 22 of this report.
2. Sec. 18 of this report.
3. T. Jorgensen, Jr., C. E. Kuyatt, Phys. Rev. *140*, 1484 (1965).
4. J. G. Cramer, F. H. Schmidt, Nuc. Inst. and Methods, *45*, 325 (1966).
5. Private communication between W. A. Kolasinski and the University of Pennsylvania Tandem Accelerator Laboratory, February 1966.
6. R. Middleton, private communication. We are grateful to Professor Middleton for supplying us with drawings prior to their publication.
7. Sec. 45 of this report.
8. H. T. Richards, F. A. Rose, P. B. Tollefsurd, preprint, University of Wisconsin.

48. Beam Bunching System for the Tandem Van de Graaff

The installation of the tandem bunching system[1] has been completed and some tests on the system's performance have been made. To provide room for the buncher (around 5 feet long) it was necessary to move the tandem ion source back from the tank. The low energy wiping slits (near the tank entrance) and the low energy chopping plates had been installed earlier.

The electronic drivers and power for the buncher are contained in a housing suspended from the buncher tube itself. This compactness is possible because the drivers use solid state devices (two RCA 2N4298 high frequency power transistors) in place of tubes. The transistors provide a signal (400 V, peak-to-peak) to the primary of an RF transformer, the secondary of which is also tuned and provides for a step-up by a factor of 8. The capacity in the secondary circuit is mostly that of the cylindrical buncher electrodes themselves, but the addition of a small variable condenser makes it possible to cover the frequency range 2 to 5 × 10^6 cps.

The high voltage step-up requires that the load be of high Q. The design Q was 100 and the measured Q was 140. The power needed to drive the buncher to its normal voltage is consequently fairly small (25 watts) and is easily handled by a pair of transistors. The main disadvantage of high Q systems is their instability. To date we have happily observed no detuning during runs or even from day to day. The lack of thermally induced drifts reflect the low power dissipation.

The low energy chopping circuit is also made of solid state devices. It operates in push-pull and provides a square wave form at the system frequency. The voltage on the chopper plates alternates between zero and the full deflection voltage, 800 V. The beam-pass (zero volt) portion of the square wave has a continuously variable duration starting at about 15 nsec. There is only one beam burst passed each cycle instead of two as in sine wave chopping. This eliminates the problem of coping with the undesired bunch.

Preliminary tests with the H_2^+ beam from the ion source show that a 30 nsec. long packet can be compressed by the buncher to 6.8 nsec. This is roughly the lower limit set by the energy spread associated with the H_2^+ breakup in the ex-

change canal. It is possible to extract an H_1^+ beam from the ion source, but it is ten to twenty times weaker than the H_2^+ beam. The H_1^+ beam compressed to 3.8 nsec. This is larger than one would expect and suggests that even the H_1^+ beam may be suffering from energy inhomogeneities. These may arise from poor regulation of the exchange canal voltage or from fringing field effects in the exchange canal. The regulation of the exchange voltage has recently been improved and it is planned to carry out further tests of the buncher system. If bunches as narrow as 1 nsec. are needed it may be necessary to add a high energy chopper to the system. But even the 6.8 nsec. bunches have already proved very useful for some studies of photons and neutrons (see Secs. 25, 31, 36). (H. Fauska, I. Halpern, J. Lilley, N. Ward, and C. Williamson)

---

1. Nuclear Physics Laboratory Annual Report, University of Washington (1966), p. 103.

---

49. Some Observations Relating to Terminal Voltage Fluctuations of the Tandem Van de Graaff

The terminal potential of the tandem Van de Graaff accelerator fluctuates by 500 to 1000 volts, even under the best of operating conditions. The pattern of the fluctuations is periodic at the frequency of the belt cycle; the dominant frequency spectrum extends from the belt frequency, which is about 2.4 Hz, to about 30-40 Hz. The voltage pattern, which is quite complicated, repeats over and over each belt cycle in a remarkably faithful manner. Although the voltage pattern is different when the corona regulator is in proper operation, it too repeats in a carbon-copy fashion.

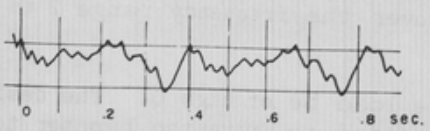

Fig. 49-1. Oscillogram tracing of terminal potential. Note that the pattern repeats each belt cycle. Peak-to-peak fluctuation is ∿2.4 kV.

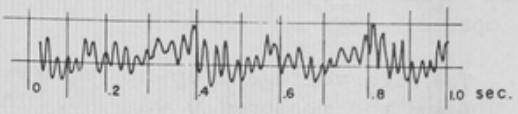

Fig. 49-2. Oscillogram tracing of terminal current. Note that the pattern repeats each belt cycle. Belt charge current = 100 μA.

A typical oscillogram of the terminal potential, as detected by the usual capacitive pickup electrodes, is shown in Fig. 49-1. Two belt periods are visible on the trace. The peak-to-peak fluctuation is ∿2.4 kV at a terminal potential of 4 MV.

By means of a shorting rod, which can be inserted through a seal in the wall of the Van de Graaff pressure vessel, we have studies the current delivered to the terminal. A typical oscillogram is shown in Fig. 49-2. The charging current

delivered to the belt was 100 μA. The peak-to-peak fluctuation is about 30 μA.

Although Fig. 49-1 and -2 do not demonstrate that the voltage fluctuations are correlated with the current, chiefly because these two oscillograms were taken at widely different times, we have verified that the expected correlation does exist. The voltage fluctuations are of course very heavily attenuated by the effective RC of the terminal.

We have also examined the momentum-analyzed beam at the image slits of the customary analyzing magnet. The beam energy does fluctuate with the same pattern as the terminal potential, which leave no doubt as to the real existence of the potential variations.

The oscillograms of Fig. 49-1 and -2 show frequencies extending from the belt frequency up to ∿60 Hz. Figure 49-2 especially shows a very prominent component containing 17 peaks per belt cycle, or a frequency of ∿40 Hz. We have observed that three different charging belts show almost exactly the same periodicity. This fact was not at first recognized, and only after examination of old oscilloscope photographs taken as a routine check on belt condition did we find that a frequency corresponding closely to 17 peaks per belt length was imbedded in each belt. One belt was removed because the current fluctuations became excessive, even though the charge and discharge screens were in good condition and properly adjusted. The second belt was removed because of accidental damage. We have some, though not conclusive, evidence that belts gradually generate a larger and larger "17-peak" structure as they age or wear.

The "17-peak" structure is evidently caused by the method of curing the rubber impregnation applied to the belt during the manufacturing process. The "curing length" is 30 inches with about a 2-inch overlap at each end.[2] The average length of a belt is 454 inches. This gives very nearly 17 cure patterns in the length of the belt. An obvious remedy would be to develop a system for a uniform and continuous curing procedure, such as between rollers.

Alternatively, if the frequency of the inhomogeneties could be increased, say by a factor of two, the terminal ripple would be reduced by a factor of about two by the RC filtering action. The High Voltage Engineering Corporation has made a special belt for us with an effective curing length of 15 inches instead of 30 inches. It is planned to install it in the near future.

Effects Due to Corona Regulator System

The corona regulator produces a phase shift of very nearly 90° for frequencies above about 10 Hz. The effective resistance of the corona discharge at 5 MV and 100 μA corona current is 5×10^{10} ohms. With an assumed effective terminal capacitance of 100 pF, the phase shift between a driving voltage on the corona points and the terminal is very close to 90° at 10 Hz. A single voltage pulse at the terminal with a width less than 0.1 second appears approximately as a differentiated pulse when the regulator is in operation. Moreover, the regulator tends to hunt at a frequency of about 20 Hz. Nevertheless, if the gain of the regulator is not too high, the terminal potential is still a pattern which repeats, carbon-copy like, each belt cycle. The corona regulator can eliminate low frequency

components, for example the belt frequency, but due to the 90° phase shift cannot eliminate the 40 Hz frequency due to the 17 peaks per belt cycle.

Charge Spread on the Belt

We constructed a circuit with which we could introduce either periodic or step function modulation of the belt charge current. Figure 49-3 shows the effect on the terminal current due to a step-function decrease in belt charge. Figure 49-3a shows the current pattern in the absence of the step, and Fig. 49-3b shows the current pattern with the step. The step occurs at the point marked, and is the voltage supplied by the belt charge circuit. That point on the belt reaches the terminal 200 msec. later, and the average current is seen to begin to change. Figure 49-3c shows the approximate difference in terminal current between Figs. 49-3a and -3b. The sharp rise charge step has spread out to a gentle rise extending over about 70-80 msec., with a 90% decrease in 60 msec. Nevertheless, the basic "17 peak" pattern remains unaltered.

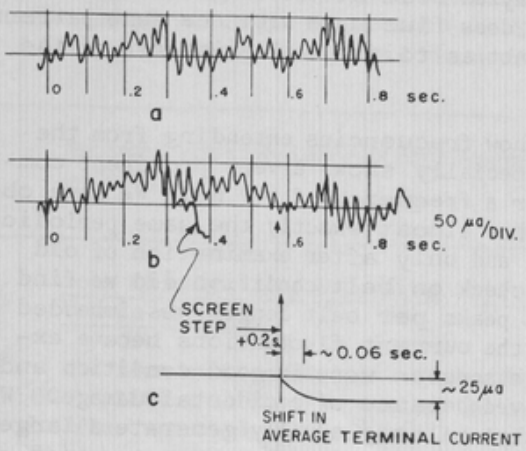

Fig. 49-3. (a) Terminal current when belt charge current is constant. (b) Terminal current when a step decrease is applied to belt charge current. (c) Approximate difference between trace (a) and (b) showing how the charge spreads out between the base and terminal.

The above observation suggests that as charge is fed to the belt it spreads out as the belt moves toward the terminal, but it tends to concentrate in a particular pattern. Since the distance the charge spreads in the time of transit from the charge screen to the terminal is greater than the distance between the inhomogeneities in the belt, it is not possible to smooth out the charge inhomogeneities by feeding an appropriate signal to the charging circuit. This means that a regulator based upon an analog memory system utilizing a tape recorder[1] will not work, unless the conductivity of the belt is substantially reduced.

Miscellaneous Observations

The terminal current ripple pattern for a given belt changes only slowly with time. We have oscilloscope photographs taken two weeks apart which show almost exactly the same pattern. However, there is some evidence that the inhomogeneities of a given belt grow over a period of months.

If the charging and take-off screens are poorly adjusted, the current pattern does not repeat each belt cycle. Thus, improper screen adjustment can cause large instabilities in operation.

The so-called self-charge generated on the belt when the impressed charging current is zero also exhibits a repeating pattern, but it is much smaller than the fluctuations with normal charging current. Thus, self-charge is not a cause of the fluctuations. With the tank at atmospheric pressure we studied the self-charge with and without the terminal pick-off screen in place and found it unchanged for the two arrangements. This suggests that self-charge is mainly on the inside of the belt.

The terminal current ripple depends upon the humidity of the tank gas and upon the length of time the belt has been dried by the tank gas. It is worse under humid conditions. This observation supports the thesis that the fluctuations are due to a balance between the rate at which charge spreads out after being deposited on the belt and the inhomogeneities of the belt. Since the charge current is maintained constant by the charging supply, the non-uniformity of the current reaching the terminal must be produced during the belt transit from the base to the terminal.

We have also studied the voltage pattern supplied to the belt by the constant current charging supply. This voltage exhibits a repeating pattern which shows definite correlation with the current pattern received at the terminal, displaced by 200 msec.(H. Fauska, J. S. Heagney, T. J. Morgan, and F. H. Schmidt)

---

1. Nuclear Physics Laboratory Annual Report, University of Washington (1966), p. 98.
2. Jacques Shaw, High Voltage Engineering Corporation, private communication.

---

50. Cyclotron

During the past year the operation of the 60-in. cyclotron has continued with relatively few major changes from previous years. An electrical failure necessitated the rebuilding of the "Dee" voltage regulator. Some improvements were incorporated in the new chassis resulting in slightly less 720-cycle ripple on the "Dee" voltage and slightly improved over-all operation. Water accumulating in the lower magnet coil tank of the main magnet caused an intermittent shorting of the lower coil to ground and subsequent loss of regulation. After the cause was discovered extensive attempts were made to clear the condition, short of dismantling the coil structure. When these attempts failed, the top layer of the upper coil and the bottom layer of the lower coil were disconnected electrically from the circuit and slightly higher currents through the remaining coils produced the required field. Cables from the cyclotron cave to the Van de Graaff counting area have been installed which allow on-line use of the computer facility.

Among the projects originating outside the laboratory and not reported elsewhere in this report, is a rather extensive project being undertaken by the materials research group at Atomics International. This project is making use of the alpha particle beam to insert helium, uniformly, into metal samples. The object of the study is to simulate the helium inclusion due to high energy neutron

fluxes. In a several hour run, helium concentrations are obtained which would require years of exposure in the highest reactor fluxes now available. The mechanical properties of the samples can then be evaluated and best choices for reactor fuel element cladding materials can be made.

The following table summarizes the operation for the period May 15, 1966 to April 15, 1967. (J. Beechel and J. S. Heagney)

Table 50-1. Statistics of Cyclotron Operation from May 16, 1966 to April 15, 1967

Division of Cyclotron Time Among Activities	Time	
Activity	Hours	Per Cent
Normal Operation	1820	50.9
Experimental Set-up	564	15.8
Cyclotron Testing	38	1.1
Scheduled Repairs	309	8.6
Unscheduled Repairs	486	13.6
Unsatisfactory Operation	207	5.8
Unrequested Time	153	4.2
Total	3577	100.0
Division of Normal Operation Among Projectiles		
Alpha Particles	1315	72.2
Protons	145	8.0
Deuterons	360	19.8
Total	1820	100.0
Bombardments for Outside Investigators		
Department of Physics - Professor McDermott	155.7	
Department of Nuclear Medicine	233.0	
Radiological Safety Division	10.5	
Oregon State University	98.7	
University of Oregon	16.0	
Western Washington State College	8.9	
Simon Fraser University	29.3	
Whitman College	8.5	
Atomics International	27.2	
Total	587.8	

X. APPENDIX

51. Nuclear Physics Laboratory Personnel

Faculty

John S. Blair, Professor
David Bodansky, Professor
John G. Cramer, Assistant Professor
Arthur W. Fairhall, Professor
George W. Farwell, Professor
James B. Gerhart, Professor
I. Halpern, Professor
Fred H. Schmidt, Professor
Robert Vandenbosch, Associate Professor

Nuclear Physics Laboratory Research Staff

Joseph P. Allen, Research Associate
Peter von Brentano, Senior Research Associate
Bernard Fernandez, Physicst[1]
Anastasios Katsanos, Research Associate
Charles D. Kavaloski, Research Assistant Professor[2]
John S. Lilley, Research Assistant Professor[3]
Paul F. Mizera, Research Associate
Ted J. Morgan, Research Associate Professor;
Supervisor, Nuclear Physics Laboratory[13]
Jack C. Norman, Instructor[4]
Gary W. Phillips, Research Associate
Patrick Richard, Research Assistant Professor
Nelson Stein, Research Assistant Professor[5]
William G. Weitkamp, Research Assistant Professor
Claude F. Williamson, Research Assistant Professor[6]

Laboratory Supervisory Personnel

Harold Fauska, Senior Physicist;
Research Electronics Supervisor
Joseph S. Heagney, Senior Physicist
Peter Momcilovich, Engineer
John W. Orth, Assistant Supervisor, Nuclear Physics Laboratory

Predoctoral Research Associates

Chemistry

Charles J. Bishop
Dennis G. Perry
Clifford Rudy
Robert W. Shaw, Jr.
Kevin L. Wolf

Physics

Wilfred J. Braithwaite
Gary M. Chenevert
Nelson Cue
Stephen M. Ferguson
Thomas D. Hayward
Roger A. Hinrichs
David L. Johnson
Wojciech A. Kolasinski
Donald M. Patterson
David C. Shreve
Derek W. Storm

Research Assistants

Chemistry

Joseph Gonyeau[7]
David A. Muga[8]

Physics

David Chamberlin
Ashish Chatterjee[7]
Juri Eenma[9]
Robert Lewis[7]
Ching C. Ling
Dennis L. Oberg
William Q. Sumner
Joseph R. Tesmer
William R. Wharton

Full-Time Technical Staff

Machine Shop

Harvey E. Bennett, Foreman
Norman E. Gilbertson
Charles E. Hart
Gustav E. Johnson
Edwin P. McArthur
Bernard Miller, Assistant Foreman
Byron A. Scott
Anthony J. Virant
Allen L. Willman

Electronic and Electrical

Noel R. Cheney, Field Engineer
Laverne H. Dunning
Robert B. Elliott[10]
Kyum-Ha Lee
George C. Monge[11]
Rod E. Stowell
Norman G. Ward

Technicians

Richard R. Clay
Emdad Hussain[12]
Carl E. Linder
Georgia Jo Rohrbaugh
George E. Saling

Design and Drafting

Robert G. Clarke[11]
Peggy Douglass
David W. Gough
Lewis E. Page

Accelerator Operators

Jacque M. Beechel
Bonnie C. Murray[11]

Others

Tylaine C. Hansen, Office Assistant
Shirley Kellenbarger, Chemist
Joanne M. Sauer, Chemist
Helene Turner, Administrative Secretary

Part-Time Technical Staff

Student Helpers

Richard F. Berthelsdorf[11]
Robert W. Eschrich[11]
John G. Marckworth
Kimball A. Milton[11]
Scott A. Morris[11]
Charles J. Peterson
Gary W. Roth
Seppo O. Sari[11]

Others

Mary A. Beard

1 On leave from SACLAY, France.
2 Now at Lowell Technological Institute, Lowell, Massachusetts.
3 Now at University of Minnesota, Minneapolis, Minnesota.
4 Now at University of Kentucky, Lexington, Kentucky.
5 Now at Yale University, New Haven, Connecticut.
6 Now at Massachusetts Institute of Technology, Cambridge, Massachusetts.
7 Research Assistant without stipend.
8 On leave of absence.
9 National Science Foundation Fellowship.
10 Retired.
11 Terminated.
12 Sponsored by International Atomic Energy Agency.
13 Deceased May 24, 1967.

52. Advanced Degrees Granted, Academic Year 1966-1967

P. F. Mizera: Ph.D. "An Investigation of Two and Three Nucleon Clustering in B^{11}, N^{15}, and F^{19} Using (α,Li) Reactions at an Incident Energy of 42 MeV."

53. List of Publications

"A b=1.0 Torodial Beta Ray Spectrometer", F.J. Bartis, Nucl. Instr. and Methods *44*, 125-132 (1966).

"Isospin Conservation in the Reaction $C^{12}(\alpha,d)N^{14}$", C.D. Zafiratos, J.S. Lilley, and F.W. Slee, Phys. Rev. *154*, 887 (1967).

"The Biased Quadrupole: A Method of Steering Accelerator Beams", J.G. Cramer and F.H. Schmidt, Nucl. Instr. and Methods *45*, 325-327 (1966).

"A Miniature Cooling System for Ge(Li) Solid-State Detectors", C.F. Williamson and J. Alster, Nucl. Instr. and Methods *46*, 341-343 (1967).

"The Charge Distribution of O^{16} Ions Produced from a Tandem Accelerator", E. Preikschat and J.G. Cramer, Rev. of Sci. Instr. *37*, 1722-1726 (1966).

"Tests of Time-Reversal Invariance in the Mg^{24} + d ⇄ Mg^{25} + p Reactions", D. Bodansky, W.J. Braithwaite, D.C. Shreve, D.W. Storm, and W.G. Weitkamp, Phys. Rev. Letters *17*, 589-592 (1966).

"The Removal of Angular Momentum by Evaporating Neutrons and Photons in the (α,3n) Reaction", B.J. Shepherd, C.F. Williamson, and I. Halpern, Phys. Rev. *17*, 806-808 (1966).

"Equilibrium Charge Distributions of 8 MeV Carbon Ions in Various Media", E. Preikschat and R. Vandenbosch, Nucl. Instr. and Methods *46*, 333-340 (1967).

"Polarization in p-α Scattering from 17 to 27 MeV", W.G. Weitkamp and W. Haeberli, Nucl. Phys. *83*, 46-64 (1966).

"Observation of the 4.12 MeV $O^{14} \rightarrow N^{14}$ Positron Spectrum Shape", G.S. Sidhu and J.B. Gerhart, Phys. Rev. *148*, 1024-1030 (1966).

Publications in Press or Submitted for Publication:

"Inelastic Scattering of 42 MeV Alpha Particles in the s-d Shell: Mg^{24}", I.M. Naqib and J.S. Blair (submitted to Phys. Rev.).

"The $Si^{28}(He^4,O^{16})O^{16}$ Reaction", R. Vandenbosch, J.C. Norman, and C.J. Bishop (Phys. Rev.).

"A Beam Centering Device for Nuclear Accelerators", H. Fauska and C.F. Williamson (Nucl. Instr. and Methods).

"(d,He^3) Studies on Zr^{90}, Y^{89}, and Sr^{88}", C.D. Kavaloski, J.S. Lilley, D.C. Shreve, and Nelson Stein (Phys. Rev.).

"Channel Analysis of Cross Sections and Angular Distributions for Fission Induced by Neutrons and Photons", R. Vandenbosch (Nucl.Phys.).

"Alpha Particle Emission During Nuclear Fission at Moderate Excitation Energies", W.D. Loveland, A.W. Fairhall, and I. Halpern (preprint).

Papers Given at Meetings and Conferences:

"Nuclear Fission", R. Vandenbosch, Gordon Research Conference on Nuclear Chemistry, June 1966.

"Proton Spin Flip in Inelastic Scattering Leading to First Excited States in Nickel Isotopes", F.H. Schmidt, W.A. Kolasinski, and J.G. Cramer, Bull. Am. Phys. Soc. II, *11*, 751 (1966).

"Energy Dependence of the Phase Rule in $Mg^{24}(\alpha,\alpha')$ Scattering", R.A. Hinrichs, J.G. Cramer, W.J. Braithwaite, Bull. Am. Phys. Soc. *11*, 908 (1966).

"Hauser-Feshbach Analysis of Cross Sections and Angular Distributions for Neutron-Induced Fission", R. Vandenbosch, International Conference on Nuclear Physics, Gatlinburg, Tennessee, September 1966.

"The Energy Dependence of the Phase Rule in the $^{24}Mg(\alpha,\alpha')$ Scattering", J.G. Cramer, R.A. Hinrichs, and W.J. Braithwaite, International Conference on Nuclear Physics, Gatlinburg, September 1966.

"Research with the University of Washington FN Tandem Accelerator", J.G. Cramer, APS meeting at Stanford University, December 1966 (invited paper).

"A Survey of the Proton Decay from Isobaric Analog States Formed in the (d,n) Reaction", P. Richard, N. Cue, and J.S. Blair, Bull. Am. Phys. Soc. *12*, 537 (1967).

"Angular Distributions and Excitation Functions of the Proton Decay from IAS Formed in the (d,n) Reaction", N. Cue, P. Richard, and J.S. Blair, Bull. Am. Phys. Soc. *12*, 527 (1967).

"Proton Spin Flip Measurements on a $d_{3/2}$ Analog Resonance in Nb^{91}", J. Cramer and P. Richard, Bull. Am. Phys. Soc. *12*, 527 (1967).

"Isobaric Analog States from the $Pb^{206}(p,p')$ Reaction between 11.9 and 16.1 MeV", J.S. Lilley, C.D. Kavaloski, Patrick Richard and Nelson Stein, Bull. Am. Phys. Soc. *12*, 537 (1967).

"Terminal Voltage Fluctuations of an FN Tandem Van de Graaff Accelerator", H. Fauska, J.S. Heagney, T.J. Morgan, and F.H. Schmidt, National Particle Accelerator Conference, Washington D.C., March 1967 (to be published in "Transactions on Nuclear Science").

"Experiments on Isobaric States in Nuclei", Peter von Brentano, Problem Symposium on Nuclear Physics, Tiblisi, USSR, April 1967.